Visualizing the Rapid Degradation and Differential Binding of Membrane-Bound Human ACE2 Protein Upon Binding and Internalization of the SARS-CoV-2 Spike RBD Protein

Paul Feinstein[1, 2*]

[1]*Department of Biological Sciences, Hunter College, City University of New York, 695 Park Avenue, New York, NY 10065*
[2] *The Graduate Center Programs in Biochemistry, Biology and CUNY Neuroscience Collaborative, 365 5th Ave, New York, NY 10016*

*Corresponding author email: Feinstein@genectr.hunter.cuny.edu

[*]Correspondence:
Paul Feinstein
695 Park Avenue
904 North Building
Department of Biology
New York, NY 10065
Feinstein@genectr.hunter.cuny.edu

Running Title: SARS2-RBD binding to ACE2

Conflict of interest: The author declares that no competing interests exist.
Keywords: SARS-CoV-2; SARS2, Spike protein; RBD, ACE2, Omicron variant, XBB.1.5 variant, NL63, ACE2 downregulation

Contributions
P.F. conceived the project. P.F. designed the experiments. P.F. performed all experiments. P.F. analyzed the data. P.F. wrote the manuscript and prepared all the figures.

Abstract:

The SARS-CoV-2 betacoronavirus infects humans through binding the Angiotensin Converting Enzyme 2 (ACE2) protein that lines the nasal cavity and lungs, followed by import into a cell utilizing the Transmembrane Protease, Serine 2 (TMPRSS2) cofactor. ACE2 binding is mediated by an approximately 200-residue portion of the SARS-CoV-2 extracellular spike protein, the receptor binding domain (RBD). Robust interactions are shown using a novel cell-based assay between an RBD membrane tethered-GFP fusion protein and a membrane-bound ACE2-Cherry fusion protein. Several observations were not predicted, including rapid and sustained interactions leading to internalization of the RBD fusion protein into ACE2-expressing cells and rapid downregulation of ACE2-Cherry fluorescence, suggesting that a membrane-associated form of RBD found on the viral coat may have long-term system-wide consequences on ACE2-expressing cells. Targeted mutation in the RBD disulfide Loop 4 led to a loss of internalization for several variants tested. However, a secreted RBD did not cause ACE2 downregulation of ACE2-Cherry fluorescence. Omicron BA.1 and BA.2 variants have altered their dependency on the amino terminus (Nt) of the ACE2 protein. In contrast, the H-CoV-NL63 RBD is only dependent on the ACE2 internal region for binding, leading to the conclusion that the RBD binding surface of ACE2 appears relatively fluid and amenable to internalizing a range of novel variants.

Introduction:

The COVID-19 worldwide pandemic continues to produce widespread illness and death. The causative agent of this disease is the Severe Acute Respiratory Syndrome coronavirus 2 (SARS-CoV-2 aka SARS2), which is similar the SARS-CoV (SARS1) virus that had a limited outbreak between 2002-2003 (1). Both SARS1 and SARS2 belong to the betacoronavirus subfamily. The spread of SARS1 was cut short by lockdowns, but followed by a second betacoronavirus, Middle East respiratory syndrome (MERS-CoV) in 2012, which continues to infect individuals (2). Vaccines against SARS2 are reducing the death caused by the proliferation of viral particles (3-5). But vaccinations tend not to halt the transmission of viral particles, which occurs in just days after infection, prior to the rise in immune response (6). In addition, the mutation rate of SARS2 is unyielding, leading to the prospect of infections by novel variants for the foreseeable future. The medical industry must find viral transmission mitigation strategies (7-9). While masks form a reasonable barrier to SARS2 infection, societies have not embraced this as a long-term solution to mitigate infections. Both vaccine protocols and drugs such as Paxlovid (10), have significantly reduced morbidities once an infection has occurred.

How are SARS1 and SARS2 infections initiated? It has been shown that the trimeric Spike coat protein for both viruses latch onto a cell via binding to a dimer of the human Angiotensin-Converting Enzyme 2 protein, ACE2, that resides in the plasma membrane. ACE2 provides 740 amino-terminal (Nt) residues in the extracellular space, whilst only a short 40-residue carboxy terminus (Ct) extends cytosolically (11-13). Unlike SARS1, SARS2 has been pre-cleaved to generate S1 and S2 subunits that remain associated by non-covalent interactions. Trimeric S1 proteins loosely associated with an uncleaved S2 subunit cannot be mimicked without using a pseudovirus. Once the SARS2 Spike S1 subunit binds an ACE2 dimer at the plasma membrane, the Transmembrane Protease, serine 2**,** TMPRSS2, catalyzes the endocytosis of the virus into the cell by cleaving the second Spike S2 subunit, revealing the S2'fusion peptide (14-16). Mitigating either binding of ACE2, functionality of TMPRSS2 (7, 8) or endocytosis could prove an effective means of suppressing disease onset. Small molecules, although not volatile, that target TMPRSS2 functionality have been identified that may limit viral load (7)

ACE2 is well expressed in the cilia or microvilli throughout epithelial cells from the nose to the lungs. In the olfactory epithelium, ACE2 is not expressed by olfactory sensory neurons (OSN) but robustly expressed on the intertwined supporting sustentacular cells (SUS) as well as Bowman's glands (17, 18). The nasal infection leads to a down-regulation of OSN-produced odorant receptor (OR) signal transduction components (19). It is not completely understood how SUS cell infection by SARS2 contributes to anosmia (6). In our pursuit of studying odorant receptor (OR) protein trafficking to the plasma membrane, we have fused ORs and other G-protein Coupled Receptors to Green Fluorescent Protein (GFP) and expressed them in an olfactory placodal cell line (OP6) with robust filopodia (20-22). Here, I have repurposed the trafficking assay to study the molecular details of how the SARS2 Spike S1 and ACE2 proteins interact.

Cellular entry for SARS2 is initiated by the cleaved Spike S protein, the 769 residue S1 subunit. Detailed analysis of the SARS1-ACE2 binding (the 193 amino acid region- the receptor binding domain, RBD) led to the identification of the SARS2-S1 RBD between residues 333-529 (23).

112 This 197-residue region recognizes three domains of ACE2 within residues 19-357. By contrast,
113 angiotensin II binds a different portion of ACE2 (24). The sufficiency of the RBD was shown in
114 binding studies using a soluble form of ACE2, sACE2, in EC50 measurements from
115 neutralization with RBD in the micromolar range and to a dimeric ACE2 protein in the
116 nanomolar range (25). The ACE2 protein traffics to the plasma membrane with a signal peptide
117 that is cleaved, resulting in the mature protein, residues 19-805. The RBD region binds to sixteen
118 ACE2 residues distributed within its amino terminal (Nt) 19-83 residues, as well as another five
119 residues within an internal region containing residues 330, 353-357. These interactions and co-
120 crystallographic studies of SARS1 and SARS2 lay the foundation of this current work (1, 26-28).
121
122 Here, the RBD domain and full-length ACE2 proteins are linked to different fluorescent proteins
123 and determined if they could interact in OP6 cells. For the Type I transmembrane ACE2 protein
124 an intracellular Cherry fusion is generated at its Carboxy terminus (Ct), whereas the 197-residue
125 SARS2 RBD was fused to a secretion peptide at its Nt and either a single transmembrane (TM)
126 domain protein or the 7-TM domain β2AR at its Ct along with an intracellular located GFP
127 fusion.
128
129 This in vitro assay allowed us to observe fast and viral-free SARS2-RBD protein binding to
130 ACE2 in cells, which mimic some of the binding and internalization properties of the pseudotype
131 virus infection of ACE2-expressing cells: 1) rapid (a few minutes) and sustained binding
132 between SARS2-RBD protein and ACE2; 2) a Spike S2 subunit independent uptake of a
133 membrane-bound RBD from one cell by other cells expressing ACE2; and 3) a downregulation
134 of ACE2-Cherry protein upon binding to RBD suggesting an unsuspected effect on ACE2
135 accessibility for binding of additional viral particles. This novel in vitro assay provides the basis
136 to identify the critical amino acid sequences involved in binding of SARS2-RBD to ACE2 and
137 its internalization. By contrast, pseudotype viruses provide data on viral replication as a
138 surrogate for RBD binding and viral membrane internalization by ACE2-expressing cells.
139
140 A multitude of generated mutations in conserved residues, despite being predicted to have
141 important roles in binding from crystal structures, do not abrogate SARS2-RBD binding to
142 ACE2 revealing the distributed nature of interactions. One critical residue that did not affect
143 plasma membrane trafficking of the protein, Y489A, nearly abolished the RBD-ACE2
144 interactions. This residue juxtaposes C488 that is critical for disulfide Loop 4 formation (C480-
145 C488). A debilitating C480A, C488A SARS2-RBD double mutant was produced, which
146 suggests disruption of disulfide bridges would abolish binding to ACE2. RBD-ACE2 binding
147 deficits were recapitulated in our assay using concentrations of disulfide-reducing agent
148 dithiothreitol (DTT) analogous to what has been demonstrated with pseudotype viruses (29).
149
150 The alphacoronavirus H-CoV-NL63 (NL63) also binds ACE2 through a 136-residue RBD
151 domain with little homology to SARS2-RBD (7% amino acid identity). Thus, it seems likely that
152 the biological properties of ACE2 make it an attractive target for cellular entry of viruses.
153 NL63-RBD contains three potential disulfide bonds with one cysteine residue common to
154 SARS2 disulfide Loop 4 and contains three other homologous residues. Again, DTT blocked
155 NL63-RBD binding to ACE2 as well. It is plausible that these or other volatile disulfide-
156 reducing agents could mitigate viral infections despite their pleiotropic effects. The ability for
157 RBD domains alone to affect ACE2 protein suggests that vaccines containing "binding

158 competent" RBD domains may alter in vivo ACE2 protein levels and lead to adverse reactions.
159 The data suggest that vaccines with mutation(s) in RBD, which cannot bind to ACE2 may lead to
160 fewer side effects. Some of the Long COVID symptoms may be a result of sustained ACE2
161 down-regulation (30).
162
163 To further pursue how RBD binds to ACE2, a structure-function mutagenesis on ACE2 was
164 undertaken in hopes of identifying an antagonist of RBD binding. Mutations around disulfide
165 Loop 4 within SARS2-RBD that reduced or abolished binding to ACE2, suggested ACE2 Nt
166 proximal regions that might be critical for binding. Here, I show mutagenesis of the ACE2 Nt
167 region identifies a swap of eight residues from the Least Horseshoe Bat (*Rhinolophus pusillus*)
168 into the Nt proximal portion of the human ACE2 (residues between 20-34), which can abolish
169 SARS2-RBD binding. But both Omicron BA.1 and BA.2-RBDs were still able to interact with
170 this ACE2 mutant. An addition of three mutations (L79A, M82A, Y83A: LMY→A) in the Nt
171 distal region of this chimeric ACE2 can completely abolish Omicron BA.1 or BA.2-RBD
172 internalization, while the control NL63-RBD from alphacoronavirus is not affected by any Nt
173 proximal or distal mutations.
174
175 However, both NL63-RBD and SARS2-RBD were both unable to bind ACE2 when its internal
176 residues K353 and D355 were both mutated. Using co-crystallization data as a guide, a double
177 mutant T500A, G502A on SARS2-RBD is also able to abolish binding to ACE2. A set of
178 peptides based on K353-G354-D355 of ACE2 were not able to inhibit either SARS2-RBD nor
179 NL63-RBD binding. The totality of the data suggests: 1) multiple weak binding sites on ACE2
180 sum to create high affinity; 2) the internal region residues may be critical for all RBD binding
181 sites necessary for ACE2 internalization; and 3) there are multiple permutations for RBD binding
182 to ACE2. The changing nature of RBD variants preferentially binding to different ACE2 residues
183 may correlate with the severity of symptoms by altering the degree of internalization by the
184 ACE2 protein.
185
186
187
188
189

190 **Results:**
191
192 **RBD Mutants**:
193 *The RBD→ACE2 cell-based binding assay*
194
195 The SARS-CoV-2 (SARS2) betacoronavirus infects cells via its furin-pre-cleaved Spike protein,
196 generating S1 and S2 subunits that remain non-covalently associated. Internalization of the
197 SARS2 virus is achieved by its membrane localization mediated by the binding of the Spike S1
198 subunit to its cellular receptor, the Angiotensin Converting Enzyme 2 (ACE2), followed by the
199 Transmembrane Protease, Serine 2 **(**TMPRSS2) cleavage of the Spike S2 subunit, revealing the
200 S2' fusion protein. There have been many strategies to characterize the molecular interactions
201 between the Spike S1 subunit and the ACE2 protein. Here, I set up an in vitro cell interaction
202 assay based on the experiments by Chan et al. (25), with a subdomain of the S1 subunit-the
203 receptor binding domain (RBD) and ACE2, both fused to different fluorescent proteins and
204 expressed in heterologous cells **(Figure 1A)**(25).
205
206 G-Protein Coupled Receptor (GPCR) trafficking to the plasma membrane (PM) has been studied
207 by my lab for the last decade, where expression vectors with GPCRs fused to fluorescent
208 proteins are transfected in an olfactory neuronal cell line (OP6) that is rich in filopodia
209 extensions (20-22). I previously showed that the presence of fluorescence in the filopodia
210 accurately correlated with PM expression (20-22). OP6 cells are grown at 33°C, which is
211 coincidentally similar to the temperature at which the nasal epithelium would be infected by
212 SARS2 in ambient air (31). I co-opted our in vitro expression system to study RBD and ACE2
213 interactions. Unless otherwise stated RBD refers to the parental SARS2 Wuhan isolate. Analysis
214 was initiated with a Cherry fusion to the carboxy terminus (Ct) of human ACE2 and a super-
215 folding variant of GFP (sfGFP) fused to the Ct of the secreted RBD. Expression of ACE2-Cherry
216 is readily observed in the filopodia **(Figure 1B-D and F).** In contrast, the secreted-
217 SARS2(sRBD)-sfGFP (s = hemagglutinin-cleavable signal) was detected only within the cell
218 (not shown). When separate transfections were co-plated and cultured overnight, on occasion an
219 ACE2-Cherry expressing cell could be seen with green particles, suggesting uptake of Secreted-
220 SARS2-sfGFP protein (not shown); The membrane of the ACE2-Cherry cells was not labeled
221 with sfGFP. These initial studies show that secretion through the membrane of sRBD-sfGFP may
222 not be occurring.
223
224 In previous studies of GPCR tagging, the nicotinic receptor α7 subunit (nrα7) signal peptide (n)
225 was shown to be effective in targeting a functional GFP added to the extracellular portion of a
226 GPCR (nGFP-GPCR) (32, 33). Thus, I tested the nrα7 signal sequence along with RBD to
227 create Secreted-SARS2-nRBD-GFP and Secreted-Delta-nRBD-GFP (delta SARS2 variant).
228 Because the delta variant was becoming dominant at the time of these experiments, it was chosen
229 for comparative purposes to the RBD (Wuhan) form. Again, no membrane GFP fluorescence
230 could be observed on ACE2-Cherry expressing cells when co-plated after transfection. But it
231 appeared that there may be some granules of GFP fluorescence within ACE2-Cherry cells after
232 12-18hr incubation. The interpretation of these results were either the sRBD-sfGFP or nRBD-
233 GFP proteins were not secreted or if they were secreted, then perhaps they were rapidly
234 internalized and degraded by the ACE2-Cherry expressing cells. Overall, these results suggested
235 a reconsideration of this first approach.

236
237 The ACE2-Cherry fusion was successfully expressed at the PM but was unsuccessful at binding
238 sRBD or nRBD-GFP particles. To prevent secretion of RBD protein, the nrα7-SARS2-RBD
239 (nRBD) was tethered to the extracellular portion of the single transmembrane domain (TM1) of
240 the mouse β2AR (the first 60 residues) that is also Ct fused to GFP. This generated nRBD-TM1-
241 GFP and a control vector nTM1-GFP. Both fusions were expressed in cells and co-cultured
242 separately with ACE2-Cherry expressing cells. As expected, nTM1-GFP trafficked to the PM
243 (34) but did not interact or transfer any fluorescence to the ACE2-expressing cells **(Figure 1B).**
244 In contrast, the nRBD-TM1-GFP fluorescence was found on the tips of the filopodia expressing
245 ACE2-Cherry **(Figure 1C and inset)**; It should be noted that ACE2-Cherry cells had well-
246 demarcated Cherry fluorescence in the filopodia, and GFP-expressing cells were not necessarily
247 nearby. This result suggested that nRBD-TM1-GFP protein may have been secreted into the
248 extracellular space. OP6 Cells do not express TMPRSS2 based on mass spectroscopy (not
249 shown), and no TMPRSS2 target sequences (Arg-Serine dimers) are found within this nRBD-
250 TM1-GFP construct; Had there been any protein digestion within GFP, then no fluorescence
251 could have been observed.
252
253 To ensure that the RBD domain is within the PM, nRBD was tethered to the full-length, 7TM
254 β2AR; These 7TM proteins cannot be secreted due to their seven hydrophobic domains.
255 Transfection, co-plating and culturing of cells with the control nβ2AR-GFP and the control
256 ACE2-Cherry (**Figure 1D**) or control β2AR-Cherry (**Figure 1E**), revealed fusion proteins on the
257 PM of the cells based on filopodial localization of the fluorescence; No transfer of fluorescence
258 was observed between cells **(Figure 1D, 1E)** (20-22). When nRBD-β2AR-GFP (henceforth
259 SARS2-RBD) expressing cells were co-cultured overnight with ACE2-Cherry expressing cells,
260 robust cell-cell contacts and filopodial binding were observed **(Figure 1F and Inset)**. Moreover,
261 ACE2-Cherry fluorescence was no longer well distributed in the cell, and green-fluorescent
262 particles could be observed within ACE2-Cherry cells as particulates. The Green fluorescent
263 particles taken up by ACE2-Cherry expressing were indeed properly folded β2AR as they were
264 able to bind a β2AR fluorescent antagonist (**Figure S1**, CellAura fluorescent $\beta_2$antagonist [(±)-
265 propranolol]). I confirmed that Delta-nRBD-β2AR-GFP (*henceforth* Delta-RBD) cells
266 expressing the variant Delta (L452R, T478K)-RBD qualitatively interacted with ACE2-Cherry
267 cells as did the SARS2-RBD form.
268
269 Our expertise in olfaction led us to consider that there may be an odor, which can interfere with
270 SARS2-RBD binding to ACE2. With our protein interaction assay in hand, 36 concentrated odor
271 mixtures from the kit "Le Nez Du Café (LNDV)"(35) were tested for their ability to antagonize
272 RBD binding to ACE2. Only one of the mixtures at a 1:500 dilution, *medicinal*, appeared to
273 qualitatively reduce, but not eliminate binding; The degree of interaction could not be quantified
274 by microscopy. Had the odor completely blocked binding, this would have been readily
275 quantifiable. Thus, a quantification procedure to measure the extent of antagonism needed to be
276 set up.
277
278 *The RBD→ACE2 flow cytometry based binding assay*
279
280 How strong is the RBD-ACE2 cell-based binding of green fluorescence in or on red fluorescent
281 cells? Would this be observed after trypsinization of co-cultures followed by single cell flow

282 cytometry or FACS analysis? The binding affinity of RBD to ACE2 has been previously
283 calculated at nanomolar equilibrium rates (Kd) (1, 25). I tested the stability of interaction with
284 overnight co-cultures for various GFP fusions against ACE2-Cherry cells, followed by
285 trypsinization, filtering and flow cytometry counts; DAPI positive single cells were quantified
286 for GFP fluorescent positive cells, Cherry fluorescent positive cells, and Cherry/GFP double
287 fluorescent positive cells that were above background. Flow cytometry counts for ACE2-Cherry
288 expressing cells were absent in GFP expression at the gate set for Cherry expression, GFP fusion
289 protein expressing cells were absent in Cherry expression at the gate set for GFP expression, and
290 the double positive window was set above both GFP and Cherry gates. GFP fusions used were:
291 nTM1, nRBD-TM1, nRBD-TM1 plus the odor mixture *medicinal*, β2AR, SARS2-RBD, SARS2-
292 RBD plus the odor mixture *medicinal*, Delta-RBD clone 1, Delta-RBD clone 2. Almost no
293 Cherry/GFP double positive cells were observed for the two controls nTM1 and β2AR **(Figure**
294 **2A).** But greater than 60-fold double fluorescent cells were observed in the other four RBD
295 conditions (56.8 ± 5.0-fold) or two RBD incubated with odor (55.9 ± 10.4-fold) **(Figure 2A).**
296 These pilot experiments clearly demonstrated that RBD-ACE2 interactions could be quantified
297 and that the odor *medicinal* **did not** mitigate binding. From this flow cytometry experiment, I
298 went on to acquire single Cherry cells, GFP cells, Cherry and GFP double fluorescent cells by
299 FACS and microscopically analyzed each population: Green cells largely contained GFP
300 fluorescence and only rare fragments of ACE2-Cherry fluorescence could be observed, Cherry
301 only cells did have some green fluorescence and the double fluorescent cells showed red cells
302 with robust green fluorescence **(Figure 2B, 2B').** Flow cytometry experiments strongly argued
303 that pieces of green-fluorescent membrane were being pulled from Delta-nRBD-β2AR-GFP
304 expressing cells.
305
306 *The RBD→ACE2 in situ single cell binding assay*
307
308 The robustness of the RBD-ACE2 interaction suggested that the observed binding may occur in a
309 short period of time. To test this idea, trypsinized Delta-nRBD-β2AR-GFP expressing cells and
310 ACE2-Cherry expressing cells were co-incubated in a tube at 37°C for 10 minutes, forming
311 doublets of green and red fluorescent cells **(Figure 2C-C''')**. Within these doublets, the
312 distribution of Cherry fluorescence (ACE2 protein) is no longer uniform and found at the edge of
313 the cell, juxtaposed to the GFP-expressing cell.
314
315 *Time course for RBD→ACE2 interactions*
316
317 Flow cytometry analysis of double fluorescent cells proved to be a robust, quantifiable method to
318 determine the degree of interactions between RBD-expressing cells and ACE2-expressing cells.
319 The speed of the interactions between these cells, led to a different version of the assay. Now,
320 transfected cells are grown separately overnight, followed by trypsinizing the "test constructs"
321 and plating them onto ACE2-expressing cells. A time course experiment was performed using
322 triplicate platings of test constructs at 10, 30, or 90 minutes (min). Following this incubation,
323 cells on target plate were washed, trypsinized, and quantified by flow cytometry analysis of
324 single cells [*Dissociate-Plate-Flow Cytometry (DPF) assay*]. As expected, nβ2AR expressing
325 cells did not interact with ACE2-expressing cells at any timepoint forming very few GFP/Cherry
326 double fluorescent cells **(Figure 2D).** But, for both nRBD-β2AR (SARS2-RBD) and Delta-
327 nRBD-β2AR (Delta-RBD) expressing cells, 4.7 and 6.1-fold increases (± 1.5 and ± 1.8,

respectively) over background in GFP/Cherry double fluorescent cells were observed in 10minutes (min), respectively; 13.4 and 13.1-fold increases (± 3.2 and ±2.7, respectively) in 30min, respectively; and 21.0 and 22.9-fold increases (± 2.8 and ±1.2, respectively) in 90min, respectively (Figure **2D).** Cell seeding is generally a slow process that takes hours, so the ~5-fold increase in double fluorescent cells at 10min was remarkable. When quantifying the ACE2-cherry fluorescent cells above background, a noticeable decline in the number red cells at 10 min was observed reaching ~3-fold fewer numbers by the 90 min timepoint, a ~60% reduction ±5% **(Figure 2D').** A 40%±16% reduction of ACE2 cell counts was observed in the pilot experiment as well **(Figure 2A')**. The rapid drop in ACE2 levels suggests either red cells have died in the 90 min period perhaps due to reorganization of membrane proteins, or ACE2 protein is being rapidly degraded through RBD binding. A decrease in ACE2-Cherry fluorescence was observed in both Cherry only and GFP/Cherry double fluorescent cells incubated with the RBD expressing cells suggesting that ACE2-Cherry fluorescence is being reduced on a per cell level. Utilizing this new assay, it was confirmed that neither Secreted-SARS2 nor Secreted-Delta gave rise to GFP/Cherry double fluorescent cells **(Figure S2A)**, nor reductions in ACE2-Cherry cell counts **(Figure S2A')**. Several control experiments further validated the assay: 1) Reducing the number of Delta-RBD cells added to ACE2-expressing cells did not alter the effect; 2) Delta-RBD cells did not interact with β2AR-Cherry cells; and most importantly the Delta-RBD cells did not cause the ACE2-expressing cells to be dislodged from the plate as GFP/Cherry doublets were not observed in the supernatant after a 90min co-culture **(Figure S2A and S2A')**. Finally, the supernatant from Delta-RBD cells grown overnight did not produce any GFP/Cherry doublets nor a decrease in ACE2-Cherry fluorescence **(Figure S2B and S2B')**. A direct test of the secreted particle possibility utilized purified His tagged-RBD protein coupled to an anti-His-488 antibody and incubated for 90min with ACE2-Cherry expressing cells. No impact could be observed on the downregulation of ACE2-Cherry fluorescence despite the formation of antibody labeling of RBD on ACE2-expressing cells (**Figure S3A and S3A'**). In sum, there was no evidence of sudden cell death nor secreted particles from the cells expressing a tethered RBD. Based on these observations, it's unlikely that the non-membrane-bound Spike S1 fragment would lead to downregulation of ACE2-Cherry.

Does cell adhesion cause downregulation of membrane proteins?

Thus far, the data show specificity between nRBD-β2AR-GFP expressing cells and ACE2-Cherry expressing cells. Yet, nonspecific interactions and ACE2-Cherry protein could be due to β2AR interaction or through the effects from an unidentified process of cell-cell adhesion. As a control Venus or Cherry fusions of the cell adhesion molecule Cadherin 2 (Cdh2) were separately transfected and co-cultured overnight in OP6 cells producing robust cell-cell contacts compared to Delta-RBD and Cdh2 **(Figure S2B)**. Interaction of Cdh2 was observed as double fluorescent cells, however the red fluorescence of CHD2-Cherry was not decreased (**Figure S2B** and **S2B'**). To rule out the RBD-ACE2 interactions were phenocopying a cell adhesion phenomenon, a series of controls using ACE2-Cherry, β2AR-Cherry, Cdh2-Cherry cells were co-incubated for 90min with β2AR-GFP, Delta-nRBD-β2AR-GFP, or Cdh2-GFP cells, followed by flow cytometry analysis; Only Delta-nRBD-β2AR-GFP and ACE2-Cherry cells led to double fluorescent cells and decreases in Cherry fluorescence of ACE2-Cherry (**Figures S2C, S2C'**). Double fluorescence cells between ACE2-Cherry and Delta-RBD GFP cells was more substantial than the adherence of Cdh2-GFP + Cdh2-Cherry cells in 90min co-cultures **(Figure**

374 **S2C and S2C').** Here it can be firmly concluded that the observed cell dynamics are derived
375 from RBD and ACE2 binding.
376
377 *RBD→ACE2 membrane reorganization*
378
379 We have previously shown that plasma membrane dynamics can be readily monitored by an
380 array of palmitoylated fluorescent proteins [20-residue sequence (aka *gap*) from Zebrafish
381 gap43] (20). To determine if the OP6 cells were undergoing general membrane changes from
382 the RBD-ACE2 binding, ACE2-Cherry and gapTeal were cotransfected (Co-EP) and Delta-
383 nRBD-β2AR-Venus cells were added and imaged after 30min **(Figure S4A-D''')**.
384 Reorganization of the ACE2-Cherry fluorescence and Delta-nRBD-β2AR-Venus was readily
385 observed, but not that of gapTeal **(Figure S4A, A')**. Quantification of fluorescent pixels showed
386 co-accumulation of Venus and Cherry fluorescence at the plasma membrane, but not Teal
387 **(Figure S4B)**. Unfortunately, quantification of these results by single cell flow cytometry is not
388 possible because Teal and Venus fluorescence are not separable by our available flow cytometry
389 machines. But flow cytometry analysis of single cells can be performed with GFP, Cherry and
390 Farred fluorescent proteins. To circumvent this issue, the assay was reorganized. Now ACE2-
391 GFP and gapFarred [codon optimized AFP (20)] were Co-EPd. Separately transfected Delta-
392 nRBD-β2AR-Cherry, Cdh2-Cherry or nβ2AR-Cherry were followed by trypsinization, co-
393 plating and imaging within 30min over time **(Figure 3A-C''')**. Quantification of fluorescent
394 pixels again showed co-accumulation of GFP and Cherry fluorescence at the plasma membrane,
395 but not Farred **(Figure 3D)**. It is notable that the effects on membrane reorganization of ACE2
396 protein was independent of Ct fluorescent protein fusion: GFP fluorescence also appeared
397 weaker suggesting it was being degraded. Flow cytometry analysis on single cells and confirmed
398 the specific interaction of Delta-nRBD-β2AR-Cherry with ACE2-GFP showing 37.8 ±6.1-fold
399 more double positive cells than controls and a 47±4.3% reduction of ACE2-GFP fluorescence;
400 Control proteins nβ2AR-Cherry and Cdh2-Cherry did not associate with ACE2-GFP nor cause
401 its downregulation **(Figure 3E and 3 E')**. Furthermore, gapFarred fluorescence was not reduced
402 to the same extent as GFP fluorescence **(Figure 3E')**.
403
404 The assay developed here to study RBD/ACE2 interactions were not developed to study the
405 previously shown of ACE2-internalization and loss. Here, SARS2-RBD interactions with ACE2
406 occur without the presence of TMPRSS2 nor S2' fusion protein to facilitate receptor-mediated
407 endocytosis. As such, lysosomal cathepsins would likely be required for endocytic entry and loss
408 of ACE2 as is found for SARS2 entry in TMPRSS2 deficient cells (36-38). There are many
409 mechanisms that could be involved in endocytosis and eventual reduction of ACE2 fluorescence
410 in addition to Clathrin-mediated processes (39, 40). To rule in/out two of the possibilities, it was
411 determined if the proteasome inhibitor MG-132 or the lysosome inhibitor bafilomycin A1
412 (BafA1) could interfere with ACE2 internalization. Neither MG-132 (**Data File S2**) nor BafA1
413 (**Figures 3F'-F''**) affected ACE2-cherry fluorescence in the context of SARS2-RBD, but more
414 double positive cells were observed with the BafA1 treatment (**Figure 3F**) suggesting an
415 increased availability (less loss) of ACE2-Cherry for binding to SARS2-RBD. Interactions
416 between SARS2-RBD and ACE2-Cherry expressing cells over 90min in the presence of
417 lysosomal inhibition did not prevent ACE2-Cherry loss nor inhibit the formation of doubled
418 positive cells. Perhaps lysosomal inhibition of ACE2-Cherry loss would be observed in an earlier
419 time point. It should be noted that ACE2-expressing cells counts are derived from expression

levels above background (**see Figure 2D')**, ACE2 fluorescence levels above background have also been calculated **(see Figures 3E', 3F'-F'', and S3A', S3B'', S3C'')**. The ACE2 internalization effects were even more profound after overnight co-plating **(Figures S4C-C''')** compared to controls **(Figures S4D-D''')**, which showed no internalization of ACE2. It should be noted that internalization of ACE2-Cherry did not lead to cell death. Finally, spinning disk imaging of the cell-based interactions with Delta-nRBD-β2AR-GFP and ACE2-Cherry cells were performed to show real-time dynamics; ACE2-Cherry reveal drastic reorganization, but not Delta-nRBD-β2AR-GFP cells within 10 minutes of imaging performed immediately after co-plating **(Figures 3G-G', 3H-H', and Movies S1A-C)**. In sum, RBD specifically reorganizes and degrades ACE2-fluorescent proteins.

Meta-Analysis of 197 residue SARS2-RBD domain

This new cell-based RBD-ACE2 interaction assay provided a novel framework to define critical RBD binding residues. Previously, the SARS1-RBD (residues 320-515) defined a 74% identical region for SARS2 (residues 333-529) **(Figure 4)**. A subset of residues that provide structural integrity and binding potential were identified by reviewing the crystallographic data (1, 28), deep mutational screening (DMS) (25, 41), in silico predicted interactions (42) and the known properties of amino acids in proteins.

DMS by two groups led to the identification of clones that can still bind ACE2. Both groups produced very similar data, but one group also controlled for RBD stability revealing 29 residues that were not mutated in 70% of the clones and thus necessary for binding **(Figure 4, red highlights within SARS1-SARS2-RBD consensus sequence)**. Ten of the 29 residues were distributed and not implicated in the folding of the RBD and thus candidates for ACE2 binding: F400, N422, Y423, S442, N487, Y489, Y495, F497, Q506, H511. Nine of the 29 residues were retained in 90% of the DMS clones **(Figure 4, green lettering and green starred)** and would appear to be critical for function including R454, N487, G502, P507 and R509 as well as the four Cysteine (Cys) residues that form disulfide bridges in Loop 2 and Loop 4. The greatest concentration of immutable residues lay between N487 and V511, which is consistent with three residues described in the literature predicted to affect binding when mutated (Y449, N487, Y489, **Figure 4** purple highlighted)(43).

As an apparent contradiction, residues predicted in silico to be critical for binding **(Figure 4, yellow highlights)** do not overlap any of the 29 relatively immutable residues from DMS clones: K417, F456, F486, Q493, Q498 (42). Among various variants produced in first two years of the pandemic only two residues (Y449, G496) are amongst the 29 residues. Finally, a set of three residues that encompass C488 from disulfide Loop 4: N487, C488, and Y489 are well conserved in all known betacoronaviruses that bind ACE2 **(Figure S5)**. Taken together, most interacting residues appear distributed, except for a stretch of residues in proximity to C480 and C488.

It is known that the alphacoronavirus H-CoV-NL63 has a 136 residue RBD domain that also binds ACE2 (NL63-RBD). This domain has only eleven residues conserved with SARS2-RBD, but four of them are colinear with the RBD disulfide Loop 4 region **(Figure S5 and S6; residues C-FPL)** (44). The NL63-RBD homology region is not among the residues predicted to interface with ACE2 **(Figure S6; RBM1-3)**, but it is interesting to note that the N578Y mutation that

466 makes a five-residue match to the SARS2-disulfide Loop 4 region (CYFPL) increases its binding
467 potential to ACE2 **(Figure S5)**(44). By contrast, the SARS2 Spike homologue, RpYN06, is
468 missing the region between C480 and C488 that comprises disulfide Loop 4 and fails to bind
469 ACE2 **(Figure S7)**(45-47). Thus, a strong argument can be made for critical ACE2 binding
470 residues reside within the RBD-disulfide Loop 4 region including the pair of Cys residues.
471
472 *RBD and disulfide Loop 4 region domain mutagenesis*
473
474 To better understand the functionality of residues within the RBD domain, an array of RBD
475 variants and mutants including disulfide Loop 4 substitutions were tested to characterize RBD
476 binding to ACE2. The SARS1, SARS2 and NL63 RBDs have been shown to bind the ACE2
477 protein with Kds in the low nM range **(Figure S5)** (1, 44, 48). SARS2 variants have not been
478 compared yet but are likely in the same range. One RBD, RaTG13 binds with a Kd in the μM
479 range (1000-fold less) (**Figure S5)** (26). All four orthologues and five SARS2 variants (Alpha,
480 Delta, Delta-Plus, Omicron-BA.1, Omicron-BA.2) were tested in our DPF assay **(Figures 4, 5,**
481 **S8)**. No differences were observed in their ability bind and reduce ACE2-Cherry expression,
482 except for NL63, which produced fewer double positive cells but more severe loss of ACE2-
483 Cherry expressing cells **(Figures 5A, 5A' and S8B')**. Alanine substitutions were used to
484 simultaneously convert all 3 high frequency mutants (>.03%) found in year 2020 (HiF2020) and
485 all 7 residues found in year 2020 and 2021 (HiF2021). None of these mutations altered binding
486 and reduction of ACE2-Cherry expression shown with SARS2-RBD **(Figure 5A, S8B, B')**.
487 Next, seven Predicted Binding Sites (P.B.S.; K417, G446, L455, F486, Q493, Q498, N501)
488 between RBD and ACE2 were converted into alanine as a group (P.B.S. 7Ala-RBD-β2AR-GFP).
489 The P.B.S 7Ala-RBD trafficked to the plasma membrane but was not observed to bind ACE2-
490 Cherry cells **(Figures 5A, 5B, S9A, S9A', S10B)**. This mutant was the first that completely
491 blocked binding **(Figures 5)**, a 6.1±3.1-fold double positive rate compared to 3.0±1.8-fold in
492 controls. One of the alanine substitutions was within the disulfide Loop 4, F486, might have been
493 predicted to be critical for RBD-ACE2 interactions. Indeed, the P.B.S. 6Ala mutant with the
494 A486F revertant could now bind to and reduce ACE2-cherry fluorescent cells **(Figures 5, S9B,**
495 **S10C)**, 85.6±10-fold double positives, almost as well as SARS-RBD **(Figure S9C and S10A)**
496 with 101.2±13.0-fold double positives. Other single reversions were not performed, but due to
497 the distributed nature of binding; It is plausible that several might also rescue binding. Among
498 the 7 residues encompassing the P.B.S., it is likely that no one residue is critical for binding
499 except F486. Yet, this residue could be heavily mutated in the DMS experiments, suggesting that
500 it does not form bonds that are necessary and sufficient of RBD binding. Taken together, DMS
501 mutagenesis along with the vast number of residue differences between RaTG13/SARS1 and
502 SARS2 along with the multiple alanine mutations suggested that critical residues for binding are
503 distributed throughout the RBD.
504
505 If RBD binding to ACE2 were distributed, then how are nanomolar Kds accomplished? Cross
506 species sequence comparisons suggest disulfide Loop 4 may be key to nucleate ACE2
507 interactions. It is known that a small tripeptide domain like Arg-Gly-Asp (RGD) can be enough
508 to achieve high affinity binding to another protein (49). Thus, a small motif within the RBD
509 domain may be all that is necessary, but no such 100% conserved three residue region exists
510 amongst RBD domains and mutants. Yet, the disulfide Loop 4 represented an interesting region
511 as the disulfide bond itself may play a critical role in recognition of the ACE2 protein **(Figure**

512 **5B)**. In the context of SARS2-RBD, small regional substitutions between C480 and 488 were
513 generated: SARS1 481-486 and RaTG13 483-486 substitutions as well as scanning alanine
514 mutants for residues 486 through 492 **(Figures 5B and S8B**). Neither SARS1 and RaTG13 Loop
515 4 substitutions nor alanine mutants within this region showed any differences in binding and
516 internalization **(Figure 5)**. Based on the P.B.S. 6Ala-RBD, the F486A alone might have
517 disrupted binding, but it did not **(Figures 5)**, again pointing to the distributed nature of RBD
518 binding to ACE2.
519
520 Alanine scanning of neighboring residues Y489, F490, P491, L492 and the Y449 residue
521 predicted to be important for binding revealed four interesting aspects of RBD binding to ACE2.
522 First, only Y489A was able to nearly abolish binding (14.7$\pm$6.6-fold double positives) and
523 reduced the loss of ACE2-Cherry fluorescence cells (30%$\pm$2.6%), while still being well
524 expressed at the plasma membrane (**Figures 5, S8, S9, S10**). In contrast, the Y449A residue
525 predicted to decrease binding of RBD had no effect. Second, C488A did not traffic well to the
526 plasma membrane, but even when it did, binding to ACE2-Cherry cells was not readily observed.
527 It seemed likely that the C488A mutation that poorly traffics RBD to the plasma membrane (PM)
528 may be due to the C480 residue forming a disulfide bond with one of the other 6 Cys residues
529 **(Figure 4).** To mirror the loss of both Cys residues found in RpYN06 **(Figure S7),** the double
530 mutant C480A, C488A-RBD was generated. This mutation traffics very well to the PM, on
531 occasion binds ACE2-Cherry expressing cells, but does not become internalized **(Figures 5, S9)**.
532 Third, neither N487A, F490A nor P491A-RBDs affected PM trafficking nor ACE2
533 binding/degradation properties of RBD. Finally, mutational analysis was expanded to the
534 Omicron (OM).BA.1 variant for Y489A and P491A mutants. But neither mutant could traffic to
535 the PM suggesting that OM.BA.1 had a different confirmational landscape to that of SARS2 or
536 any previous variant **(Figures 5 and S10)**. The failure of Y489A-OM.BA.1-RBD mutation to
537 allow PM trafficking suggests a disruption of C480-C488 disulfide bond formation and further
538 points to an altered Loop 4 confirmation in the Y489A-SARS2-RBD mutation. Overall, the data
539 strongly implicate the formation of the disulfide Loop 4 bond as a critical feature of RBD-ACE2
540 interactions.
541
542 *Blocking RBD binding using a disulfide reducing agent*
543
544 The analysis RBDs from NL63 and betacoronaviruses such as SARS1, SARS2 and its variants
545 define a continuum of RBD residues necessary for allowing its internalization by ACE2. These
546 data argue that it would be difficult to find an airborne molecule, which would specifically
547 disrupt contacts between the changing landscape of RBD and ACE2 interactions. But the
548 disulfide Loop 4 analysis suggested that critical Cysteine residues involved in disulfide bridges
549 were common to all RBD domains could be a targeted to mitigate infection. That said, the
550 volatile reducing agent Dithiothreitol (DTT) was able to disrupt SARS2 pseudotype virus
551 infections on ACE2-expressing cells in the millimolar range (29, 50). DTT has a strong
552 characteristic odor with a modest vapor pressure of 1.28 x10^{-4} mm Hg at 25C. A derivative of
553 DTT, dithiobutylamine (DTBA) was identified in 2012 that had similar properties, but more
554 resistant to changes in pKA and reduces disulfide bonds in small proteins more quickly (51). The
555 RBD-ACE2 solution binding assay (**Figure 2C-C'''**) was utilized to assess GFP-Cherry in
556 concentration series (0mM, 0.5mM, and 2mM) for DTT and DTBA. SARS2-RBD-β2AR-GFP
557 or OM.BA.1-RBD-β2AR-GFP and ACE2-Cherry GFP/Cherry doublets were readily observed in

558 the 0mM DTT and DTBA conditions for both SARS2 and OM.BA.1-RBD (**Figure 6A**). In the
559 2mM DTT condition it was difficult to find SARS2-RBD or OM.BA.1-RBD bound to ACE2
560 (Figure **6B and inset**). In contrast, RBD interactions were not observed in 2mM DTBA. The
561 effect of reducing agents on SARS2 and OM.BA.1-RBDs in the solution binding assay mirrored
562 what was already tested using pseudotype viruses, showing that binding assay strategy could be
563 set up to screen for other volatile compounds for their ability to disrupt disulfide bonds. Finally,
564 the NL63-RBD with a different set of disulfide bonds was quantified in the presence of 2mM
565 DTT and 2mM DTBA in the plate binding assay with ACE2-Cherry. 2mM DTBA completely
566 removed the ACE2-Cherry cells from the tissue culture plate, but the 2mM DTT did not, and
567 these interactions were quantified by flow cytometry; the 2mM DTT prevented double
568 fluorescent cells from forming and prevented downregulation of ACE2-Cherry fluorescence
569 (**Figure 6C and 6C'**). Thus, a limited exposure of disulfide bonds in RBDs using a volatile
570 disulfide reducing agents could provide a new strategy to mitigate viral infections.
571
572 **ACE2 Mutants:**
573 *ACE2 Amino terminal domain mutagenesis*
574
575 SARS2-RBD is predicted to bind many residues on ACE2 through mostly hydrogen bonding (1,
576 28). These interaction domains can be separated into Nt proximal region: residues 19-45; Nt
577 distal region: residues 79, 82-83, Internal region 1: residue 330, and Internal region 2: residues
578 353-357. Both RaTG13 and SARS1 RBDs are predicted to bind the same three regions with
579 some variation in specific residues **(Figure 7A)**. The ACE2 Nt proximal region is poorly
580 conserved (<50% homology) across 408 species from residues 19-27 but becomes increasingly
581 more conserved from residues 28-45 (>50% homology)(52). By contrast, the ACE2 Nt distal
582 region retains conservation only in residue Y83 (>50%) and the Internal region residues of 330
583 and 353-357 are also highly conserved (>50%) (**Figure 7A, B**). In comparison, NL63-RBD has
584 reduced contacts with the divergent Nt proximal region, no contacts with the divergent Nt distal
585 region, and expanded contacts with the conserved Internal region 1 (27). The regional overlap in
586 binding to ACE2 for NL63-RBD and SARS2-RBD (SARS1 and RaTG13 as well) is remarkable
587 despite the near absence of protein homology. The disulfide Loop 4 region of SARS2 is strongly
588 implicated to bind only the ACE2 Nt proximal and distal regions (**Figure 7B)**. Mapping studies
589 show that both N487 and Y489 are in involved in coordinating binding at both the Nt proximal
590 and distal regions (**Figure 7B**), suggesting that disruption of this contacts might abolish binding
591 (1).
592
593 Utilizing our co-plating in vitro assay and guided by the co-crystal studies of SARS2-RBD and
594 ACE2, a set of eight mutations (Group I) targeting key residues in the Nt domain with either
595 alanine or alteration in charge character **(Figure 8A)**. Another three mutations targeted multiple
596 residues that would coordinate ACE2 Proximal and Distal regions by N487/Y489 residues.
597 These multiple alanine substitutions at key ACE2 residues: Q24A, Y83A; T27A, F28A, K31A,
598 Y83A; or L79A, M82A, Y83A (LMY→A). None of the eight sets of point mutations had any
599 effect on blocking ACE2 Nt contacts with SARS2-RBD. These results seem at odds with the co-
600 crystal data, but not with the alanine-substituted SARS2-RBD mutants that also failed to disrupt
601 binding and internalization.
602

603 It has been shown that ACE2 from three species *R. pusillus*, Chicken, and Turkey either poorly
604 or do not bind SARS1 or SARS2-RBD domains (53-55). This lack of binding is believed to be a
605 distributed consequence of residues along the entirety of the ACE2 protein. But sequence
606 analysis showed that Aves/Reptilla (**Figure 7A**) were more variable than the entire set of 408
607 ACE2 aligned residues. This divergence set forth a hybrid ACE2 Nt approach substituting the
608 first 43 residues: five mutants based on *R. pusillus* (Group II), and six mutants based on Chicken
609 (Group III).
610
611 *R. pusillus* ACE2 has only nine differences with the human ACE2 protein between Q19 and L45,
612 in the Nt proximal region where SARS2-RBD is predicted to bind. Three hybrids referred to as
613 Pusillus (Pus) and number of amino acids (AA) were generated with different number of
614 substitutions (5 amino acids)-Pus5AA, Pus7AA and Pus8AA and tested with SARS2-RBD.
615 Neither the Pus5AA nor Pus7AA disrupted binding/internalization. But the Pus8AA completely
616 disrupted/internalization **(Figures 8A-C, S11)**, which is consistent with the idea that Y489A and
617 the Loop 4 region are important for SARS2-RBD binding to Nt ACE2. All variants and mutants
618 of SARS2-RBD failed to bind or be internalized by Pus8AA: Delta, HiFrequency2020 3Ala (3
619 Alanine substitutions in the most common changes observed 2020), HiFrequency2021 7Ala
620 (7Alanine substitutions in the most common changes observed in 2021), Predicted Binding Site
621 (P.B.S.)-7Ala (7 Alanine substitutions from in silico prediction programs)(42), P.B.S. 6 Ala (one
622 fewer substitution) as well as SARS1, and RaTG13 **(Figure S11)**. Surprisingly, RBD-OM.BA.1
623 and OM.BA.2 (**Figures 8A, 9A-F, S11)** were unaffected, as well as NL63-RBD (**Figure 8D**); all
624 three RBDs were still bound and internalized by the Pus8AA substitution. This might have been
625 expected for NL63 due to its paucity of contacts with the ACE2 Nt proximal region (**Figure 7A)**.
626
627 F28 is strongly conserved in ACE2 and is predicted to interact with the critical SARS2 residue
628 Y489, but an F28A mutation did not block SARS2-RBD internalization. To extend these
629 observations, F28A was added to the ACE2 Pus8AA hybrid to determine if OM.BA.1 or BA.2
630 would be blocked from binding/internalization, but no decrease in binding was observed (**Figure**
631 **8A)**. These observations conclude that there is a differential reliance on the ACE Nt proximal
632 region for SARS2 versus OM.BA.1, OM.BA.2 and NL63-RBDs, suggesting multiple modes of
633 ACE2 binding/internalization. Subsequent RBD variants OM.BA.4/BA.5 (both with L452R,
634 F486V and R493Q relative to OM.BA.2) do not bind to the ACE2 Pus8AA Nt mutant,
635 suggesting this newer variant had interactions more like that of SARS2-RBD. Finally, data from
636 ACE2 deep mutational screening (DMS) (25, 41) show that SARS2-RBD-H34S does not block
637 interactions, yet the wild type H34 residue in ACE2 Pus7AA hybrid did rescue SARS2-RBD
638 binding. Taken together Pusillus AA hybrids might change conformation of the Nt region or
639 disrupt specific residue interactions between SARS-RBD and ACE2. AlphaFold analysis of
640 ACE2 Pus8AA hybrid did not reveal change to the **helix** (residues 20-52)-**turn**-**helix** (residues
641 55-81) structure of the Nt proximal and distal regions, respectively (**Figure S12**). However, the
642 amino terminus did adopt novel conformations that perhaps disrupt its contacts with the RBD
643 Loop 4 region. By contrast Pus7AA maintains the H34 residue, which is predicted to interact
644 with SARS2 residues Q493, L455, and Y453. But this interaction is unlikely to be critical as
645 chicken14AA containing H34V does not block binding nor does H34S (25). Taken together, the
646 Pus8AA hybrid likely changes the conformation and contacts of the Nt proximal region, leading
647 to a destabilized interaction between SARS-RBD and ACE2.
648

649 My proposed model of disulfide Loop 4 interactions suggested that it coordinates its binding
650 between the ACE2 Nt proximal and distal Regions (ACE2 residues 79-83). Based on the ACE2
651 Pus8AA mutation, SARS2 may primarily utilize the ACE2 Nt proximal region and conversely,
652 OM.BA.1 and OM.BA.2 RBDs might primarily utilize the Nt distal region. None of the Group I
653 mutations analyzed, including the Nt distal region mutant LMY→A altered OM.BA.1
654 binding/internalization **(Figure 8A)**. The RBD domains of OM.BA.1 and OM.BA.2 contain 16
655 mutations that differ from SARS2, which perhaps caused them to rely on both the Nt proximal
656 and distal regions. To test this idea, the ACE2 Pus8AA hybrid was combined with the LMY→A
657 mutant. Pus8AA + LMY→A was finally able to block OM.BA.1 and OM.BA.2 RBDs from
658 being bound and internalized (**Figures 8A, 9G-I, S11**), confirming the hypothesis; the NL63-
659 RBD, which does not bind to the ACE2 Nt distal regions, was unaffected as expected (**Figure**
660 **9J-L**). These Group II ACE2 mutants show that SARS2, OM.BA.1 and NL63 RBDs have
661 differential contact points to promote their binding/internalization
662
663 In contrast to the Group II hybrids, Chicken ACE2 mutants (Group III) containing both the Nt
664 proximal and distal region substitutions did not block SARS2, OMBA.2 nor NL63 RBDs from
665 binding and internalization. Group III data suggest that some combination ACE2 Pus8AA
666 residues can block SARS2-RBD binding by a robust change in contact residues (**Figures 7A, 7B,**
667 **8A**). The totality of data for OM.BA.1 and OM.BA.2 RBD binding point to a conformational
668 shift in their RBDs that alters their usage for ACE2 Nt Proximal and Distal regions. Consistent
669 with this conclusion, both Y489A and P491A are properly trafficked to the plasma membrane for
670 the SARS2-RBD, whereas analogous mutations in OM.BA1-RBD fail to traffic to the plasma
671 membrane likely due to a change in conformation leading to failure in the formation of the
672 correct cysteine bonds (56).
673
674 Mice cannot be infected by SARS2, which is why mutant mice strains have been generated with
675 the human ACE2 CDS replacing the mouse ACE2 gene (57). A third hybrid (Group IV) with the
676 mouse (m)ACE Nt proximal and distal was made with 25 of the first 94 residues altered (**Figures**
677 **8A, S13**). This Group IV hybrid contained mutations at similar residues to the Pus8AA as well as
678 a LMY→TSF mutation. Yet, no alteration in binding or internalization was observed for SARS2,
679 OM.BA.1 and NL63 RBDs. Thus, substantial changes in the ACE2 Nt proximal and distal
680 regions suggest a lack of specificity for RBD binding. Interactions were quantified for four
681 ACE2 substitutions by our Dissociation-Plate-Flow Cytometry *(DPF) assay*: Pus8AA, Pus8AA
682 +LMY→A, and mACE2 Nt 1-94 with RBDs from SARS2, OM.BA.1, NL63 and a newer variant
683 XBB.1.5 (**Figure 10A-A'**).
684
685 Indeed, flow cytometry quantification of double positives for SARS2, OM.BA.1, NL63
686 mimicked the co-plating assay results with XBB.1.5 showing binding and internalization like
687 that of OM.BA.1 in all four Nt ACE2 hybrids (**Figure 10A, Supplemental Data File S2**). In
688 contrast to OM.BA.1, XBB.1.5 did not cause a change in fluorescence to Pus8AA or Pus8AA
689 +LMY→A-Cherry cells. OM.BA.1, despite a lack of robust binding to Pus8AA +LMY→A
690 (8.75±1.94), still showed modest reduction to its fluorescence (17.2%±2.2%) (**Figure 10A'**).
691 Finally, a fourth mutant mACE 1-357 was tested, which abolished binding for RBDs SARS2
692 (1.45±1.37), OM.BA.1 (5.71±0.89), and XBB.1.5 (3.98±2.08), but not for NL63 (26.7±1.60)
693 (**Figure 10A**). An interaction could be observed for OM.BA.1 by the 24.8%±0.04% loss of

694 ACE2 fluorescence (**Figure 10A'**). These data are consistent with NL63 having a greater set of
695 contacts with residues 321-330 of ACE2 (**Figure 11A**).
696
697
698 *Co-transfection of membrane tethered RBDs and ACE2*
699
700 In vitro co-plating, while simple, requires visual inspection of RBD-expressing cell touching an
701 ACE2-expressing cell. This assay is robust but can be difficult to quantify weak binding without
702 internalization. The *DPF assay* is very quantitative, but more labor-intensive. To more quickly
703 rule out weak interactions, a co-transfection and plating assay was set up to see if protein
704 interactions could be observed within the same cells, as is reminiscent of the interactions
705 published decades ago for other cell surface receptors and ligands, the SEVENLESS-BOSS (58)
706 proteins as well as the NOTCH-DELTA (59) proteins. A priori, it was not known if membrane-
707 bound RBD and ACE2 proteins could interact if co-expressed. Here, it was expected that
708 interactions between expressed proteins would be at a higher probability compared to those
709 between cells. Co-transfection between nβ2AR-GFP (n=signal peptide) with ACE2-Cherry in the
710 same cells and imaged after 16 hrs reveals robust membrane trafficking for both proteins in the
711 same cells (**Figures S14A-A''**). By contrast, co-transfection of SARS2-RBD with ACE2-Cherry
712 shows only robust SARS2-RBD at the membrane and filopodia with ACE2-Cherry internalized
713 (**Figures S14B-B'')**. Internalization of ACE2 by RBD through intra- or intercellular interactions
714 may be clathrin dependent (40);. This final piece of evidence firmly concludes that ACE2-Cherry
715 is subordinate to the effects of the SARS2-RBD protein and does not cause cell death. This co-
716 transfection assay confirms and extend the results observed on ACE2-Cherry membrane
717 localization: Y489A (**Figure S14C-C''**) and P.B.S 7Ala (**Figure S14D-D''**) do not affect ACE2
718 internalization, C480A, C488A (**Figures S14E-E''**) had little effect; and P.B.S. 6Ala (**Figures**
719 **S14G-G''**) did not block internalization.
720
721 Consistent with co-plating experiments, co-transfection of SARS2 and OM.BA.5 RBDs with
722 Pus8AA hybrid ACE2 did not show binding/internalization (**Figures S15A-A'', S15B-B''**)
723 whereas co-transfection with OM.BA.1 RBD did show internalization (**Figures S15C-C''**).
724 Surprisingly, OM.BA.1 RBD did internalize Pus8AA +LMY→A (**Figures S15D-D''**), despite it
725 not forming double fluorescent cells by *DPF assay* (**Figure 10**), but perhaps consistent with the
726 loss of fluorescence (**Figure 10**). Co-transfection proved an effective way for simultaneously
727 assessing the membrane trafficking of ACE2 and RBD mutants as well as determining if proteins
728 could interact. It is likely that co-transfection reveals less stable contacts between RBD and
729 ACE2, which still allow for the internalization of the ACE2-Cherry protein (compare **Figures**
730 **S14E-E'** to co-plating in and DPF assay results in **Figures 11F-F'**). It should be noted that co-
731 transfection results likely mimics SARS2 viral production within ACE2-expressing cells.
732
733 *ACE2 Internal region mutagenesis*
734
735 Interpretation of the data thus far suggests the ACE2 Nt proximal region is necessary for
736 SARS2-RBD binding/internalization and both ACE2 Nt proximal and distal regions are
737 necessary for OM.BA.1 and BA.2-RBDs; Neither region is necessary for NL63-RBD
738 binding/internalization. SARS2-, SARS1-, RaTG13- and NL63-ACE2 crystal structures map
739 residues to two additional Internal regions of ACE2: residues 321-326 (PNMTQG); 330 (N) and

740 353-356 (KGDF), with NL63 contacting all these residues, with SARS2, SARS1 and RaTG13
741 contacting different subsets (**Figure 11A**). All four of these RBDs contact ACE2 conserved
742 residues K353 and G354 (**Figure 11A**). G354 contact is not likely as important as the D355
743 contacts found in three RBDs (*not* SARS1). NL63-RBD being unaffected by the
744 Pus8AA+LMY→A mutant nor mACE2 1-357 suggests that this Internal region is key to
745 triggering binding and internalization of all RBDs. It was previously shown that ACE2 mutants
746 K353A and D353A nearly abolish all SARS and NL63 infections (48, 60, 61). Several alanine
747 substitutions tested this region for interfering with SARS2 or NL63 binding/internalization:
748 quadruple mutant-N330A, K353A, G354A, D355A, the double mutant-K353A and D355A, and
749 individual mutations in K353A and D355A (**Figure 11A**). The NKGD→A and KD→A mutants
750 blocked both SARS2 and NL63-RBD binding and internalization (**Figures 11A-D, S15E-E'',**
751 **S15F-F''**). But the individual K353A and D355A mutations had no effect (**Figure 11A**). The
752 internal region mutants point to a common binding site on ACE2 that all RBDs utilize for
753 binding/internalization.
754
755 Crystal studies of RBD with ACE2 suggest K353-G354-D355 in ACE2 interacts predominantly
756 with T500 and G502 in the SARS2-RBD, a region distinct from the Loop 4 region (1, 28). G502,
757 P507, and R509 all represented immutable residues from DMS studies suggesting they could all
758 be key residues for ACE2 interaction. Co-transfections were carried out for this region of
759 SARS2-RBD: T500A, G502A, P507A, P509A and T500A, G502A double mutant (**Figures 11E,**
760 **S14H'-H'' through S14L-L''**). Only the double mutant T500A, G502A was able to completely
761 abolish ACE2 binding (**Figures S14J-J''**). These data argue that two regions of SARS2-RBD
762 work together to coordinate binding with ACE2: T500 and G502 coordinate the internal region
763 of ACE2 while Y489 and the Loop 4 disulfide bond (C480-C488) coordinate the Nt distal and
764 proximal residues. Perhaps the effect of these mutations is not universal across variants as the
765 Y489A mutation in OM.BA.1 disrupted membrane trafficking, likely due to a disruption in RBD
766 folding (**Figure 11E**). The *DPF assay* was once again utilized to compare and quantify these
767 three types of mutations in the SARS2, XBB.1.5 and OM.BA.1 RBDs (**Figures 11F, F', S14E-**
768 **E', S14F-F'**); Both C480A, C488A (3.04±1.04) and T500A, G502A (7.87±4.80) disrupted
769 binding/internalization (double positives) of ACE2 across all variants (**Figures 11E, 11F-F'**).
770 The sum of all RBD mutations produced suggest binding is localized to a stretch of residues
771 between Y489-G502, which is also where blocking antibodies target (28).
772
773 *Can RBD binding to ACE2 be antagonized by KGD containing peptides?*
774

775 A common binding site on ACE2 for both NL63 and SARS2-RBDs suggested that a competitive
776 antagonist based on the Internal region 2 amino acid sequence could be derived. Six peptides
777 were generated and tested for functional antagonism in the solution binding assay at micromolar
778 concentrations (**Figure S16A**). None of the peptides interfered with RBD-ACE2 binding for both
779 NL63 and SARS2-RBDs. However, one of the peptides (GKGD) caused red fluorescence of
780 ACE2-Cherry cells to surround SARS2-RBD expressing cells (**Figure S16A**). Because the
781 tripeptide Lys-Gly-Asp (KGD) is like the high affinity Arg-Gly-Asp (RGD) tripeptide for
782 fibronectin (49), two RGD containing peptides for blocking activity were also tested at
783 micromolar concentrations, but neither had any impact. Next, the GKGD peptide alone was
784 tested in the *DPF assay* with a preincubation of 100μM GKGD peptide, followed by flow
785 cytometry analysis for both SARS2 and NL63-RBDs (**Figures S16B-B'**); Again, no mitigation

786 of SARS2-ACE2 binding was observed. Finally, purified His-tagged SARS2-RBD (60ng, ~250
787 residues) was added to ACE2 cells with or without preincubation with 49µg of the 4-residue
788 GKDG peptide in the *DPF assay*; Despite a ~50,000x molar excess of peptide, no decrease in
789 RBD binding was observed (**Figures S16C-C''**). Higher than 100µM peptide concentrations
790 were not tested due to rampant nonspecific effects at mM presentation of compounds. Taken
791 together, these data suggest that small KGD-containing peptides do not bind RBDs with
792 sufficient affinity to block ACE2 binding.
793
794
795 **Discussion:**
796
797 **RBD Mutants**
798 *Spike S1 subunit-RBD interactions with ACE2 are critical for cellular internalization*
799
800 Respiratory coronaviruses like SARS1, SARS2 and NL63 utilize their spike protein to bind to
801 ACE2 on the surface of cells that line the respiratory epithelium(44, 60). Mapping studies from
802 SARS1 identified the minimum protein sequence necessary to bind to ACE2, a 193 amino acid
803 region-the receptor binding domain (RBD), which is also found in SARS2 (1, 23, 41). Binding
804 studies with SARS1 and SARS2 RBDs show roughly the same high affinity binding to ACE2,
805 which does not correlate to viral transmission rates (62, 63). One of the key differences in viral
806 transmission rates is the addition of 12 nucleotides within the Spike protein, creating a four-
807 amino acid RRAR-furin cleavage target after residue 684, allowing for pre-activation(64, 65),
808 splitting the protein into an Nt-S1 and Ct-S2 subunits (66). The liberation of residues 1-684 (S1),
809 containing the RBD from 333-529, likely provides easier access for binding to ACE2 and for
810 TMPRSS2 to cleave at the S2 subunit and reveal the S2' Fusion Peptide (67). It is thought that
811 the RBD association with ACE2 allows proximity access to the plasma membrane located
812 TMPRSS2; The S2' Fusion Peptide subsequently drives membrane fusion events for SARS1,
813 SARS2 and NL63. The work here suggests that the RBD association with ACE2 may also take
814 part in the viral transmission and/or internalization process. In this regard the natural propensity
815 of ACE2 to be internalize makes it an attractive target for coronaviruses but is unlikely the only
816 target as RpYN06 which does not bind ACE2, must be internalized by a distinct membrane
817 target.
818
819 *Binding efficiencies and homologies between RBD across species.*
820
821 There are 9 betacoronavirus and 1 alphacoronavirus with measured Kd of binding between RBD
822 and human ACE2. SARS1 and SARS2 have been measured at 58nM and 16nM respectively(62).
823 High affinity is a trademark of most of these coronaviruses except for RaTG13 and RsYN04,
824 which bind in the micromolar range (26, 45). The only alpha coronavirus that binds to ACE2,
825 does so at 17nM (48), nearly identical to that of the SARS2 RBD. H-CoV-NL63 is a common
826 human "cold virus" and has not caused a worldwide pandemic, which again argues that affinity
827 by itself does not correlate with virulence (68). SARS1& SARS2-RBDs completely lack
828 substantial NL63-RBD amino acid homology or common tertiary structures but co-crystal
829 studies with ACE2 reveal similar contact sites within its Nt and Internal regions (27). This
830 convergence on ACE2 contacts suggests that only certain regions can provide high affinity

interactions and/or mediate its internalization, both of which may be critical to viral transmission.

An in vitro RBD-ACE2 binding assay.

It has recently been shown that SARS2 infection of the olfactory system is a critical step for infection to prosper (69). These results argue that propagation of the preliminary infection allows for both asymptomatic dissemination of the SARS2 virus as well as symptomatic consequences of deeper respiratory infections within ACE2/TMPRSS2 expressing cells that line the respiratory tract. If a compound can be identified to block the SARS2-Spike S1 subunit binding to ACE2 in the olfactory epithelium, then it stands to reason viral transmission rates could be reduced. The in vitro system set up here robustly traffics RBD domains and ACE2 to the plasma membrane. The filopodia that exhibit RBD-β2AR-GFP fluorescence are 1μm or less, which is like the average size of a betacoronavirus particle, 0.1 μm (70-72). Thus, filopodial membrane interactions with the plasma membrane (PM) of the ACE2-Cherry expressing cells may show similarities to interactions between viruses that infect new cells. A 1000-fold range of RBDs with published affinities were tested, yet no differences were observed in the assay, consistent with pseudotype virus assays (53-55). Overall, the in vitro assay may represent a higher throughput strategy to study the molecular details of RBD binding to ACE2.

ACE2-Cherry protein relocalizes upon binding to RBD-β2AR

The RBD portion of spike proteins function by bringing its respective coronavirus to the PM where enzymes like TMPRSS2 cleave the spike protein liberating a S2 Fusion Peptide whose function is to fuse viral and cellular membranes and enable endosome-independent entry (66). One of the surprising findings here is that ACE2 by itself promotes internalization of RBD tethered to β2AR. In addition, rapid loss of ACE2-Cherry fluorescence at the PM (<10min) without formation of red/green doublet cells (**Figures 2D'**) suggests that reversable RBD binding is sufficient to trigger ACE2-Cherry loss. The mechanism of ACE2-Cherry loss is not known, but targeted degradation seems likely as other membrane localized proteins are not being lost (**Figures 3, S4**). It has been published that the SARS2 S protein also causes the loss of ACE2 expression in HEK-293A cells over the course of several hours and that this process can be reduced by the lysosomal inhibitor BafA1. Here I show membrane levels of ACE2-Cherry in OP6 cells over the 90minute interaction period with SARS2-RBD are still reduced (**Figure 3F'**), but the number of double positive cells did increase suggesting that ACE2 proteins were perhaps more stabilized at the membrane (**Figure 3F**). In this context, NL63-RBD double positives also increased, but just below statistical significance (**Data File S2**).

Meta-Analysis and mutational analysis of RBD reveal critical residues around disulfide Loop 4

The realization of a functional RBD-ACE2 interaction assay led to a meta-analysis of RBD mutations that were either derived from natural selection during infection (Variants) or DMS analysis by two laboratories (25, 41). Variants typically contain two or more mutations. By contrast DMS mutations are single substitutions of all 19 amino acids at each of the 197 residues of RBD, leading to an analysis of nearly 4000 mutants. DMS shows the distributed nature of RBD binding to ACE2. The mapped SARS2-RBM with ACE2 constitutes a 74 amino acid

877 region of which DMS meta-analysis suggests 7 of these residues (R454, C480, N487, C488,
878 G502, P507, R509) to be necessary for binding to ACE2. Six of these residues are predicted to
879 have critical roles in the RBD double beta barrel configuration: Positively charged residues R454
880 and R509 likely connect to D667 and D442, respectively and neither are predicted to bind ACE2;
881 residues C480 and C488 form the Loop 4 disulfide bond; and finally alpha helical breaking
882 residues G502 and P507 that likely promote formation of the R509-D442 bridge. This leaves
883 only N487 that would be necessary for binding and indeed is predicted to make contacts with
884 both ACE2 Nt proximal and distal residues Q24 and Y83, respectively. But the N487A mutation
885 in RBD and both Q24A and Y83A mutations in ACE2 also did not affect binding or
886 internalization. Thus, none of these 7 residues would appear to confer the specificity of RBD-
887 ACE2 binding.
888
889 Two additional analyses were performed looking at the most abundant mutations at multiple
890 positions in the RBD in years 2020 (HiF2020-3 residues) and 2021 (HiF2021-7residues).
891 Alanine mutants at all seven positions K417, N439, L452, S477, T478, E484, and N501 had no
892 effect on the binding or internalization of ACE2. A second set of seven alanine substitutions of
893 in silico predicted binding sites (P.B.S.): K417A, G446A, L455A, F486A, Q493A, Q498A,
894 N501A. This P.B.S. 7Ala-RBD mutant did block binding and internalization. Two of these
895 residues, L455 and F486 are not mutated in OM.BA.1, suggesting that one or both may be
896 critical for binding. Reversion of residue 486 to phenylalanine in the P.B.S. 6Ala-RBD mutant
897 did indeed rescue RBD binding and internalization by ACE2. But the F486A mutation alone in
898 RBD and corresponding mutations in ACE2 at M82A and Y83A did not abolish binding and
899 internalization. Thus, the totality of these alanine mutations, like the meta-analysis of the DMS,
900 point to a distributed binding between RBD and ACE2.
901
902 A distributed nature of RBD binding seems antithetical to Kds with nanomolar affinities. DMS
903 analyses of binding max studies reveal several residues G447, N448, Y449, N487, and Y489 that
904 are critical for binding with Y489 being the most critical (43), yet Y449A, N487A did not affect
905 binding and internalization; Y489A did prove critical. Juxtaposed to Y489 is the Loop 4
906 disulfide bond C480-C488 that is absent in the RBD RpYN06 and does not bind to ACE2(45). A
907 logical conclusion is that Loop 4 may be critically important for RBD binding or "attachment" to
908 the Nt of ACE2. All Loop 4 residues between C480 to C488 were substituted with SARS1 and
909 RaTG13 as well as single alanine substitutions between F486 and L492. From all these swaps it
910 did not appear that any one residue was key to the functionality of Loop 4, but rather supported
911 the idea that formation of Loop 4 itself is critical. By contrast, blocking the formation of Loop 4
912 with the double alanine substitution of C480 and C488 prevented internalization of RBD by
913 ACE2-expressing cells. Despite this result, it is not possible for Y489 alone to confer non-
914 covalent high affinity binding to ACE2. Perhaps the disulfide Loop 4 is an anchor onto the Nt of
915 ACE2 that was not observed by the crystallographic studies (1). Finally, DMS mutations (25,
916 41) would have predicted that N487A to be as debilitating as Y489A, which was not observed.
917 Overall, the mutagenesis and meta-analysis failed to identify a contiguous stretch of a few
918 residues that would bind ACE2.
919
920 The alphacoronavirus NL63 RBD has a completely different primary sequence and folding
921 compared to RBDs of RaTG13, SARS1, and SARS2 as well as its RBM region is split over three
922 surfaces, yet all binds similar regions on ACE2. But the amino acid identity is limited to just

923 eleven residues with four of them surrounding the SARS2 Loop 4 region: C488, F490, P491 and
924 L492 (C577, F579, P580, L581 in NL63); This region of NL63 RBD is not implicated in any
925 RBM, but a N578Y mutation a generates a five amino acid match to SARS2 from C488-L492
926 and improves the NL63 RBD binding Kd 2-fold. In addition, the NL63 C577 residue is part of
927 disulfide Loop 3 (**See Figure S6**). Taken together, the residues surrounding the disulfide Loop 4
928 in SARS2 is likely one of the critical regions for RBD interaction with ACE2. It is also possible
929 that Loop 4 (Loop 3 in NL63) serves no "binding" but rather as a hook onto the ACE2 amino
930 terminus where it interacts. As such, neither SARS2-Y489W-RBD nor SARS2-Y489H-RBD
931 mutations disrupted binding and internalization with ACE2 despite Histidine's remarkably
932 different properties as a charged polar group. These results suggest that the effect of Y489A is
933 not a change in the direct interaction between it and ACE2, but perhaps a more subtle change to
934 the Loop 4 positioning relative to the ACE2 amino terminus. The Y489A-OM.BA.1-RBD
935 mutation disrupts PM trafficking, which may result from a failure to form the disulfide bridge
936 C480-C488 like results for C488A-RBD.
937
938 *Could odors act to mitigate SARS-CoV-2 binding?*
939
940 The initial drive to study RBD/ACE2 interactions was to identify an odor that could mitigate
941 infections. But none of the 36 odor mixtures from the "Le Nez du Café" were able to mitigate
942 formation of RBD/ACE2 double positive cells nor reduction of ACE2 expression levels. A more
943 directed approach could focus on the complete set of 4000 "relevant" odors for humans
944 (https://ifrafragrance.org/priorities/ingredients/ifra-transparency-list) or the 230 Key Food Odors,
945 and 800 common human odors (http://www.flavornet.org) that exist in everyday products. A
946 recent study suggested that Honeysuckle extract might mitigate infection (73).
947
948 A second approach would be to identify critical di or tri-peptide motifs for antagonism within the
949 197 residue RBD. But RBD mutagenesis did produce one tangible target: the disulfide bridge
950 between C480 and C488. It is shown here and at other laboratories that DTT and a more pH
951 stable version DTBA can mitigate RBD/ACE2 binding, albeit at high concentrations. Both
952 compounds are volatile and perceived as having a foul smell due to their thiol groups. These
953 odors could be masked by sweet-smelling odors. Additionally, there may be other odors that are
954 more volatile and capable of disrupting the disulfide linkage, which could represent another
955 solution to reduce rates of infections by an inhalation regimen. Like many chemotherapies, a
956 reducing agent lacks specificity and would damage other proteins but could have value in short-
957 term decreases in the viral load. Paxlovid is very good at reducing the SARS2 viral load despite
958 many unwanted side effects (74).
959
960 Vaccines provide IgG responses that can limit viral amplifications, but unfortunately, mucosal
961 protection (IgA) in the nasal epithelium wanes more quickly (75). Thus, most individuals are not
962 immune to infection and the subsequent viral amplification within the sustentacular cells that
963 carry ACE2 and TMPRSS2 expression. If inhibitors can block this initial viral insult (7), then
964 extent of disease would likely be mitigated as well.
965
966
967
968

969 **ACE2 Mutants**
970
971 *The disulfide Loop 4 region interacts with Nt proximal and distal regions of ACE2*
972
973 The importance of disulfide Loop 4 located residues F486, N487 and Y489 from RBD analysis,
974 would seem to correlate with the Nt region in ACE2 as critical for binding. RBD residues 486-
975 489 bridge Nt proximal region residues Q24, T27, F28 with Nt distal region residues L79, M82,
976 Y83 (LMY) (**See Figure 7B**). But ACE2 mutations (Group I) targeting these residues did not
977 affect RBD binding and internalization. Group II Nt Hybrids with *R. pusillus* sequences
978 abolished SARS2-RBD interactions, but not OM.BA.1. Combining Nt proximal *R. pusillus*
979 residues and Nt distal substitutions LMY→A did lead to a complete block in binding and
980 internalization by OM.BA.1-RBD. These results suggest that the 15 amino acid differences in
981 OM.BA.1-RBD lead to a new protein conformation, which is consistent with the absence of
982 Y489A protein trafficking in a OM.BA.1-RBD. At first approximation, these data argue that Nt
983 proximal and distal ACE2 regions are necessary for binding and internalization of SARS2 and
984 OM.BA.1-RBDs. But the Nt mACE 1-94 hybrid still providing binding and internalization,
985 suggest a lack of specificity.
986
987 *SARS-CoV-2 and H-CoV-NL63 both require common Internal ACE2 region for binding*
988
989 The NL63-RBD binding and internalization by ACE2 was unaffected by any of the 20 Group
990 I/II/III/IV Nt proximal or distal mutations. Those results are consistent with the co-crystals
991 showing only a few contacts by NL63-RBD in the Nt proximal and distal domains. By contrast,
992 NL63-RBD has extensive contacts in both Internal regions 1 and 2 whereas SARS2-RBD has
993 more of its contacts to Internal region 2. Previously, it was shown that K353A had substantial
994 impact on both NL63 and SARS2-RBD binding in pseudovirus infections but did not abolish it.
995 Our co-plating and co-transfection assays also did not reveal complete blocks in binding and
996 internalization. While the single substitution D355A did not have an impact, the double mutant
997 KD→A abolished NL63 binding and blocked internalization of SARS2-RBD. The internal
998 region represents a second ACE2 site, when mutated, abolishes nanomolar SARS2-RBD
999 binding, consistent with the prediction that high affinity SARS2-RBD binding is distributed. The
1000 K353A, D355A double mutation is more proximal to the collectrin (neck) region (residues 616-
1001 742) of ACE2 involved in its dimerization (76). It will be interesting to determine if
1002 internalization of ACE2 is proceeded by RBDs binding to ACE2 dimers, which then reduces the
1003 affinity for the neck region dimers leading to ACE2 internalization. Such internalization is
1004 capable of pinching off membrane from neighboring cells with membrane-bound RBD proteins.
1005 Finally, post-translational modifications within the RBD such as asparagine deamidation in
1006 N405, N481 and N501 (77, 78) could alter binding to ACE2, however, OM.BA.1 and XBB.1.5
1007 have Y501 between the critical T500 and G502 residues involved in internal region 2 binding. It
1008 is worth noting that NL63-RBD interacts with K353 and D355 of ACE2 with a similar three-
1009 residue stretch, S535-P536-G537 (48) vs. T500-N501/Y501-G502, again suggesting a common
1010 interaction mechanism.
1011
1012 Based on the RBD mutants identified here, it appears the most critical RBD region for
1013 interaction with ACE2 may be further refined to a 23-residue region from C480 to G502, which
1014 encompasses the Loop 4 disulfide bond (C480-C488). It is noteworthy that this region represents

1015 the highest density of residue contacts specific to the m396 neutralizing antibody against SARS2
1016 (28, 79). The disruption of RBD variant binding with the double mutants C480A, C488A and
1017 T500A, G502A suggest this region remains critical for any new variant binding to ACE2. It is
1018 possible that a peptide inhibitor against this 23-residue stretch could be the basis of a competitive
1019 or allosteric inhibitors. Several SARS2-RBD and ACE2 peptide inhibitors have been
1020 successfully developed (80, 81) that can mitigate binding. With the emergence of new variants,
1021 some of these inhibitors will likely lose efficacy. Although none of our KGD or RGD containing
1022 peptides antagonized binding of RBDs, it remains possible that a cyclized or other derivative
1023 peptide could do so in the future (49).
1024
1025 It has been suggested that infections through other RBD receptors could negate the attempts to
1026 mitigate RBD-ACE2 interactions to control the spread of SARS2 (82-84). While this is true,
1027 ACE2 remains the entry protein for two distinct coronaviruses, suggesting it is the target protein
1028 that is best expressed on the target cells for viral propagation. It is worth noting that the early
1029 phase of SARS2 infections in the nasal epithelium target cells allow for viral amplification with
1030 minimal IgG response. The RGD/KGD motif on the SARS2 spike protein has also been
1031 implicated in binding to integrins and RGD/KGD binding sites on ACE2 may be competing for
1032 co-receptor usage (85-87). Both possibilities underscore the complexities in the SARS2 infection
1033 process. Disrupting RBD binding in the nasal epithelium would mitigate all these possible co-
1034 receptor interactions.
1035
1036 A model emerges (**See Figures 12, S17**) whereby the Internal region 2 on ACE2 may be
1037 critically important for stable RBD-ACE2 binding/internalizations but require secondary
1038 contacts for stabilization. In the case of NL63-RBD, those additional contacts are in the Internal
1039 region 1 and for SARS-RBDs, those additional contacts are in the Nt proximal and distal regions.
1040 It still may be possible to identify a high affinity agonist to RBD based on the NL63/SARS2
1041 target KGD motif in ACE2 that could mitigate binding. Finally, peptides against both the Nt and
1042 Internal region binding sites might work synergistically to inhibit the spread of SARS-CoV-2.
1043
1044
1045 *Implications:*
1046
1047 *ACE2 downregulation:* The rapid downregulation by a membrane-bound RBD independent of
1048 stable binding suggests that the efficiency of RBD binding and internalization might limit
1049 availability of ACE2 protein for future infections. It's unclear how many full-length Spike
1050 proteins that are membrane-bound exist on a virion. On the other hand, the S2-associated S1
1051 particle may mimic the membrane-bound RBD interactions observed. Thus, the loss of ACE2
1052 protein at the plasma membrane before S2 liberation of the Fusion Peptide, might lead to fewer
1053 viral particles that can infect target cells. We do not know the rate of *in vivo* ACE2
1054 internalization by RBD and its eventual replacement to the plasma membrane, but this could be
1055 studied in the future using mice expressing the human ACE2 protein and membrane-bound
1056 RBDs. Reduction in levels of ACE2 will likely affect the Renin-Angiotensin System by
1057 increasing Angiotensin II and over activating Angiotensin II receptor type 1 (AT1R), potentially
1058 leading to long-term physiological consequences such as Long Covid(30).
1059

1060 The binding assay shown here reveals properties of RBD distinct from other observations that
1061 show the SARS2 pseudotype virus causing ACE2 degradation (88-90). It seems plausible that
1062 vaccines using RBD domains capable of binding ACE2 may lead to unwanted side effects
1063 produced from downregulation of ACE2 in recipients, such as short or long-term alterations in
1064 the Renin-Angiotensin System (RAS)(91-93). In addition, a combination of an immune response
1065 to the antigen and alterations in RAS may also lead to unwanted side effects (94). In this regard,
1066 Pfizer produced several versions of RBD vaccines; if this hypothesis is true, then observed
1067 vaccine side effects may have similarities to some of the COVID-19 symptoms. Notably, the
1068 full-length Spike protein has fewer side effects than just the RBD alone (95, 96). It is worth
1069 exploring the possibility of fewer side effects with vaccines expressing RBD containing
1070 mutations such as Y489A, P.B.S. 7Ala, or double mutants C480A-C488A and T500A-G502A
1071 that reduce binding to ACE2. The latter two double mutants can work across three variants.
1072
1073 *Internal regions of ACE2:* The published NL63-RBD affinities to ACE2 are similar those of
1074 SARS2, but likely utilize internal regions of ACE2 as the key region for its binding and
1075 internalization. It is worth noting that NL63-RBD is more robust at reducing ACE2 fluorescence
1076 and **Figure 11A'**, which also suggests that the better a protein binds to the internal ACE2 region,
1077 the more robust its internalization. The changing nature of SARS2-RBD binding to ACE2 argues
1078 that variants could emerge that rely more on the ACE2 internal region for binding like NL63-
1079 RBD. It is unclear how COVID-19 disease progression would occur if ACE2 were to be more
1080 rapidly internalized.
1081
1082 A nanobody or peptide blocking strategy targeting the KGD region of ACE2 within the nasal
1083 epithelium could radically reduce the ability of SARS2-CoV-2 to infect sustentacular cells. Such
1084 a peptide might feature the consensus binding residues Ser/Thr-X-Gly found in all SARS2 and
1085 NL63 RBDs described here. Mitigating viral amplification in the nasal cavity will likely lead to
1086 reduced viral particles, fewer symptoms, and most importantly less asymptomatic spread, which
1087 could lead to an improved prognosis for the current and future pandemics.
1088
1089
1090 *Limitations of the study:*
1091
1092 The experiments described here are aimed at generating a simple in vitro system for the rapid
1093 characterizing the Spike protein-ACE2 interaction domain, specifically the receptor binding
1094 domain (RBD). I extend the findings by Starr et al and Chan et al, who performed structure-
1095 future relationships between RBD and ACE2 interactions. The focus on the RBD alone is partly
1096 because the full-length Spike protein is pre-cleaved, generating S1 and S2 fragments that remain
1097 noncovalently associated. There may be value in testing some of these mutations in the context
1098 of a pseudovirus. We could test a few mutations in the context of membrane-bound S1 Spike
1099 proteins, but the net result would likely be adding more steric hindrance to ACE2 binding as has
1100 been shown for furin-mutated Spike protein (64).
1101
1102 I was surprised that the addition of a transmembrane to RBD not only bound to ACE2-Cherry
1103 but also reduced fluorescence levels. Loss of ACE2-Cherry fluorescence was not dependent on a
1104 β2AR-GFP expressing cells as well. Finally, cell adhesion between differentially labeled CDH2
1105 molecules did not lead to loss of CDH2-Cherry. The observed correlation between the degree of

1106 fluorescence loss and the degree of RBD binding is decorrelated when XBB.1.5-RBD is used in
1107 the context of an ACE2-Cherry (Figure S3C), ACE2-Cherry (Pus8AA), or when exogenous
1108 RBD protein is added. The decorrelation between binding and loss of ACE2 fluorescence
1109 suggests that ACE2 may lose its fluorescence due to internalization, and this event is mediated
1110 by a disruption of its ability to dimerize.
1111
1112 Because RBDs from both SARS2 and NL63 differentially bind the same spectrum of residues on
1113 ACE2, it becomes unclear if these are the only residues necessary and sufficient for RBD
1114 internalization. In this regard, residues involved in ACE2 dimerization may indirectly affect loss
1115 of ACE2-Cherry fluorescence upon membrane-RBD binding.
1116
1117

1118 **Materials and Methods:**
1119
1120 **RBD and ACE2 constructs:** See details of DNA sequences in **Supplemental Data File S1**.
1121 D1794 (is the β2AR with an internal EcoR1 site added (does not alter residue) for rapid cloning
1122 of 5'ends. ACE2-Cherry (human ACE2 coding sequence with an internal EcoR1 site mutation
1123 (does not alter residues). RBD and ACE2 mutants made by gblocks (IDT) and sequenced after
1124 subcloning (see **Supplemental Data File S1**). SARS1 RBD from (23), SARS2 and RaTG13 are
1125 equivalent regions. NL63 RBD from NCBI. All RBD variants have been codon optimized.
1126
1127 hemagglutinin-cleavable signal sequence: (MKTIIALSYIFCLVFA) was initially used to test
1128 secreted version (25). All membrane tethered Nt RBD constructs used nicotinic receptor α7
1129 subunit signal peptide: (MGLRALMLWLLAATGLVRESLQGEFQRKLYPVATM) (32, 33).
1130
1131 **Cell culture and Imaging:**
1132 Mouse olfactory placode cells [OP6 (97), a gift from Jane Roskams], were maintained as
1133 previously described in Dulbecco's modified Eagle's medium (DMEM 1X Gibco) supplemented
1134 with 10% fetal bovine serum (FBS Gibco) and 1% penicillin/streptomycin (Pen Strep Millipore)
1135 at 33°C. I transiently transfected plasmid DNA constructs using the Amaxa Nucleofector
1136 (Lonza) with PBS at 60%-70% confluency according to the manufacturer's protocol. Transfected
1137 cells were allowed to recover for 16-18 hours at 33°C and express the plasmid DNA before
1138 imaging.
1139
1140 I have previously characterized β2AR and odorant receptor fluorescent protein fusions (20-22).
1141 Cells grown at 33°C and imaged 16hrs post-transfection. Typically, 15ug of DNA was
1142 electroporated (EPd) into 0.5 million OP6 cells. Imaging performed LSM510 confocal
1143 microscope or Spinning Disk microscope as previously performed (20).
1144
1145 Electroporation of 0.5 million OP6 cells with ACE2 plasmid (Cherry) is plated and grown
1146 overnight, and expression was typically found in 1-5% of cells. Electroporation of 0.5 million
1147 OP6 cells with an RBD or other plasmids are plated and grown overnight. Expression of these
1148 plasmids was typically 2-4 fold better than the ACE2 containing plasmids.
1149
1150 **Analysis of flow cytometry values:**
1151 Trypsinized and analyzed 100K-250K DAPI (live cells). Green, Red and Green&Red cells.
1152 Fluorescent counts acquired. Total green fluorescent cells = (Green&Red Cells + Green cells)
1153 divided by DAPI total. Normalize total green cells are based on the experimental control counts.
1154 Total red cells= (Red&Green cells + Red cells) divided by DAPI total. Normalized total Red
1155 cells are based on the experiment controls for each experiment. Total Red&Green cells were
1156 obtained by gating and dividing by Green Cell value and normalized by controls within an
1157 experiment, then multiplied by Normalized Green Value.
1158
1159
1160 **RBD/ACE2 Interaction analysis:**
1161 • **In vitro co-plate binding assay**: RBD and ACE2 DNA constructs were separately EPd into
1162 OP6 cells, seeded (co-plated) onto the same 30cm^2 dishes, and imaged after 16hrs.

1163 Internalization of green fluorescence by red cells was obvious whether green cells were in
1164 proximity. When internalization was not observed, then images were captured for at least 3
1165 cells where Green/Red cells are touching**.**

1166 • **In vitro co-EP assay:** 10ug of RBD and 10ug of ACE2 DNA constructs were Co-EPd into
1167 OP6 cells, seeded onto 30cm^2 dishes, and imaged after 1µ6hrs. At least 3 coexpressing cells
1168 were imaged for each.

1169 • **Dissociation-Plate-Flow cytometry (*DPF*) assay:** 15ug of RBD and 15ug of ACE2 DNA
1170 constructs were separately EPd into OP6 cells and seeded onto different 30cm^2 dishes. RBD
1171 cells were trypsinized and seeded for the desired time onto the 16hrs grown ACE2-
1172 expressing cells in 30cm^2 dishes, then trypsinized, spun down, resuspended, filtered and
1173 counted by flow cytometer.

1174 • **In solution binding assay:** 15ug of RBD and 15ug of ACE2 DNA constructs were
1175 separately EPd into OP6 cells and seeded onto different 30cm^2 dishes. Both RBD cells and
1176 ACE2-expressing cells were trypsinized, spun down, resuspended in 300µl of media. 50µl of
1177 each population were mixed into an Eppendorf tube and put in a 37°C water bath for 10min
1178 to 1hr. A 10µl aliquot was pipetted onto coverslip and imaged. Images were taken such that
1179 many cells were in the field of view. If doublets formed, then it was apparent throughout the
1180 field of view.

1181

1182 Flow cytometry and FACS were performed using a Becton Dickinson Aria II equipped with 5
1183 lasers (BD bioscience). Gates were drawn as determined by negative controls to separate
1184 positive and negative populations for each florescent protein. Typically, 300,000 events (yielding
1185 about 250,000 DAPI positive cells) were recorded for each flow cytometry analysis, and the data
1186 was analyzed using BD FACSDiva 9.0.1. Calculations and graphs were made in GraphPad
1187 Prism. Mean and standard deviations were derived in Excel. See **Supplemental Data File S2** for
1188 details.

1189

1190 **Peptides and antibodies**

1191 Peptides synthesized from GenScript. RGD purchased from R&D systems, #7723/10mg.
1192 Cilengitide purchased from Tocris, #5870.

1193

1194 His Tag Alexa Fluor 488-conjugated Antibody Catalog #: IC050G from R&D systems.
1195 2019-nCoV RBD, His tag Cat#40592-V08H from SinoBiologicals

1196

1197 **Live-imaging**

1198 OP6 cells transfected with RBD and/or ACE2 constructs imaged on a Zeiss LSM 510
1199 microscope using a Zeiss Plan-APO 25X water immersion objective in culture media for Figures
1200 1, 2, 3, 6, S1, S4, S9 and S10. GFP/Venus expressing cells excited at 488- collected at BP500-
1201 545 and Cherry expressing cells at 561 nm-collected at LP575 nm. All images were acquired
1202 using the multitracking feature.

1203

1204 **Logo plots and space filling model of ACE2**

1205 https://weblogo.berkeley.edu/logo.cgi used to generate Logo plots in Figures 7, 11.

1206

1207 Modifications of space filling model of ACE2 structure from Wu et al, 2020 (pdb_00006m0j)
1208 used to generate Figures 12 and S17.

β2AR antagonist:
CellAura fluorescent $\beta_2$antagonist [(±)-propranolol]**,** HB7820 from Hello Bio
https://www.hellobio.com/cellaura-fluorescent-beta2-antagonist-propranolol.html?q=7820 (98).

His Tag Alexa Fluor® 488-conjugated Antibody Catalog #: IC050G from R&D systems.
2019-nCoV RBD, His tag Cat#40592-V08H from SinoBiologicals

Odors:
Le Nez du Café Revelation Kit Odors-36 Scent concentrations from Expresso Parts.

Acknowledgements:

Special thanks to Masayo Omura for providing logistical and intellectual support that helped drive the success of these experiments. Many thanks to Masayo Omura, Ivan Rodriguez, Sergio Bernal-Garcia, and Thomas Bozza for advice on the experimental design and interpretation of results; Mary Slavinsky and Masayo Omura for technical support in plasmid production; Livia Johnson and Diana Bratu for advice on utilizing the spinning disk microscope; and Sergio Bernal -Garcia for help with GraphPad Prism and Fiji. Thanks to Ivan Rodriguez, Vincent Racaniello, Masayo Omura, and Sergio Bernal Garcia for providing feedback on the manuscript. Tomas Baumgartner Manager, Flow Cytometry Core Facility, Weill Cornell Medicine for support on flow cytometry of single cells. GISAID (http://cov-glue-viz.cvr.gla.ac.uk/mutations.php) for SARS-CoV2 database. Many thanks to Delia Tomoiaga, Claude Rose Levine, and Mark Levine for supporting my efforts to design novel experiments that might help tackle the pandemic of our lifetime. This work was supported by Hunter College and NIH grants# NIH R01 NS091439-01 and NIH R01 DC020764-01.

All data generated are found in the supplementary files of this manuscript.

References:

1. Wang Q, Zhang Y, Wu L, Niu S, Song C, Zhang Z, Lu G, Qiao C, Hu Y, Yuen KY, Wang Q, Zhou H, Yan J, Qi J. Structural and Functional Basis of SARS-CoV-2 Entry by Using Human ACE2. Cell. 2020;181(4):894-904 e9. Epub 2020/04/11. doi: 10.1016/j.cell.2020.03.045. PubMed PMID: 32275855; PMCID: PMC7144619.
2. Perlman KMaS. Coronaviruses, Including Severe Acute Respiratory Syndrome (SARS) and Middle East Respiratory Syndrome (MERS)
. Mandell, Douglas, and Bennett's Principles and Practice of Infectious Diseases 2015
. 2015(Chapter 157):1928–36.e2. Epub 2014 Oct 31. doi: 10.1016/B978-1-4557-4801-3.00157-0
; PMCID: PMC7151770.
3. Borah P, Deb PK, Al-Shar'i NA, Dahabiyeh LA, Venugopala KN, Singh V, Shinu P, Hussain S, Deka S, Chandrasekaran B, Jaradat DMM. Perspectives on RNA Vaccine Candidates for COVID-19. Front Mol Biosci. 2021;8:635245. Epub 2021/04/20. doi: 10.3389/fmolb.2021.635245. PubMed PMID: 33869282; PMCID: PMC8044912.

4. Park JW, Lagniton PNP, Liu Y, Xu RH. mRNA vaccines for COVID-19: what, why and how. Int J Biol Sci. 2021;17(6):1446-60. Epub 2021/04/29. doi: 10.7150/ijbs.59233. PubMed PMID: 33907508; PMCID: PMC8071766.
5. Drozdzal S, Rosik J, Lechowicz K, Machaj F, Szostak B, Przybycinski J, Lorzadeh S, Kotfis K, Ghavami S, Los MJ. An update on drugs with therapeutic potential for SARS-CoV-2 (COVID-19) treatment. Drug Resist Updat. 2021;59:100794. Epub 2022/01/08. doi: 10.1016/j.drup.2021.100794. PubMed PMID: 34991982; PMCID: PMC8654464.
6. Killingley B, Mann AJ, Kalinova M, Boyers A, Goonawardane N, Zhou J, Lindsell K, Hare SS, Brown J, Frise R, Smith E, Hopkins C, Noulin N, Londt B, Wilkinson T, Harden S, McShane H, Baillet M, Gilbert A, Jacobs M, Charman C, Mande P, Nguyen-Van-Tam JS, Semple MG, Read RC, Ferguson NM, Openshaw PJ, Rapeport G, Barclay WS, Catchpole AP, Chiu C. Safety, tolerability and viral kinetics during SARS-CoV-2 human challenge in young adults. Nat Med. 2022;28(5):1031-41. Epub 2022/04/02. doi: 10.1038/s41591-022-01780-9. PubMed PMID: 35361992.
7. Shapira T, Monreal IA, Dion SP, Buchholz DW, Imbiakha B, Olmstead AD, Jager M, Desilets A, Gao G, Martins M, Vandal T, Thompson CAH, Chin A, Rees WD, Steiner T, Nabi IR, Marsault E, Sahler J, Diel DG, Van de Walle GR, August A, Whittaker GR, Boudreault PL, Leduc R, Aguilar HC, Jean F. A TMPRSS2 inhibitor acts as a pan-SARS-CoV-2 prophylactic and therapeutic. Nature. 2022;605(7909):340-8. Epub 2022/03/29. doi: 10.1038/s41586-022-04661-w. PubMed PMID: 35344983; PMCID: PMC9095466 US10988505B2) that cover matriptase and other type II transmembrane serine proteases inhibitors for treating and preventing viral infections, respiratory disorders, inflammatory disorders, pain disorders, tissue disorders, hyperproliferative disorders, and disorders associated with iron overload. The remaining authors declare that they have no competing interests.
8. Hoffmann M, Kleine-Weber H, Schroeder S, Kruger N, Herrler T, Erichsen S, Schiergens TS, Herrler G, Wu NH, Nitsche A, Muller MA, Drosten C, Pohlmann S. SARS-CoV-2 Cell Entry Depends on ACE2 and TMPRSS2 and Is Blocked by a Clinically Proven Protease Inhibitor. Cell. 2020;181(2):271-80 e8. Epub 2020/03/07. doi: 10.1016/j.cell.2020.02.052. PubMed PMID: 32142651; PMCID: PMC7102627.
9. Han DP, Penn-Nicholson A, Cho MW. Identification of critical determinants on ACE2 for SARS-CoV entry and development of a potent entry inhibitor. Virology. 2006;350(1):15-25. Epub 2006/03/03. doi: 10.1016/j.virol.2006.01.029. PubMed PMID: 16510163; PMCID: PMC7111894.
10. Hashemian SMR, Sheida A, Taghizadieh M, Memar MY, Hamblin MR, Bannazadeh Baghi H, Sadri Nahand J, Asemi Z, Mirzaei H. Paxlovid (Nirmatrelvir/Ritonavir): A new approach to Covid-19 therapy? Biomed Pharmacother. 2023;162:114367. Epub 2023/04/06. doi: 10.1016/j.biopha.2023.114367. PubMed PMID: 37018987; PMCID: PMC9899776.
11. Jonsdottir HR, Dijkman R. Coronaviruses and the human airway: a universal system for virus-host interaction studies. Virol J. 2016;13:24. Epub 2016/02/08. doi: 10.1186/s12985-016-0479-5. PubMed PMID: 26852031; PMCID: PMC4744394.
12. Leon Fodoulian JT, Daniel Rossier, Madlaina Boillat, Chenda Kan, Véronique Pauli, Kristof Egervari, Johannes A. Lobrinus, Basile N. Landis, Alan Carleton, Ivan Rodriguez. SARS-CoV-2 receptor and entry genes are expressed by sustentacular cells in the human olfactory neuroepithelium. bioRxiv 20200331013268; doi: https://doiorg/101101/20200331013268. 2020.

1299 13. David H. Brann TT, Caleb Weinreb, Marcela Lipovsek, Koen Van den Berge, Boying
1300 Gong, Rebecca Chance, Iain C. Macaulay, Hsin-jung Chou, Russell Fletcher, Diya Das, Kelly
1301 Street, Hector Roux de Bezieux, Yoon-Gi Choi, Davide Risso, Sandrine Dudoit, Elizabeth
1302 Purdom, Jonathan S. Mill, Ralph Abi Hachem, Hiroaki Matsunami, Darren W. Logan, Bradley J.
1303 Goldstein, Matthew S. Grubb, John Ngai, Sandeep Robert Datta. Non-neuronal expression of
1304 SARS-CoV-2 entry genes in the olfactory system suggests mechanisms underlying COVID-19-
1305 associated anosmia. bioRxiv 20200325009084; doi: https://doiorg/101101/20200325009084.
1306 2020.
1307 14. Iwata-Yoshikawa N, Kakizaki M, Shiwa-Sudo N, Okura T, Tahara M, Fukushi S, Maeda
1308 K, Kawase M, Asanuma H, Tomita Y, Takayama I, Matsuyama S, Shirato K, Suzuki T, Nagata
1309 N, Takeda M. Essential role of TMPRSS2 in SARS-CoV-2 infection in murine airways. Nat
1310 Commun. 2022;13(1):6100. Epub 2022/10/16. doi: 10.1038/s41467-022-33911-8. PubMed
1311 PMID: 36243815; PMCID: PMC9568946.
1312 15. Beaudoin CA, Pandurangan AP, Kim SY, Hamaia SW, Huang CL, Blundell TL, Vedithi
1313 SC, Jackson AP. In silico analysis of mutations near S1/S2 cleavage site in SARS-CoV-2 spike
1314 protein reveals increased propensity of glycosylation in Omicron strain. J Med Virol.
1315 2022;94(9):4181-92. Epub 2022/05/17. doi: 10.1002/jmv.27845. PubMed PMID: 35575289;
1316 PMCID: PMC9348480.
1317 16. Koch J, Uckeley ZM, Doldan P, Stanifer M, Boulant S, Lozach PY. TMPRSS2
1318 expression dictates the entry route used by SARS-CoV-2 to infect host cells. Embo J.
1319 2021;40(16):e107821. Epub 2021/06/24. doi: 10.15252/embj.2021107821. PubMed PMID:
1320 34159616; PMCID: PMC8365257.
1321 17. Brann DH, Tsukahara T, Weinreb C, Lipovsek M, Van den Berge K, Gong B, Chance R,
1322 Macaulay IC, Chou HJ, Fletcher RB, Das D, Street K, de Bezieux HR, Choi YG, Risso D,
1323 Dudoit S, Purdom E, Mill J, Hachem RA, Matsunami H, Logan DW, Goldstein BJ, Grubb MS,
1324 Ngai J, Datta SR. Non-neuronal expression of SARS-CoV-2 entry genes in the olfactory system
1325 suggests mechanisms underlying COVID-19-associated anosmia. Sci Adv. 2020;6(31). Epub
1326 2020/09/17. doi: 10.1126/sciadv.abc5801. PubMed PMID: 32937591.
1327 18. Fodoulian L, Tuberosa J, Rossier D, Boillat M, Kan C, Pauli V, Egervari K, Lobrinus JA,
1328 Landis BN, Carleton A, Rodriguez I. SARS-CoV-2 Receptors and Entry Genes Are Expressed in
1329 the Human Olfactory Neuroepithelium and Brain. iScience. 2020;23(12):101839. Epub
1330 2020/12/01. doi: 10.1016/j.isci.2020.101839. PubMed PMID: 33251489; PMCID:
1331 PMC7685946.
1332 19. Zazhytska M, Kodra A, Hoagland DA, Frere J, Fullard JF, Shayya H, McArthur NG,
1333 Moeller R, Uhl S, Omer AD, Gottesman ME, Firestein S, Gong Q, Canoll PD, Goldman JE,
1334 Roussos P, tenOever BR, Jonathan BO, Lomvardas S. Non-cell-autonomous disruption of
1335 nuclear architecture as a potential cause of COVID-19-induced anosmia. Cell.
1336 2022;185(6):1052-64 e12. Epub 2022/02/19. doi: 10.1016/j.cell.2022.01.024. PubMed PMID:
1337 35180380; PMCID: PMC8808699.
1338 20. Bubnell J, Pfister P, Sapar ML, Rogers ME, Feinstein P. beta2 adrenergic receptor
1339 fluorescent protein fusions traffic to the plasma membrane and retain functionality. PLoS One.
1340 2013;8(9):e74941. Epub 2013/10/03. doi: 10.1371/journal.pone.0074941. PubMed PMID:
1341 24086401; PMCID: PMC3781101.
1342 21. Bubnell J, Jamet S, Tomoiaga D, D'Hulst C, Krampis K, Feinstein P. In Vitro Mutational
1343 and Bioinformatics Analysis of the M71 Odorant Receptor and Its Superfamily. PLoS One.

2015;10(10):e0141712. Epub 2015/10/30. doi: 10.1371/journal.pone.0141712. PubMed PMID: 26513476; PMCID: PMC4626375.
22. Jamet S, Bubnell J, Pfister P, Tomoiaga D, Rogers ME, Feinstein P. In Vitro Mutational Analysis of the beta2 Adrenergic Receptor, an In Vivo Surrogate Odorant Receptor. PLoS One. 2015;10(10):e0141696. Epub 2015/10/30. doi: 10.1371/journal.pone.0141696. PubMed PMID: 26513247; PMCID: PMC4626089.
23. Wong SK, Li W, Moore MJ, Choe H, Farzan M. A 193-amino acid fragment of the SARS coronavirus S protein efficiently binds angiotensin-converting enzyme 2. J Biol Chem. 2004;279(5):3197-201. Epub 2003/12/13. doi: 10.1074/jbc.C300520200. PubMed PMID: 14670965; PMCID: PMC7982343.
24. Towler P, Staker B, Prasad SG, Menon S, Tang J, Parsons T, Ryan D, Fisher M, Williams D, Dales NA, Patane MA, Pantoliano MW. ACE2 X-ray structures reveal a large hinge-bending motion important for inhibitor binding and catalysis. J Biol Chem. 2004;279(17):17996-8007. Epub 2004/02/03. doi: 10.1074/jbc.M311191200. PubMed PMID: 14754895; PMCID: PMC7980034.
25. Chan KK, Dorosky D, Sharma P, Abbasi SA, Dye JM, Kranz DM, Herbert AS, Procko E. Engineering human ACE2 to optimize binding to the spike protein of SARS coronavirus 2. Science. 2020;369(6508):1261-5. Epub 2020/08/06. doi: 10.1126/science.abc0870. PubMed PMID: 32753553.
26. Liu K, Pan X, Li L, Yu F, Zheng A, Du P, Han P, Meng Y, Zhang Y, Wu L, Chen Q, Song C, Jia Y, Niu S, Lu D, Qiao C, Chen Z, Ma D, Ma X, Tan S, Zhao X, Qi J, Gao GF, Wang Q. Binding and molecular basis of the bat coronavirus RaTG13 virus to ACE2 in humans and other species. Cell. 2021;184(13):3438-51 e10. Epub 2021/06/18. doi: 10.1016/j.cell.2021.05.031. PubMed PMID: 34139177; PMCID: PMC8142884.
27. Wu K, Li W, Peng G, Li F. Crystal structure of NL63 respiratory coronavirus receptor-binding domain complexed with its human receptor. Proc Natl Acad Sci U S A. 2009;106(47):19970-4. Epub 2009/11/11. doi: 10.1073/pnas.0908837106. PubMed PMID: 19901337; PMCID: PMC2785276.
28. Lan J, Ge J, Yu J, Shan S, Zhou H, Fan S, Zhang Q, Shi X, Wang Q, Zhang L, Wang X. Structure of the SARS-CoV-2 spike receptor-binding domain bound to the ACE2 receptor. Nature. 2020;581(7807):215-20. Epub 2020/04/01. doi: 10.1038/s41586-020-2180-5. PubMed PMID: 32225176.
29. Grishin AM, Dolgova NV, Landreth S, Fisette O, Pickering IJ, George GN, Falzarano D, Cygler M. Disulfide Bonds Play a Critical Role in the Structure and Function of the Receptor-binding Domain of the SARS-CoV-2 Spike Antigen. J Mol Biol. 2022;434(2):167357. Epub 2021/11/16. doi: 10.1016/j.jmb.2021.167357. PubMed PMID: 34780781; PMCID: PMC8588607.
30. Khazaal S, Harb J, Rima M, Annweiler C, Wu Y, Cao Z, Abi Khattar Z, Legros C, Kovacic H, Fajloun Z, Sabatier JM. The Pathophysiology of Long COVID throughout the Renin-Angiotensin System. Molecules. 2022;27(9). Epub 2022/05/15. doi: 10.3390/molecules27092903. PubMed PMID: 35566253; PMCID: PMC9101946.
31. Keck T, Leiacker R, Riechelmann H, Rettinger G. Temperature profile in the nasal cavity. Laryngoscope. 2000;110(4):651-4. Epub 2000/04/14. doi: 10.1097/00005537-200004000-00021. PubMed PMID: 10764013.
32. Jeanneteau F, Diaz J, Sokoloff P, Griffon N. Interactions of GIPC with dopamine D2, D3 but not D4 receptors define a novel mode of regulation of G protein-coupled receptors. Mol Biol

1390 Cell. 2004;15(2):696-705. Epub 2003/11/18. doi: 10.1091/mbc.e03-05-0293. PubMed PMID:
1391 14617818; PMCID: PMC329290.
1392 33. Weill C, Ilien B, Goeldner M, Galzi JL. Fluorescent muscarinic EGFP-hM1 chimeric
1393 receptors: design, ligand binding and functional properties. J Recept Signal Transduct Res.
1394 1999;19(1-4):423-36. Epub 1999/03/11. doi: 10.3109/10799899909036662. PubMed PMID:
1395 10071775.
1396 34. Parvanova I. Getting at the Surface: A Promoter and Coding Sequence Characterization
1397 of an Odorant Receptor. CUNY Academic Works. 2019.
1398 35. McMahon C, Scadding GK. Le Nez du Vin--a quick test of olfaction. Clin Otolaryngol
1399 Allied Sci. 1996;21(3):278-80. Epub 1996/06/01. doi: 10.1111/j.1365-2273.1996.tb01741.x.
1400 PubMed PMID: 8818503.
1401 36. Lu Y, Zhu Q, Fox DM, Gao C, Stanley SA, Luo K. SARS-CoV-2 down-regulates ACE2
1402 through lysosomal degradation. Mol Biol Cell. 2022;33(14):ar147. Epub 2022/10/27. doi:
1403 10.1091/mbc.E22-02-0045. PubMed PMID: 36287912; PMCID: PMC9727799.
1404 37. Shang C, Zhuang X, Zhang H, Li Y, Zhu Y, Lu J, Ge C, Cong J, Li T, Tian M, Jin N, Li
1405 X. Inhibitors of endosomal acidification suppress SARS-CoV-2 replication and relieve viral
1406 pneumonia in hACE2 transgenic mice. Virol J. 2021;18(1):46. Epub 2021/03/01. doi:
1407 10.1186/s12985-021-01515-1. PubMed PMID: 33639976; PMCID: PMC7914043.
1408 38. Jackson CB, Farzan M, Chen B, Choe H. Mechanisms of SARS-CoV-2 entry into cells.
1409 Nat Rev Mol Cell Biol. 2022;23(1):3-20. Epub 2021/10/07. doi: 10.1038/s41580-021-00418-x.
1410 PubMed PMID: 34611326; PMCID: PMC8491763.
1411 39. Szewczyk-Roszczenko OK, Roszczenko P, Shmakova A, Finiuk N, Holota S, Lesyk R,
1412 Bielawska A, Vassetzky Y, Bielawski K. The Chemical Inhibitors of Endocytosis: From
1413 Mechanisms to Potential Clinical Applications. Cells. 2023;12(18). Epub 2023/09/28. doi:
1414 10.3390/cells12182312. PubMed PMID: 37759535; PMCID: PMC10527932.
1415 40. Bayati A, Kumar R, Francis V, McPherson PS. SARS-CoV-2 infects cells after viral
1416 entry via clathrin-mediated endocytosis. J Biol Chem. 2021;296:100306. Epub 2021/01/22. doi:
1417 10.1016/j.jbc.2021.100306. PubMed PMID: 33476648; PMCID: PMC7816624.
1418 41. Starr TN, Greaney AJ, Hilton SK, Ellis D, Crawford KHD, Dingens AS, Navarro MJ,
1419 Bowen JE, Tortorici MA, Walls AC, King NP, Veesler D, Bloom JD. Deep Mutational Scanning
1420 of SARS-CoV-2 Receptor Binding Domain Reveals Constraints on Folding and ACE2 Binding.
1421 Cell. 2020;182(5):1295-310 e20. Epub 2020/08/26. doi: 10.1016/j.cell.2020.08.012. PubMed
1422 PMID: 32841599; PMCID: PMC7418704.
1423 42. Jawad B, Adhikari P, Podgornik R, Ching WY. Key Interacting Residues between RBD
1424 of SARS-CoV-2 and ACE2 Receptor: Combination of Molecular Dynamics Simulation and
1425 Density Functional Calculation. J Chem Inf Model. 2021;61(9):4425-41. Epub 2021/08/25. doi:
1426 10.1021/acs.jcim.1c00560. PubMed PMID: 34428371; PMCID: PMC8409146.
1427 43. Harvey WT, Carabelli AM, Jackson B, Gupta RK, Thomson EC, Harrison EM, Ludden
1428 C, Reeve R, Rambaut A, Consortium C-GU, Peacock SJ, Robertson DL. SARS-CoV-2 variants,
1429 spike mutations and immune escape. Nat Rev Microbiol. 2021;19(7):409-24. Epub 2021/06/03.
1430 doi: 10.1038/s41579-021-00573-0. PubMed PMID: 34075212; PMCID: PMC8167834.
1431 44. Li W, Sui J, Huang IC, Kuhn JH, Radoshitzky SR, Marasco WA, Choe H, Farzan M. The
1432 S proteins of human coronavirus NL63 and severe acute respiratory syndrome coronavirus bind
1433 overlapping regions of ACE2. Virology. 2007;367(2):367-74. Epub 2007/07/17. doi:
1434 10.1016/j.virol.2007.04.035. PubMed PMID: 17631932; PMCID: PMC2693060.

1435 45. Zhou H, Ji J, Chen X, Bi Y, Li J, Wang Q, Hu T, Song H, Zhao R, Chen Y, Cui M,
1436 Zhang Y, Hughes AC, Holmes EC, Shi W. Identification of novel bat coronaviruses sheds light
1437 on the evolutionary origins of SARS-CoV-2 and related viruses. Cell. 2021;184(17):4380-91
1438 e14. Epub 2021/06/21. doi: 10.1016/j.cell.2021.06.008. PubMed PMID: 34147139; PMCID:
1439 PMC8188299.
1440 46. Temmam S, Vongphayloth K, Baquero E, Munier S, Bonomi M, Regnault B,
1441 Douangboubpha B, Karami Y, Chretien D, Sanamxay D, Xayaphet V, Paphaphanh P, Lacoste V,
1442 Somlor S, Lakeomany K, Phommavanh N, Perot P, Dehan O, Amara F, Donati F, Bigot T,
1443 Nilges M, Rey FA, van der Werf S, Brey PT, Eloit M. Bat coronaviruses related to SARS-CoV-2
1444 and infectious for human cells. Nature. 2022;604(7905):330-6. Epub 2022/02/17. doi:
1445 10.1038/s41586-022-04532-4. PubMed PMID: 35172323.
1446 47. Lin HX, Feng Y, Tu X, Zhao X, Hsieh CH, Griffin L, Junop M, Zhang C.
1447 Characterization of the spike protein of human coronavirus NL63 in receptor binding and
1448 pseudotype virus entry. Virus Res. 2011;160(1-2):283-93. Epub 2011/07/30. doi:
1449 10.1016/j.virusres.2011.06.029. PubMed PMID: 21798295; PMCID: PMC7114368.
1450 48. Wu K, Chen L, Peng G, Zhou W, Pennell CA, Mansky LM, Geraghty RJ, Li F. A virus-
1451 binding hot spot on human angiotensin-converting enzyme 2 is critical for binding of two
1452 different coronaviruses. J Virol. 2011;85(11):5331-7. Epub 2011/03/18. doi: 10.1128/JVI.02274-
1453 10. PubMed PMID: 21411533; PMCID: PMC3094985.
1454 49. Kapp TG, Rechenmacher F, Neubauer S, Maltsev OV, Cavalcanti-Adam EA, Zarka R,
1455 Reuning U, Notni J, Wester HJ, Mas-Moruno C, Spatz J, Geiger B, Kessler H. A Comprehensive
1456 Evaluation of the Activity and Selectivity Profile of Ligands for RGD-binding Integrins. Sci
1457 Rep. 2017;7:39805. Epub 2017/01/12. doi: 10.1038/srep39805. PubMed PMID: 28074920;
1458 PMCID: PMC5225454.
1459 50. Mancek-Keber M, Hafner-Bratkovic I, Lainscek D, Bencina M, Govednik T, Orehek S,
1460 Plaper T, Jazbec V, Bergant V, Grass V, Pichlmair A, Jerala R. Disruption of disulfides within
1461 RBD of SARS-CoV-2 spike protein prevents fusion and represents a target for viral entry
1462 inhibition by registered drugs. FASEB J. 2021;35(6):e21651. Epub 2021/05/19. doi:
1463 10.1096/fj.202100560R. PubMed PMID: 34004056; PMCID: PMC8206760.
1464 51. Lukesh JC, 3rd, Palte MJ, Raines RT. A potent, versatile disulfide-reducing agent from
1465 aspartic acid. J Am Chem Soc. 2012;134(9):4057-9. Epub 2012/02/23. doi: 10.1021/ja211931f.
1466 PubMed PMID: 22353145; PMCID: PMC3353773.
1467 52. Damas J, Hughes GM, Keough KC, Painter CA, Persky NS, Corbo M, Hiller M, Koepfli
1468 KP, Pfenning AR, Zhao H, Genereux DP, Swofford R, Pollard KS, Ryder OA, Nweeia MT,
1469 Lindblad-Toh K, Teeling EC, Karlsson EK, Lewin HA. Broad host range of SARS-CoV-2
1470 predicted by comparative and structural analysis of ACE2 in vertebrates. Proc Natl Acad Sci U S
1471 A. 2020;117(36):22311-22. Epub 2020/08/23. doi: 10.1073/pnas.2010146117. PubMed PMID:
1472 32826334; PMCID: PMC7486773.
1473 53. Mou H, Quinlan BD, Peng H, Liu G, Guo Y, Peng S, Zhang L, Davis-Gardner ME,
1474 Gardner MR, Crynen G, DeVaux LB, Voo ZX, Bailey CC, Alpert MD, Rader C, Gack MU,
1475 Choe H, Farzan M. Mutations derived from horseshoe bat ACE2 orthologs enhance ACE2-Fc
1476 neutralization of SARS-CoV-2. PLoS Pathog. 2021;17(4):e1009501. Epub 2021/04/10. doi:
1477 10.1371/journal.ppat.1009501. PubMed PMID: 33836016; PMCID: PMC8059821 following
1478 competing interests: M.F., H.M. and B.D.Q had filed a patent for the application of ACE2-Fc
1479 variants as a SARS-CoV-2 treatment. M.R.G., C.C.B., M.D.A., and M.F. are all cofounders of,

and have an equity interest in Emmune Inc., a biotech company that specializes in the development of antibody-like antiviral therapies.
54. Conceicao C, Thakur N, Human S, Kelly JT, Logan L, Bialy D, Bhat S, Stevenson-Leggett P, Zagrajek AK, Hollinghurst P, Varga M, Tsirigoti C, Tully M, Chiu C, Moffat K, Silesian AP, Hammond JA, Maier HJ, Bickerton E, Shelton H, Dietrich I, Graham SC, Bailey D. The SARS-CoV-2 Spike protein has a broad tropism for mammalian ACE2 proteins. PLoS Biol. 2020;18(12):e3001016. Epub 2020/12/22. doi: 10.1371/journal.pbio.3001016. PubMed PMID: 33347434; PMCID: PMC7751883.
55. Li Y, Wang H, Tang X, Fang S, Ma D, Du C, Wang Y, Pan H, Yao W, Zhang R, Zou X, Zheng J, Xu L, Farzan M, Zhong G. SARS-CoV-2 and Three Related Coronaviruses Utilize Multiple ACE2 Orthologs and Are Potently Blocked by an Improved ACE2-Ig. J Virol. 2020;94(22). Epub 2020/08/28. doi: 10.1128/JVI.01283-20. PubMed PMID: 32847856; PMCID: PMC7592233.
56. Liu X, Garriga P, Khorana HG. Structure and function in rhodopsin: correct folding and misfolding in two point mutants in the intradiscal domain of rhodopsin identified in retinitis pigmentosa. Proc Natl Acad Sci U S A. 1996;93(10):4554-9. Epub 1996/05/14. doi: 10.1073/pnas.93.10.4554. PubMed PMID: 8643442; PMCID: PMC39315.
57. Choi CY, Gadhave K, Villano J, Pekosz A, Mao X, Jia H. Generation and characterization of a humanized ACE2 mouse model to study long-term impacts of SARS-CoV-2 infection. J Med Virol. 2024;96(1):e29349. Epub 2024/01/08. doi: 10.1002/jmv.29349. PubMed PMID: 38185937; PMCID: PMC10783855.
58. Cagan RL, Kramer H, Hart AC, Zipursky SL. The bride of sevenless and sevenless interaction: internalization of a transmembrane ligand. Cell. 1992;69(3):393-9. Epub 1992/05/01. doi: 10.1016/0092-8674(92)90442-f. PubMed PMID: 1316239.
59. Langridge PD, Struhl G. Epsin-Dependent Ligand Endocytosis Activates Notch by Force. Cell. 2017;171(6):1383-96 e12. Epub 2017/12/02. doi: 10.1016/j.cell.2017.10.048. PubMed PMID: 29195077; PMCID: PMC6219616.
60. Mathewson AC, Bishop A, Yao Y, Kemp F, Ren J, Chen H, Xu X, Berkhout B, van der Hoek L, Jones IM. Interaction of severe acute respiratory syndrome-coronavirus and NL63 coronavirus spike proteins with angiotensin converting enzyme-2. J Gen Virol. 2008;89(Pt 11):2741-5. Epub 2008/10/22. doi: 10.1099/vir.0.2008/003962-0. PubMed PMID: 18931070; PMCID: PMC2886958.
61. Brown EEF, Rezaei R, Jamieson TR, Dave J, Martin NT, Singaravelu R, Crupi MJF, Boulton S, Tucker S, Duong J, Poutou J, Pelin A, Yasavoli-Sharahi H, Taha Z, Arulanandam R, Surendran A, Ghahremani M, Austin B, Matar C, Diallo JS, Bell JC, Ilkow CS, Azad T. Characterization of Critical Determinants of ACE2-SARS CoV-2 RBD Interaction. Int J Mol Sci. 2021;22(5). Epub 2021/03/07. doi: 10.3390/ijms22052268. PubMed PMID: 33668756; PMCID: PMC7956771.
62. Chan KK, Tan TJC, Narayanan KK, Procko E. An engineered decoy receptor for SARS-CoV-2 broadly binds protein S sequence variants. Sci Adv. 2021;7(8). Epub 2021/02/19. doi: 10.1126/sciadv.abf1738. PubMed PMID: 33597251; PMCID: PMC7888922.
63. Butowt R, Bilinska K, von Bartheld CS. Olfactory dysfunction in COVID-19: new insights into the underlying mechanisms. Trends Neurosci. 2023;46(1):75-90. Epub 2022/12/06. doi: 10.1016/j.tins.2022.11.003. PubMed PMID: 36470705; PMCID: PMC9666374.
64. Essalmani R, Jain J, Susan-Resiga D, Andreo U, Evagelidis A, Derbali RM, Huynh DN, Dallaire F, Laporte M, Delpal A, Sutto-Ortiz P, Coutard B, Mapa C, Wilcoxen K, Decroly E, Nq

1526 Pham T, Cohen EA, Seidah NG. Distinctive Roles of Furin and TMPRSS2 in SARS-CoV-2
1527 Infectivity. J Virol. 2022;96(8):e0012822. Epub 2022/03/29. doi: 10.1128/jvi.00128-22. PubMed
1528 PMID: 35343766; PMCID: PMC9044946.
1529 65. Papa G, Mallery DL, Albecka A, Welch LG, Cattin-Ortola J, Luptak J, Paul D,
1530 McMahon HT, Goodfellow IG, Carter A, Munro S, James LC. Furin cleavage of SARS-CoV-2
1531 Spike promotes but is not essential for infection and cell-cell fusion. PLoS Pathog.
1532 2021;17(1):e1009246. Epub 2021/01/26. doi: 10.1371/journal.ppat.1009246. PubMed PMID:
1533 33493182; PMCID: PMC7861537.
1534 66. Peacock TP, Goldhill DH, Zhou J, Baillon L, Frise R, Swann OC, Kugathasan R, Penn R,
1535 Brown JC, Sanchez-David RY, Braga L, Williamson MK, Hassard JA, Staller E, Hanley B,
1536 Osborn M, Giacca M, Davidson AD, Matthews DA, Barclay WS. The furin cleavage site in the
1537 SARS-CoV-2 spike protein is required for transmission in ferrets. Nat Microbiol. 2021;6(7):899-
1538 909. Epub 2021/04/29. doi: 10.1038/s41564-021-00908-w. PubMed PMID: 33907312.
1539 67. Yu S, Zheng X, Zhou B, Li J, Chen M, Deng R, Wong G, Lavillette D, Meng G. SARS-
1540 CoV-2 spike engagement of ACE2 primes S2' site cleavage and fusion initiation. Proc Natl Acad
1541 Sci U S A. 2022;119(1). Epub 2021/12/22. doi: 10.1073/pnas.2111199119. PubMed PMID:
1542 34930824; PMCID: PMC8740742.
1543 68. Rawat P, Jemimah S, Ponnuswamy PK, Gromiha MM. Why are ACE2 binding
1544 coronavirus strains SARS-CoV/SARS-CoV-2 wild and NL63 mild? Proteins. 2021;89(4):389-
1545 98. Epub 2020/11/20. doi: 10.1002/prot.26024. PubMed PMID: 33210300; PMCID:
1546 PMC7753379.
1547 69. Tang AT, Buchholz DW, Szigety KM, Imbiakha B, Gao S, Frankfurter M, Wang M,
1548 Yang J, Hewins P, Mericko-Ishizuka P, Leu NA, Sterling S, Monreal IA, Sahler J, August A,
1549 Zhu X, Jurado KA, Xu M, Morrisey EE, Millar SE, Aguilar HC, Kahn ML. Cell-autonomous
1550 requirement for ACE2 across organs in lethal mouse SARS-CoV-2 infection. PLoS Biol.
1551 2023;21(2):e3001989. Epub 2023/02/07. doi: 10.1371/journal.pbio.3001989. PubMed PMID:
1552 36745682; PMCID: PMC9934376.
1553 70. Astuti I, Ysrafil. Severe Acute Respiratory Syndrome Coronavirus 2 (SARS-CoV-2): An
1554 overview of viral structure and host response. Diabetes Metab Syndr. 2020;14(4):407-12. Epub
1555 2020/04/27. doi: 10.1016/j.dsx.2020.04.020. PubMed PMID: 32335367; PMCID: PMC7165108.
1556 71. Leijnse N, Barooji YF, Arastoo MR, Sonder SL, Verhagen B, Wullkopf L, Erler JT,
1557 Semsey S, Nylandsted J, Oddershede LB, Doostmohammadi A, Bendix PM. Filopodia rotate and
1558 coil by actively generating twist in their actin shaft. Nat Commun. 2022;13(1):1636. Epub
1559 2022/03/30. doi: 10.1038/s41467-022-28961-x. PubMed PMID: 35347113; PMCID:
1560 PMC8960877.
1561 72. Maslanka Figueroa S, Fleischmann D, Beck S, Tauber P, Witzgall R, Schweda F,
1562 Goepferich A. Nanoparticles Mimicking Viral Cell Recognition Strategies Are Superior
1563 Transporters into Mesangial Cells. Adv Sci (Weinh). 2020;7(11):1903204. Epub 2020/06/17.
1564 doi: 10.1002/advs.201903204. PubMed PMID: 32537398; PMCID: PMC7284201.
1565 73. Lin PC, Lee YR, Liu LT, Chiou SS, Chen PC, Tsai CY, Tsai JJ. Honeysuckle extracts as
1566 a potential inhibitor of SARS-CoV-2 infection. Front Pharmacol. 2025;16:1517585. Epub
1567 2025/05/19. doi: 10.3389/fphar.2025.1517585. PubMed PMID: 40385477; PMCID:
1568 PMC12083240.
1569 74. Zaharuddin Z, Md Hussin NS, Karuppannan M. Real-world analysis of safety,
1570 tolerability, and adherence to nirmatrelvir-ritonavir (paxlovid) in primary care COVID-19

1571 outpatients. Sci Rep. 2024;14(1):24750. Epub 2024/10/22. doi: 10.1038/s41598-024-75192-9.
1572 PubMed PMID: 39433826; PMCID: PMC11494129.
1573 75. Havervall S, Marking U, Svensson J, Greilert-Norin N, Bacchus P, Nilsson P, Hober S,
1574 Gordon M, Blom K, Klingstrom J, Aberg M, Smed-Sorensen A, Thalin C. Anti-Spike Mucosal
1575 IgA Protection against SARS-CoV-2 Omicron Infection. N Engl J Med. 2022;387(14):1333-6.
1576 Epub 2022/09/15. doi: 10.1056/NEJMc2209651. PubMed PMID: 36103621; PMCID:
1577 PMC9511632.
1578 76. Zhu J, Su, Y., and Tang, Y. Disrupting ACE2 Dimerization Mitigates the Infection by
1579 SARS-CoV-2 Pseudovirus. Frontiers in Virology. 2022;Virol., 03 July 2022(2).
1580 77. Lorenzo R, Defelipe LA, Aliperti L, Niebling S, Custodio TF, Low C, Schwarz JJ,
1581 Remans K, Craig PO, Otero LH, Klinke S, Garcia-Alai M, Sanchez IE, Alonso LG. Deamidation
1582 drives molecular aging of the SARS-CoV-2 spike protein receptor-binding motif. J Biol Chem.
1583 2021;297(4):101175. Epub 2021/09/10. doi: 10.1016/j.jbc.2021.101175. PubMed PMID:
1584 34499924; PMCID: PMC8421091.
1585 78. Beaudoin CA, Petsolari E, Hamaia SW, Hala S, Alofi FS, Pandurangan AP, Blundell TL,
1586 Chaitanya Vedithi S, Huang CL, Jackson AP. SARS-CoV-2 Omicron subvariant spike N405
1587 unlikely to rapidly deamidate. Biochem Biophys Res Commun. 2023;666:61-7. Epub
1588 2023/05/14. doi: 10.1016/j.bbrc.2023.04.088. PubMed PMID: 37178506; PMCID:
1589 PMC10152834.
1590 79. Yi C, Sun X, Ye J, Ding L, Liu M, Yang Z, Lu X, Zhang Y, Ma L, Gu W, Qu A, Xu J,
1591 Shi Z, Ling Z, Sun B. Key residues of the receptor binding motif in the spike protein of SARS-
1592 CoV-2 that interact with ACE2 and neutralizing antibodies. Cell Mol Immunol. 2020;17(6):621-
1593 30. Epub 2020/05/18. doi: 10.1038/s41423-020-0458-z. PubMed PMID: 32415260; PMCID:
1594 PMC7227451.
1595 80. Chopra A, Shukri AH, Adhikary H, Lukinovic V, Hoekstra M, Cowpland M, Biggar KK.
1596 A peptide array pipeline for the development of Spike-ACE2 interaction inhibitors. Peptides.
1597 2022;158:170898. Epub 2022/10/25. doi: 10.1016/j.peptides.2022.170898. PubMed PMID:
1598 36279985; PMCID: PMC9585897.
1599 81. Cao L, Goreshnik I, Coventry B, Case JB, Miller L, Kozodoy L, Chen RE, Carter L,
1600 Walls AC, Park YJ, Strauch EM, Stewart L, Diamond MS, Veesler D, Baker D. De novo design
1601 of picomolar SARS-CoV-2 miniprotein inhibitors. Science. 2020;370(6515):426-31. Epub
1602 2020/09/11. doi: 10.1126/science.abd9909. PubMed PMID: 32907861; PMCID: PMC7857403.
1603 82. Beaudoin CA, Jamasb AR, Alsulami AF, Copoiu L, van Tonder AJ, Hala S, Bannerman
1604 BP, Thomas SE, Vedithi SC, Torres PHM, Blundell TL. Predicted structural mimicry of spike
1605 receptor-binding motifs from highly pathogenic human coronaviruses. Comput Struct Biotechnol
1606 J. 2021;19:3938-53. Epub 2021/07/09. doi: 10.1016/j.csbj.2021.06.041. PubMed PMID:
1607 34234921; PMCID: PMC8249111.
1608 83. Eslami N, Aghbash PS, Shamekh A, Entezari-Maleki T, Nahand JS, Sales AJ, Baghi HB.
1609 SARS-CoV-2: Receptor and Co-receptor Tropism Probability. Curr Microbiol. 2022;79(5):133.
1610 Epub 2022/03/17. doi: 10.1007/s00284-022-02807-7. PubMed PMID: 35292865; PMCID:
1611 PMC8923825.
1612 84. Alipoor SD, Mirsaeidi M. SARS-CoV-2 cell entry beyond the ACE2 receptor. Mol Biol
1613 Rep. 2022;49(11):10715-27. Epub 2022/06/27. doi: 10.1007/s11033-022-07700-x. PubMed
1614 PMID: 35754059; PMCID: PMC9244107.
1615 85. Beddingfield BJ, Iwanaga N, Chapagain PP, Zheng W, Roy CJ, Hu TY, Kolls JK, Bix
1616 GJ. The Integrin Binding Peptide, ATN-161, as a Novel Therapy for SARS-CoV-2 Infection.

JACC Basic Transl Sci. 2021;6(1):1-8. Epub 2020/10/27. doi: 10.1016/j.jacbts.2020.10.003. PubMed PMID: 33102950; PMCID: PMC7566794.
86. Beaudoin CA, Hamaia SW, Huang CL, Blundell TL, Jackson AP. Can the SARS-CoV-2 Spike Protein Bind Integrins Independent of the RGD Sequence? Front Cell Infect Microbiol. 2021;11:765300. Epub 2021/12/07. doi: 10.3389/fcimb.2021.765300. PubMed PMID: 34869067; PMCID: PMC8637727.
87. Kliche J, Kuss H, Ali M, Ivarsson Y. Cytoplasmic short linear motifs in ACE2 and integrin beta(3) link SARS-CoV-2 host cell receptors to mediators of endocytosis and autophagy. Sci Signal. 2021;14(665). Epub 2021/01/14. doi: 10.1126/scisignal.abf1117. PubMed PMID: 33436498; PMCID: PMC7928716.
88. Zamorano Cuervo N, Grandvaux N. ACE2: Evidence of role as entry receptor for SARS-CoV-2 and implications in comorbidities. Elife. 2020;9. Epub 2020/11/10. doi: 10.7554/eLife.61390. PubMed PMID: 33164751; PMCID: PMC7652413.
89. Sui Y, Li J, Venzon DJ, Berzofsky JA. SARS-CoV-2 Spike Protein Suppresses ACE2 and Type I Interferon Expression in Primary Cells From Macaque Lung Bronchoalveolar Lavage. Front Immunol. 2021;12:658428. Epub 2021/06/22. doi: 10.3389/fimmu.2021.658428. PubMed PMID: 34149696; PMCID: PMC8213020.
90. Ugo Bastolla1* PC, David Abia1, Maria-Laura Garcia-Bermejo3 and Manuel Fresno1. Is Covid-19 Severity Associated With ACE2 Degradation? Frontiers in Drug Discovery. 2022(January 2022 | Volume 1 | Article 789710). Epub 10.3389/fddsv.2021.789710.
91. Trougakos IP, Terpos E, Alexopoulos H, Politou M, Paraskevis D, Scorilas A, Kastritis E, Andreakos E, Dimopoulos MA. Adverse effects of COVID-19 mRNA vaccines: the spike hypothesis. Trends Mol Med. 2022;28(7):542-54. Epub 2022/05/11. doi: 10.1016/j.molmed.2022.04.007. PubMed PMID: 35537987; PMCID: PMC9021367.
92. Angeli F, Spanevello A, Reboldi G, Visca D, Verdecchia P. SARS-CoV-2 vaccines: Lights and shadows. Eur J Intern Med. 2021;88:1-8. Epub 2021/05/11. doi: 10.1016/j.ejim.2021.04.019. PubMed PMID: 33966930; PMCID: PMC8084611.
93. Zappa M, Verdecchia P, Spanevello A, Visca D, Angeli F. Blood pressure increase after Pfizer/BioNTech SARS-CoV-2 vaccine. Eur J Intern Med. 2021;90:111-3. Epub 2021/06/24. doi: 10.1016/j.ejim.2021.06.013. PubMed PMID: 34158234; PMCID: PMC8206586.
94. Forte E. Circulating spike protein may contribute to myocarditis after COVID-19 vaccination. Nat Cardiovasc Res. 2023;2(2):100. Epub 2023/02/01. doi: 10.1038/s44161-023-00222-0. PubMed PMID: 39196056.
95. Walsh EE, Frenck RW, Jr., Falsey AR, Kitchin N, Absalon J, Gurtman A, Lockhart S, Neuzil K, Mulligan MJ, Bailey R, Swanson KA, Li P, Koury K, Kalina W, Cooper D, Fontes-Garfias C, Shi PY, Tureci O, Tompkins KR, Lyke KE, Raabe V, Dormitzer PR, Jansen KU, Sahin U, Gruber WC. Safety and Immunogenicity of Two RNA-Based Covid-19 Vaccine Candidates. N Engl J Med. 2020;383(25):2439-50. Epub 2020/10/15. doi: 10.1056/NEJMoa2027906. PubMed PMID: 33053279; PMCID: PMC7583697.
96. Haas JW, Bender FL, Ballou S, Kelley JM, Wilhelm M, Miller FG, Rief W, Kaptchuk TJ. Frequency of Adverse Events in the Placebo Arms of COVID-19 Vaccine Trials: A Systematic Review and Meta-analysis. JAMA Netw Open. 2022;5(1):e2143955. Epub 2022/01/19. doi: 10.1001/jamanetworkopen.2021.43955. PubMed PMID: 35040967; PMCID: PMC8767431 scholarship from the German Academic Exchange Service (Deutscher Akademischer Austauschdienst) during the conduct of the study. No other disclosures were reported.

97. Illing N, Boolay S, Siwoski JS, Casper D, Lucero MT, Roskams AJ. Conditionally immortalized clonal cell lines from the mouse olfactory placode differentiate into olfactory receptor neurons. Mol Cell Neurosci. 2002;20(2):225-43. Epub 2002/07/03. doi: 10.1006/mcne.2002.1106. PubMed PMID: 12093156.

98. Ma G, Syu GD, Shan X, Henson B, Wang S, Desai PJ, Zhu H, Tao N. Measuring Ligand Binding Kinetics to Membrane Proteins Using Virion Nano-oscillators. J Am Chem Soc. 2018;140(36):11495-501. Epub 2018/08/17. doi: 10.1021/jacs.8b07461. PubMed PMID: 30114365; PMCID: PMC6211285.

99. Hati S, Bhattacharyya S. Impact of Thiol-Disulfide Balance on the Binding of Covid-19 Spike Protein with Angiotensin-Converting Enzyme 2 Receptor. ACS Omega. 2020;5(26):16292-8. Epub 2020/07/14. doi: 10.1021/acsomega.0c02125. PubMed PMID: 32656452; PMCID: PMC7346263.

100. Argentinian AntiCovid C. Structural and functional comparison of SARS-CoV-2-spike receptor binding domain produced in Pichia pastoris and mammalian cells. Sci Rep. 2020;10(1):21779. Epub 2020/12/15. doi: 10.1038/s41598-020-78711-6. PubMed PMID: 33311634; PMCID: PMC7732851.

1681 **Figures:**

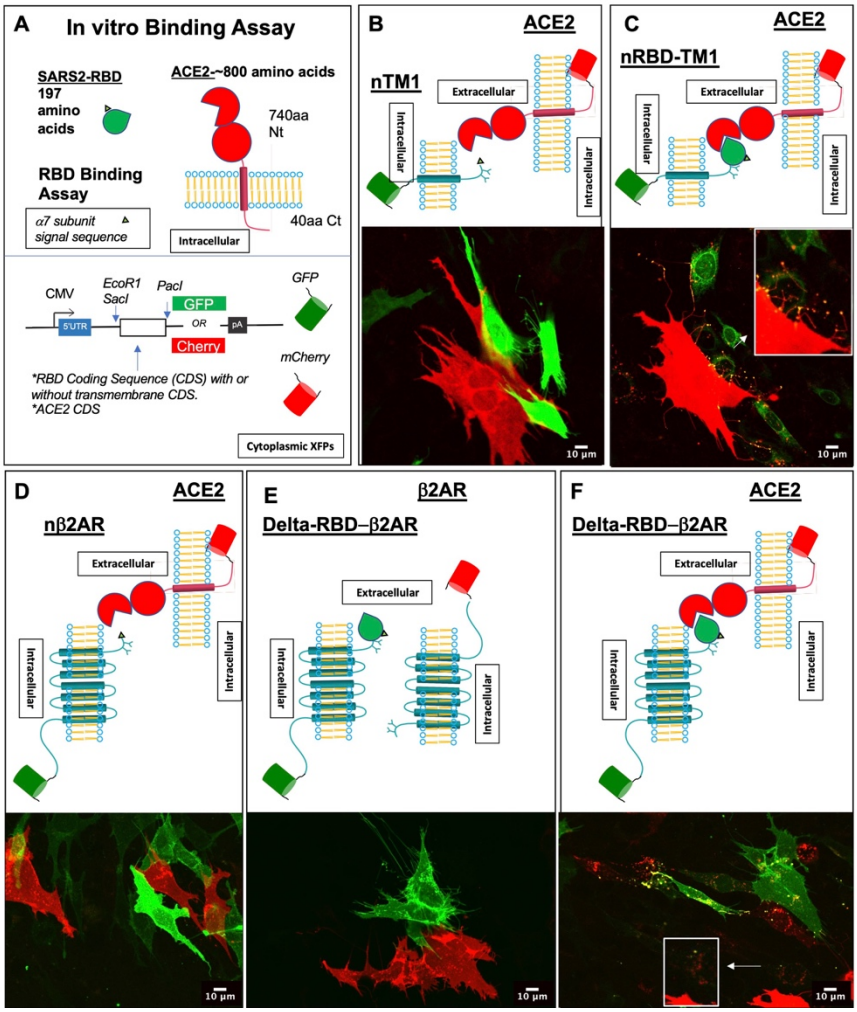

1682

1683 **Figure 1: An in vitro substitute for SARS2 virus binding to ACE2-expressing cells.**
1684 **A.** Experimental system to identify a compound that mitigates SARS2-RBD and ACE2 binding
1685 in cell lines. Expression vectors with Cherry and GFP contain EcoR1-PacI restriction sites,
1686 whereby cloning of SARS2-RBD variants or ACE2 mutants will generate in frame fusion
1687 proteins. **B.-F.** Confocal images of separate electroporations into OP6 cells and co-plated
1688 overnight (O/N). All RBD constructs contain the nicotinic receptor α7 subunit (n) signal
1689 sequence at their N-termini **B.** Expression and co-plating of the first 60amino acids of β2AR
1690 (nTM1) to GFP and human ACE2 fused to Cherry. No double fluorescent cells observed: red
1691 (Cherry) and green (GFP). **C.** SARS2-RBD-β2AR-TM1 (nRBD-TM1) is fused to GFP and co-
1692 plated with ACE2-Cherry expressing cells. Red filopodia (20) are seen with green fluorescent on
1693 its distal points (see inset, magnification). **D.** Control co-plating of nβ2AR-GFP and ACE2-
1694 Cherry expressing cells show no double fluorescence. **E.** Control co-plating of the Delta variant,
1695 Delta-RBD-β2AR-GFP and β2AR-Cherry expressing show no double fluorescence. **F.** Co-
1696 plating Delta-RBD-β2AR-GFP and ACE2-Cherry expressing cells show dramatic internalization
1697 of GFP fluorescently tagged protein and no obvious morphology to the ACE2-Cherry expressing
1698 cells. Inset shows filopodia of ACE2-Cherry cells with GFP. Scale bars at 10µm**.**

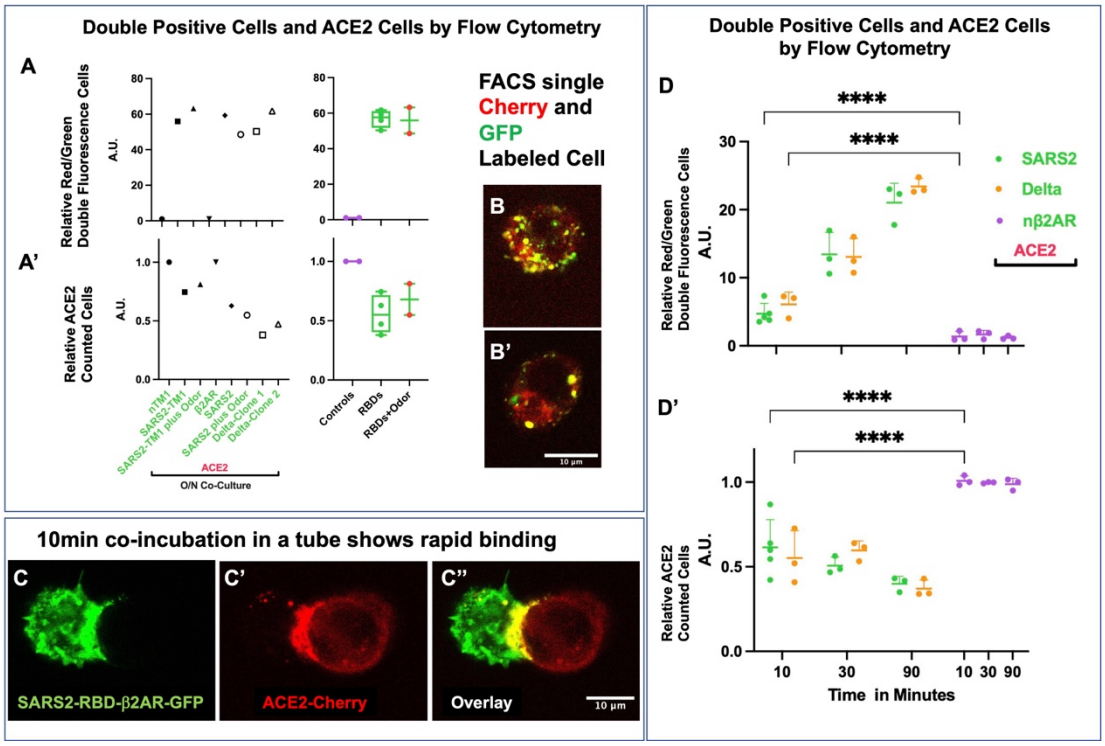

Figure 2: Quantifying RBD-ACE2 interactions by single cell flow cytometry analysis. **A and A'.** Initial experiments aimed a quantifying interaction. RBD-TM1/ RBD-β2AR-GFP fusion constructs and controls co-plated after separate electroporation (EP) and left to interact for 16hrs. nTM1, SARS2-TM1, SARS2-TM1 plus overnight (O/N) LNDV odor mixture 35 (1:500), β2AR, SARS2, SARS2 plus LNDV odor mixture 35 (1:500), and two clones of Delta (1 and 2). In all cases where an RBD was present, double fluorescent cells were observed at 60x WT values, which were in the single digits. Data were performed in triplicate, but when all the WT or RBD containing cells are analyzed in aggregate, then highly statistically significant data is obtained. Values are normalized to controls (Y-axis arbitrary units, A. U.). Surprisingly, ACE2 fluorescence was diminished in all cases RBD was present and again, when cells are analyzed in aggregate, data is highly significant. **B and B'.** Two double fluorescence cells shown by confocal imaging, revealing red cells with green speckles. **C-C''.** *Dissociated Cell-based Assay* Confocal imaging of a dissociated green cell adhering to a dissociated red cell that are acutely mixed for 10min at 37°C; Many of the cells were found to interact with an overt relocalization of the ACE2-Cherry protein (**C'**). **D and D'** *Dissociate, Plate, Flow cytometry (DPF) Assay*: values in are normalized to controls (Y-axis arbitrary units, A. U.). The speed of the interaction observed in **C**, was recapitulated by layering dissociating EPd test constructs on ACE2-cherry cells in triplicate including for 3 time points: 10min, 30min and 90min, followed by dissociation and flow cytometry counting. ACE2-Cherry cells at all time points are from the same set of EPs were plated O/N on individual 30cm plates. GFP fluorescent cells, Control nβ2AR, SARS2-RBD and Delta-RBD cells were seeded onto sets of 30cm plates in triplicate. After O/N growth, individual 30cm plates of cells were trypsinized and plated on top of ACE2-Cherry cells for the defined time. Like the O/N co-cultures, the trypsinization-co-plating-flow cytometry analysis revealed double fluorescence in 10min as well as a near 50% reduction in ACE2-Cherry expressing cells

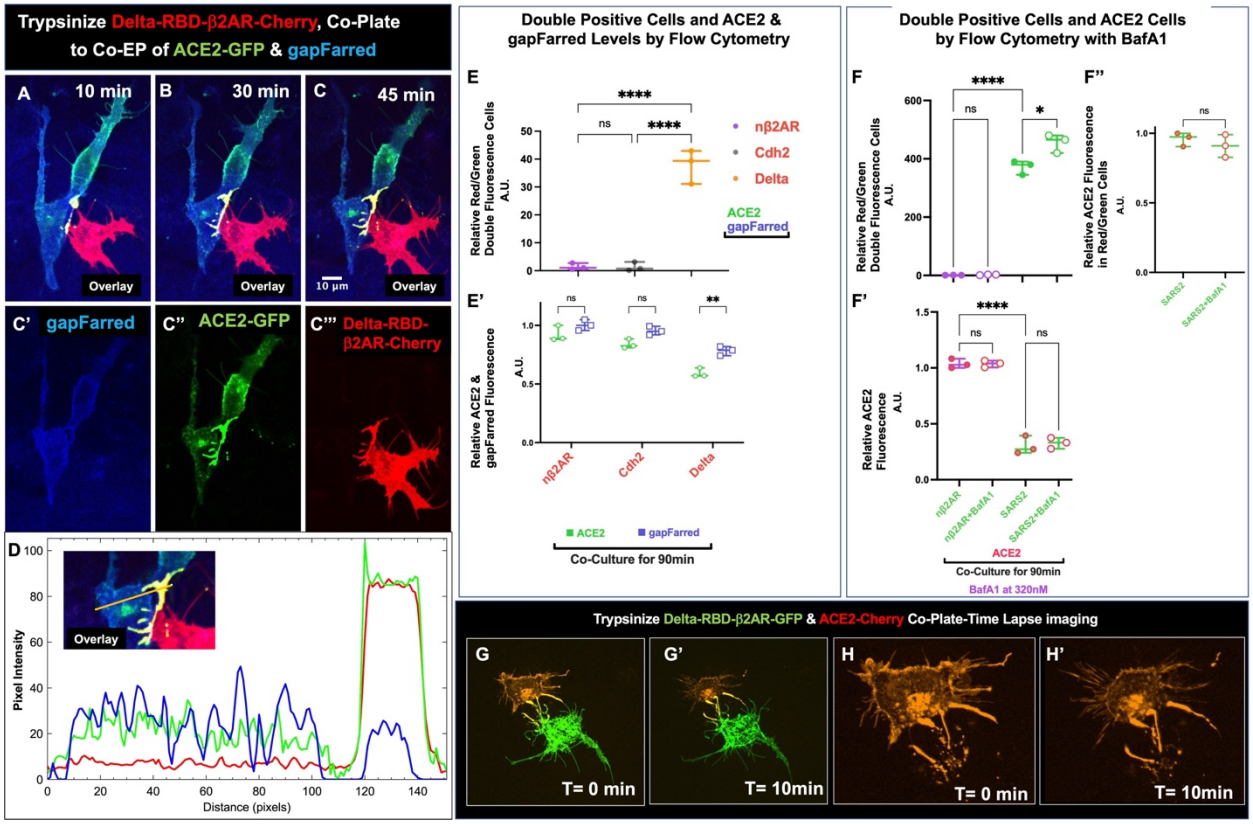

Figure 3: RBD-Cherry affects ACE2-GFP, but not gapFarred (see also Figure S4)
A-C. Confocal images for Co-EP of ACE2-GFP and gapFarred. After 16hrs Delta-RBD-Cherry cells are trypsinized and plated onto ACE2/gapFarred cells. **A-C'''**. In less than 10min after plating, aggregation of both Delta-RBD and ACE2 fusion proteins is observed, but not gapFarred (a M71Q mutation in Cherry was utilized to reduce detection in. Farred spectrum). **D**. Histogram of fluorescence intensity changes in **C-C'''** also reveals aggregation of Delta-RBD and ACE2 fusion proteins, but not the membrane localized protein gapFarred. **E and E'** *DPF Assay*: values in are normalized to controls (Y-axis arbitrary units, A. U.). Flow cytometry analysis of the Delta-RBD plated cells onto double fluorescent ACE2-GFP/gapFarred cells for 90min reveals double fluorescent cells (Red/Green) and a reduction of ACE2 fluorescence (Green) relative to two controls, nβ2AR and Cdh2**.** gapFarred fluorescence did show reduced expression in the context of Delta-RBD, but not to the same extent. **F. F'.** Spinning disk confocal imaging of O/N EPd ACE2-Cherry and Delta-RBD- nβ2AR-GFP cells coplated for 10min, which reveals altered morphology of the red fluorescent cells, but not the green, fluorescent cells (**see also Movies S1A-C**).

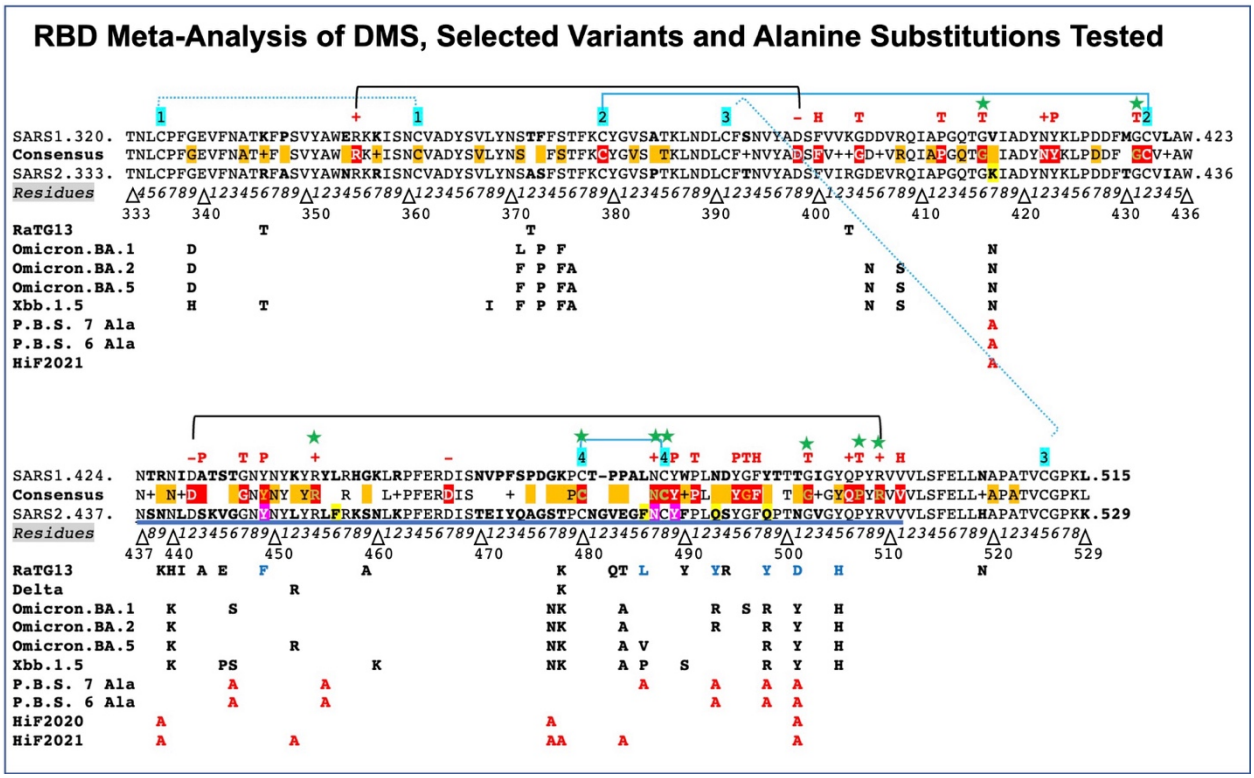

Figure 4: RBD Meta-Analysis of Deep Mutational Screening, Identified Variants, Mutations Tested.
Alignment of SARS1 and SARS2 reveals 74% amino acid identity (145 residues) over the 197 residues of the Receptor Binding Domain (RBD). SARS2 Residue numbers from 333 to 529 are shown. Consensus residues are shown between SARS1 and SARS2**:** The + denoting similar amino acids (15 residues). Eight conserved Cysteine residues denoted by blue numbers and brackets with their proposed linkages: 1-1 (SARS2,336-361), 2-2 (SARS2,379-432), 3-3 (SARS2,391-525), 4-4 (SARS2,480-488) (99). Meta-analysis of Deep Mutational Screening of RBD reveals 29 residues (Red highlighted residues in the consensus) that are retained in 70% of the mutations and thus deemed immutable (25, 41). Orange highlighted residues or shaded regions in the consensus denote where mutations are found in SARS2 at a frequency greater than 0.03% or found in the omicron variant (http://cov-glue-viz.cvr.gla.ac.uk/mutations.php through 2021)(43); two residues are labelled with orange lettering as they reside among the highly conserved red highlighted residues, **Y449** and **G496**). In contrast to the variant residues, 9 red highlighted residues with green lettering, also denoted with green stars (G416, G431, R454, C480, N487, C488, G502, P507, R509) were deemed absolutely necessary, which include one pair of Cysteine residues C480-C488, three Glycines and one Proline that promote Beta turns and two Arginines that likely contribute to RBD structural integrity through interactions with conserved Aspartic Acid residues: black brackets (R355-D398 @2.8Å; D442-R509 @3.1Å; R454-D467 @3.4Å)(100) (100)**. Most of the red highlighted residues promote structural integrity of the RBD domain:** Red highlighted Glycines and Prolines are denoted with a red T, charged residues are denoted with red + or -, and hydrophobic residues are denoted with red H and polar Tyrosine/Serine with a red P.

Receptor Binding Motif (RBM): N437-R510 is underlined in SARS2. Amino acid differences are bolded with 5 Yellow highlighted residues (K417, F456, F486, Q493, Q498, N501) in SARS2 have been modeled by density function calculation to be the key residues that SARS2 tightly bind to ACE2 compared to SARS. Three residues Y449, N487 and Y489, highlighted in purple for SARS2 are predicted to be critical for strong association with ACE2.

RBD Variants Analyzed: RaTG13-RBD (blue residues predicted to be relevant for binding) (54), Delta variant-RBD **B.1.617.2**, Omicron variant-RBD **B.1.1.529 (OM.BA.1)**, Omicron variant-RBD **B.1.1.529.2 (OM.BA.2), OM.BA.5,** and **XBB1.5.**

Multiple Alanine Mutants analyzed to look at critical residues for RBM-ACE2 interaction: Predicted Binding Sites (P.B.S.): K417A, G446A, L455A, F486A, Q493A, Q498A, N501A, alters 4 of the modeled residues (bold), plus two additional residues implicated (28, 42). **P.B.S. 6Ala:** returns F486 within Disulfide Loop 4 (480-488). **HiFrequency variations in 2020 SARS2 variants:** N439A, S477A, N501A **HiFrequency variations in 2021 SARS2 variants**: K417A, N439A, L452A, S477A, T478A, E484A, N501A

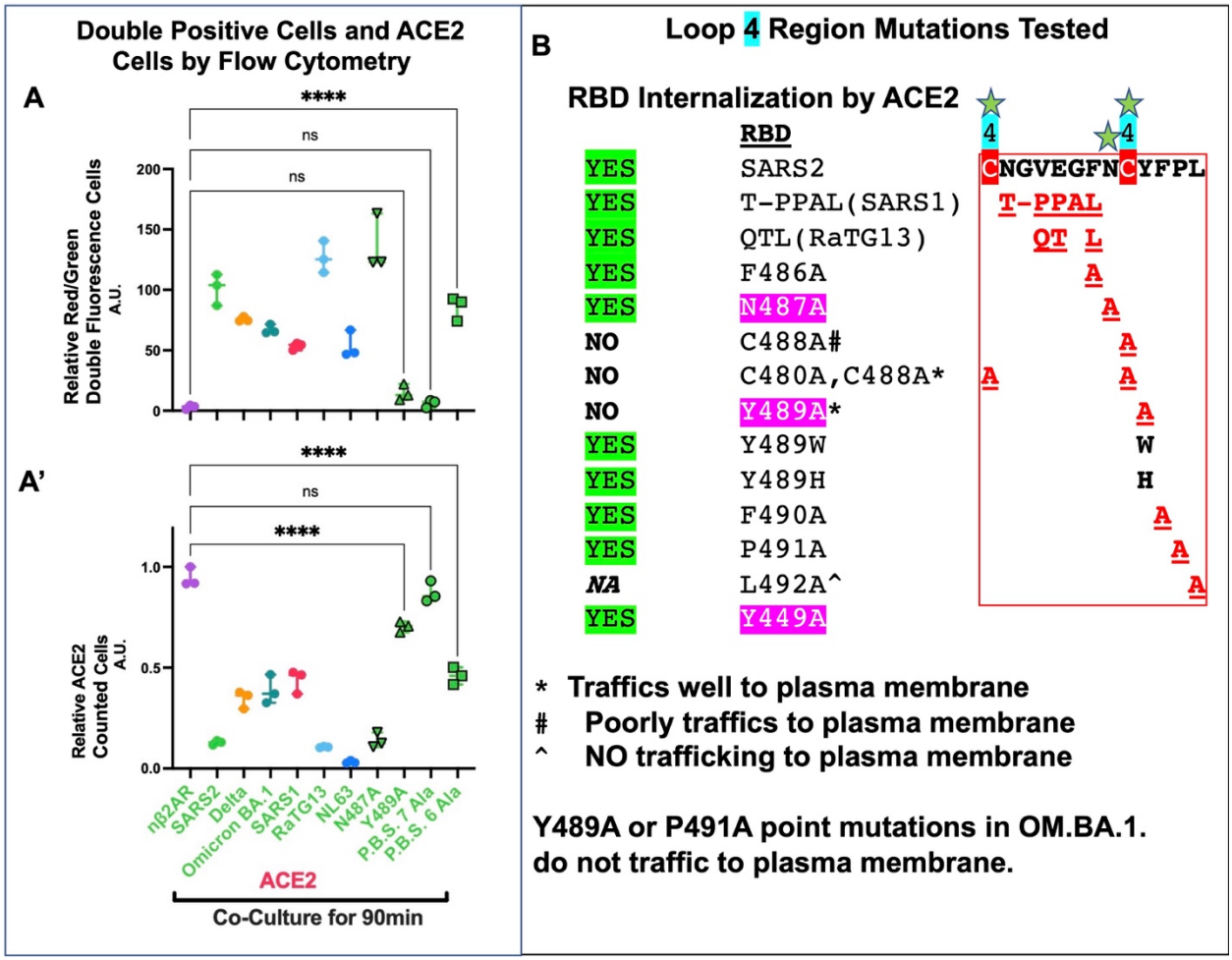

Figure 5: RBD Variants, Orthologues and Loop 4 mutants.
A, A'. RBD Variants and Orthologues: *DPF assay*: values are normalized to controls (Y-axis arbitrary units, A. U.). Three Variants of Concern were tested for their ability to bind and be internalized by ACE2: Delta, OM.BA.1 and OM.BA.2 (not shown) and two RBD orthologues SARS1 and RaTG13 tested. All 5 of these RBDs were internalized by ACE2 in an indistinguishable manner, despite the measured binding of RaTG13 being 1000-fold less than SARS1 and SARS2. Four multiple alanine mutants were also tested (HiF2020, HiF2021, P.B.S. 7Ala, P.B.S. 6Ala). Neither the three-alanine mutation in HiF2020 nor the seven-alanine mutation in HiF2021 had any effect on RBD internalization by ACE2-expressing cells. In contrast, the seven-alanine mutation in P.B.S. did abolish RBD binding. When F486A was reverted (A486F), RBD internalization by ACE2-expressing cells was readily observed. The divergent RBD orthologue in H-CoV-NL63 could function in the in vitro plate binding assay. NL63-RBD (136 residues) is known to bind to similar domains on ACE2 through three non-contiguous RBM regions (**See Figures S5, S6**). Indeed NL63-RBD was very efficient at being internalized by ACE2-expressing cells. Single cell flow cytometry binding assay scoring for reduction of ACE2 levels is inverse proportional to the formation of Red/Green cells. NL63-RBD was more robust at downregulating ACE2 than all other RBDs tested, which also accounts for the reduced number of Red/Green single cells. **B. Loop 4 mutants:** Meta-Analysis from DMS suggested that key Loop 4 Cysteines, N487 and Y489 were critical for RBM interaction

with ACE2. Focusing in on Loop 4, residue substitutions in SARS2 that match SARS1 and RaTG13 are characterizing. In addition, alanine scanning substitutions between F486 to L492 are characterized including Y449A for comparison. In O/N co-plating of constructs or by *DPF assay*, nearly all RBD orthologues, Loop 4 substitutions, and alanine substitutions were internalized by ACE2-expressing cells except for three: C488A and L492A, neither of which showed significant trafficking to the plasma membrane (PM) and Y489A, which robustly trafficked to PM, bound, but was not internalized by ACE2-expressing cells **(Figures S8, S9)**. The single cell flow cytometry binding assay results parallel the qualitative in vitro plate binding assay showing absence of Red/Green cells for P.B.S. mutant and near absence for Y489A. The P.B.S.+F486 nicely shows rescue. Based on cross species conservation, both Y489A and P491A were made in the OM.BA.1 variant, but unlike SARS2, both were unable to traffic to the PM **(Figure S10)**.

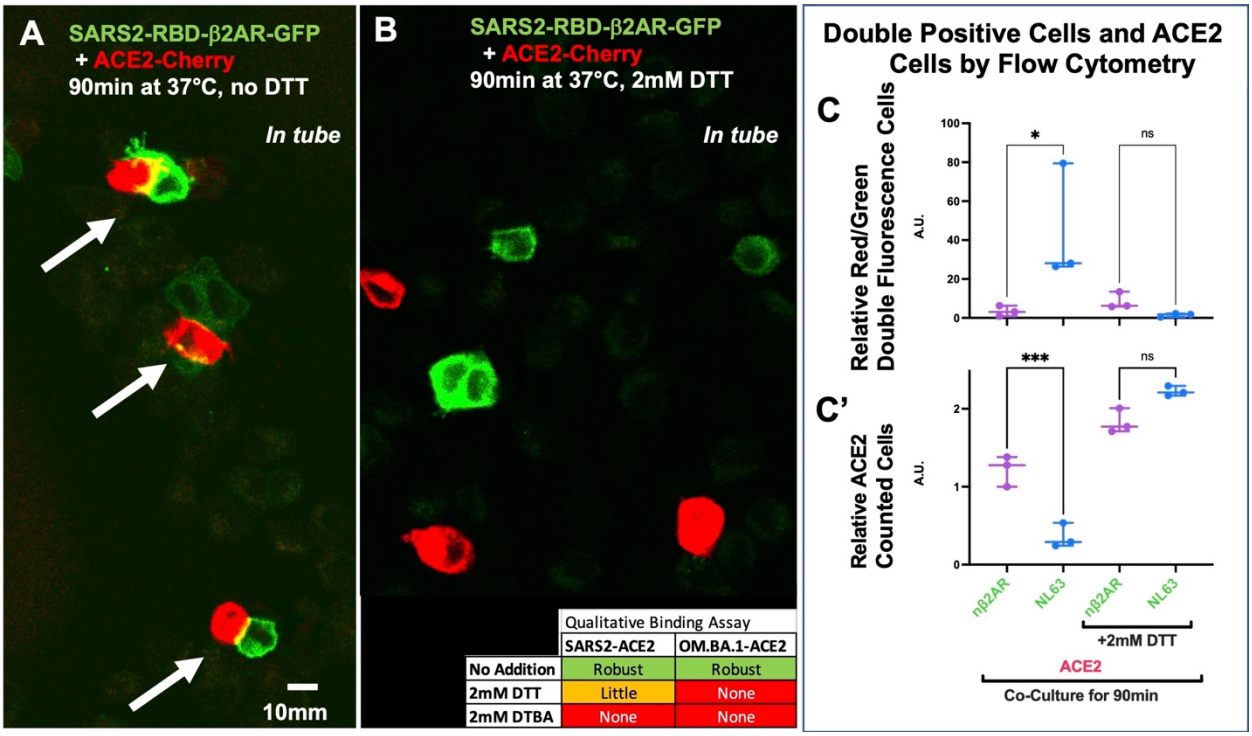

Figure 6: Disulfide Bond Reducing Agents Block RBD-ACE2 Association.
A, B. *Dissociated Cell-based Assay*: SARS2-RBD (Green) or ACE2-Cherry (Red) by low magnification confocal microscopy which affords visualization of 10-15 Green and Red cells. Qualitative analysis of binding was performed after 90min incubation at 37°C for SARS2-RBD. Red/Green doublets (white arrows) were readily observed in at least 3 fields of view. Addition of 2mM DTT limits this interaction where doublets are rarely found. In contrast 2mM DTBA abolished the visualization of doublets (see inset). Both 2mM DTT and 2mM DTBA abolished doublet visualization for OM.BA.1-RBD as well. **C and C'** *DPF assay*: values are normalized to controls (Y-axis arbitrary units, A. U.). NL63-RBD binding to ACE2 was tested by 90min incubation. NL63-RBD shows both increased numbers of Red/Green single cells, but also a decrease in ACE2 expression. By contrast addition of 2mM DTT abolished Red/Green single cells and ACE2 expression levels were not reduced.

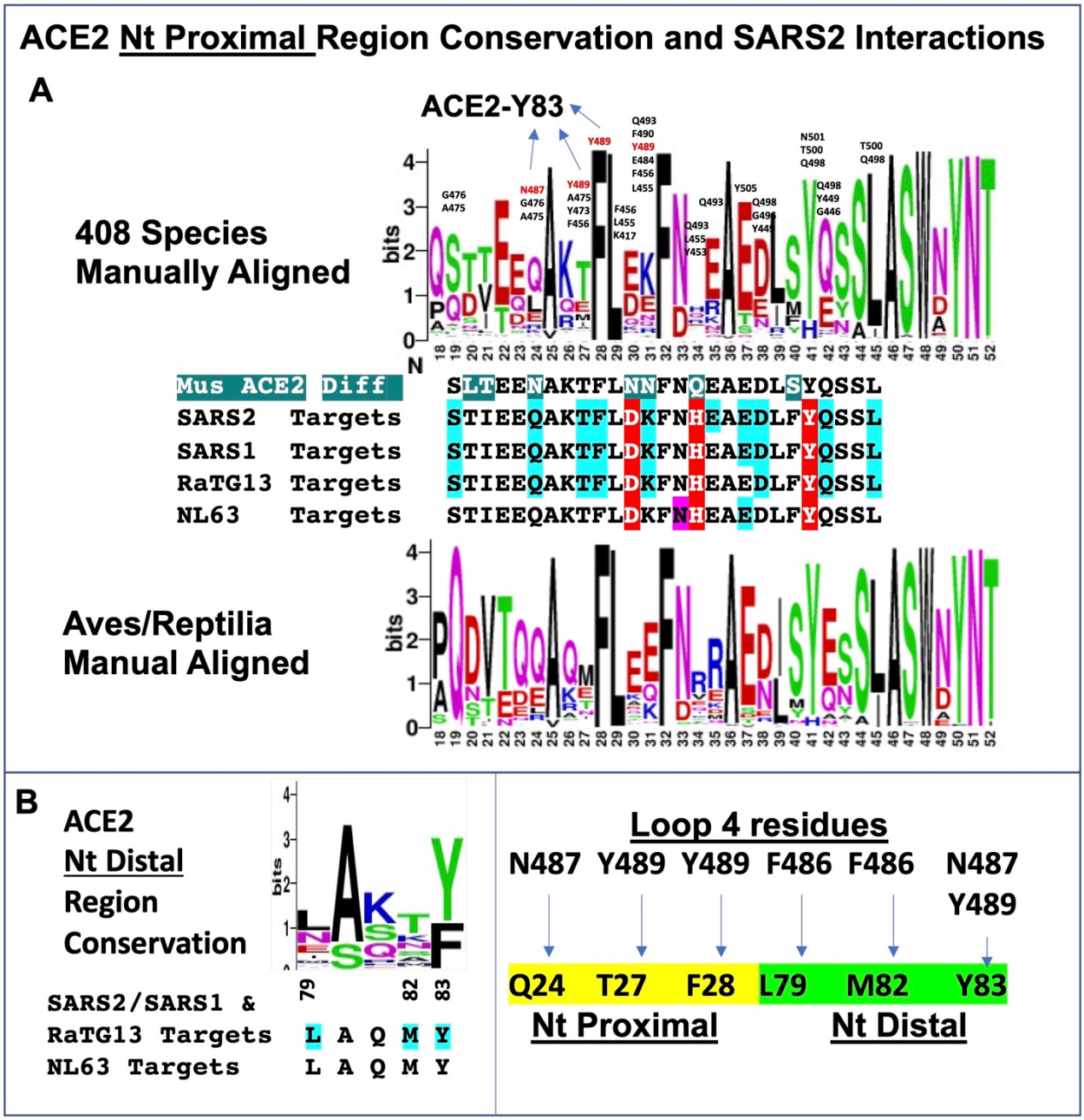

Figure 7: Conservation of ACE2 N-terminus and Predicted SARS2 Contact Sites.
A. ACE2 Nt. Proximal Region. Logo plot of 408 ACE2 species (52) manually aligned starting from residue 18, the last residue before the signal peptide is spliced. ACE2 conserved residues between 22-41 appear to have a periodicity consistent with forming an alpha-helix whereby they would nominally be on the same face. SARS2 point of contacts are predominantly to the non-conserved ACE2 residues 19, 24, 27, 30, 31, 34, 35, 37, 38 and 42; conserved ACE2 residues F28, Y41, and L45. SARS2 contacting residues annotated within Logo plot. SARS2 N487 and Y489 residues in red also interact with ACE2-residue 83 (**See B**.). Logo plot of Aves/Reptilla is shown, which has a divergent amino terminus. Between Logo Plots reveals comparisons for SARS2-RBD, SARS1-RBD, RaTG13-RBD, and NL63-RBD predicted binding sites to human ACE2 (Residues: blue highlighted occur in $^{3}/_{4}$ RBDs, red highlighted occur in $^{4}/_{4}$ RBDs, purple

1857 highlight is NL63 specific). **B. ACE2 Nt Distal Region**. Predicted binding sites of human
1858 ACE2 for SARS2, SARS2, RaTG13 and NL63 (blue highlighted occur in $^{3}/_{4}$ RBDs). SARS2
1859 residue F486 interacts with L79 and M82 whereas, N487 and Y489 serve to coordinate ACE2
1860 protein, Nt amino region and Y83. F486, N487, Y489 are all near disulfide Loop

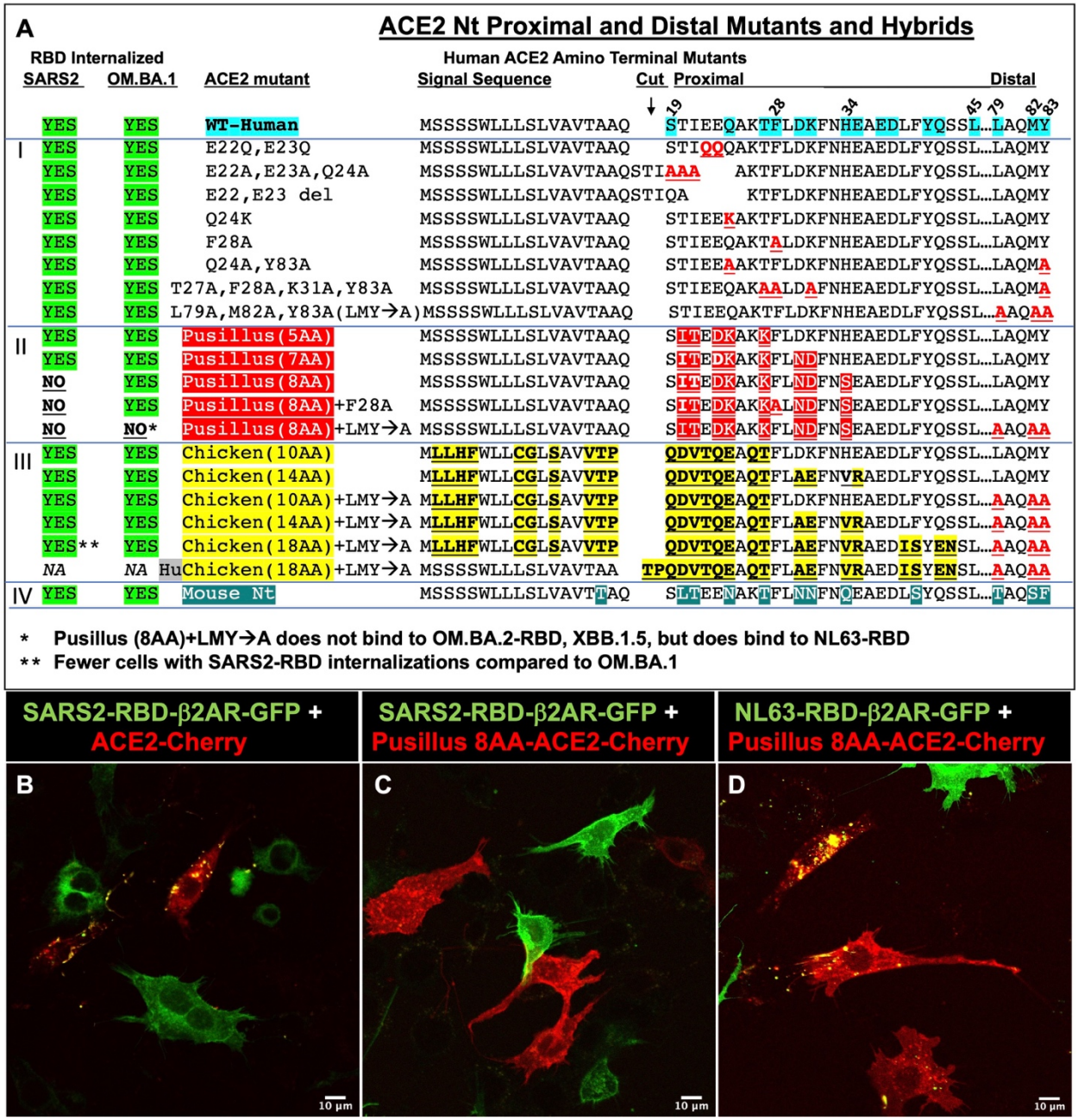

Figure 8: Amino Terminal human ACE2 Mutants

A. Twenty variants of human ACE2 (**Group I, II, III, IV**) were generated with amino-terminal mutations in the first 83 amino acids of the predicted protein. Only one mutant, HuChicken(18AA), did not show red fluorescence at the plasma membrane (PM). When RBD (green) internalization occurred, most of the red cells (ACE2 mutant) had internalized green fluorescence. To score for the absence of binding (as was performed for RBD mutants), at least three touching Red/Green cells had to be observed with no green-RBD internalizations (see **Figure 3**). **Group I mutants**: Based on crystallographic studies showing residues in the WT (wildtype) ACE2 (turquoise) that interact with SARS2-RBD. Mutations carrying T27A, F28A,

K31A, Y83A is based on 4 residues that increase the affinity of RBD to ACE2 (25). No block of Internalization for green fluorescence for red fluorescence cells were observed in all eight variants for both SARS2 and OM.BA.1-RBD expressing cells. **Group II mutants**: Based on *R. pusillus* ACE2 not binding to SARS2-RBD (53, 54). Internalization of SARS2-RBD was observed for mutants containing the 8 amino acid substitutions, but they did not affect OM.BA.1-RBD internalization. Addition of F28A (a key residue in Y489 interaction) had no effect on OM.BA.1-RBD internalization. Only the addition of L79A, M82A and Y83A was able to abolish OM.BA.1-RBD internalization. **Group III mutants**: Based on Chicken ACE2 not binding to SARS2-RBD (53-55). In contrast *R. pusillus* mutants, none of these six mutants were able to abolish Internalization of green fluorescence in red fluorescence cells. It should be noted that NL63-RBD was internalized by both Pusillus 8AA and Pusillus 8AA+LMY→A (**see Figure 9**). **Group IV mutant**: Nt Residues 1-94 are replaced with Mouse Nt residues, which have no effect on binding/internalization of SARS2-RBD or OM.BA.1-RBD. **B-D.** Utilizing LSM510, representative confocal images for co-plated RBD variants and ACE2-Cherry cells. **B.** Internalization of SARS2-RBD byACE2-Cherry cells, **C**. No internalization of SARS2-RBD by Pus8AA-ACE2-Cherry cells, **D**. NL63-RBD still shows internalization by Pus8AA-ACE2-Cherry cells.

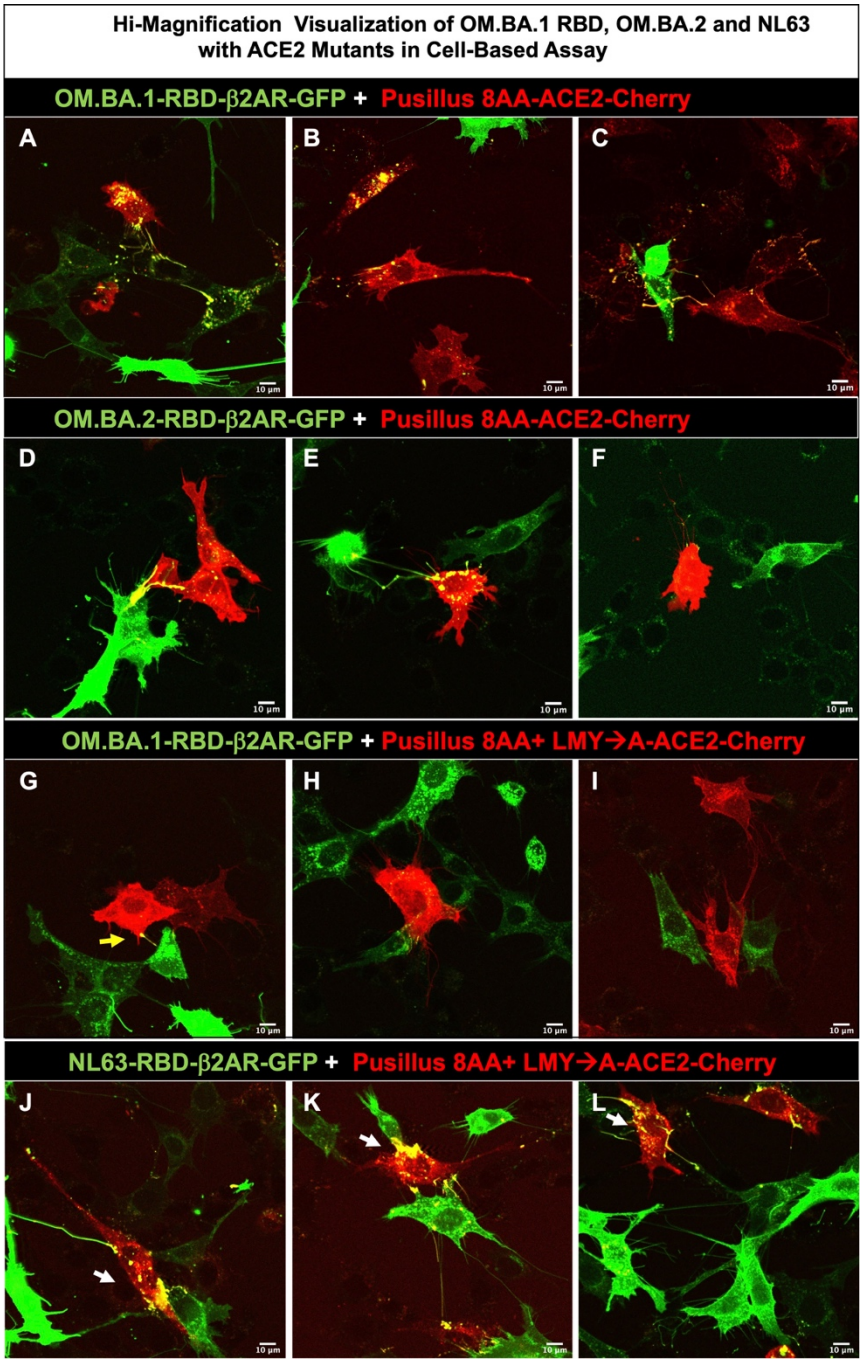

Figure 9: Visualization of OMBA.1 RBD mutants and NL63-RBD in Cell-Based assay with ACE2 mutants.
A-I. Utilizing LSM510, confocal images for co-plated RBD variants and mutants with ACE2-Cherry cells. **A-C**. Three representative images showing OM.BA.1-RBD protein readily internalized into Pus8AA-ACE2 expressing cells. **D-F**. Three representative images showing OM.BA.2-RBD protein readily internalized into Pus8AA-ACE2 expressing cells. **G-I.** Three representative images showing OM.BA.1-RBD protein **not** internalized by Pus8AA+LMY→A-ACE2-expressing cells. **J-L.** In contrast, three representative images showing NL63-RBD protein readily internalized by Pus8AA+LMY→A-ACE2-expressing cells.

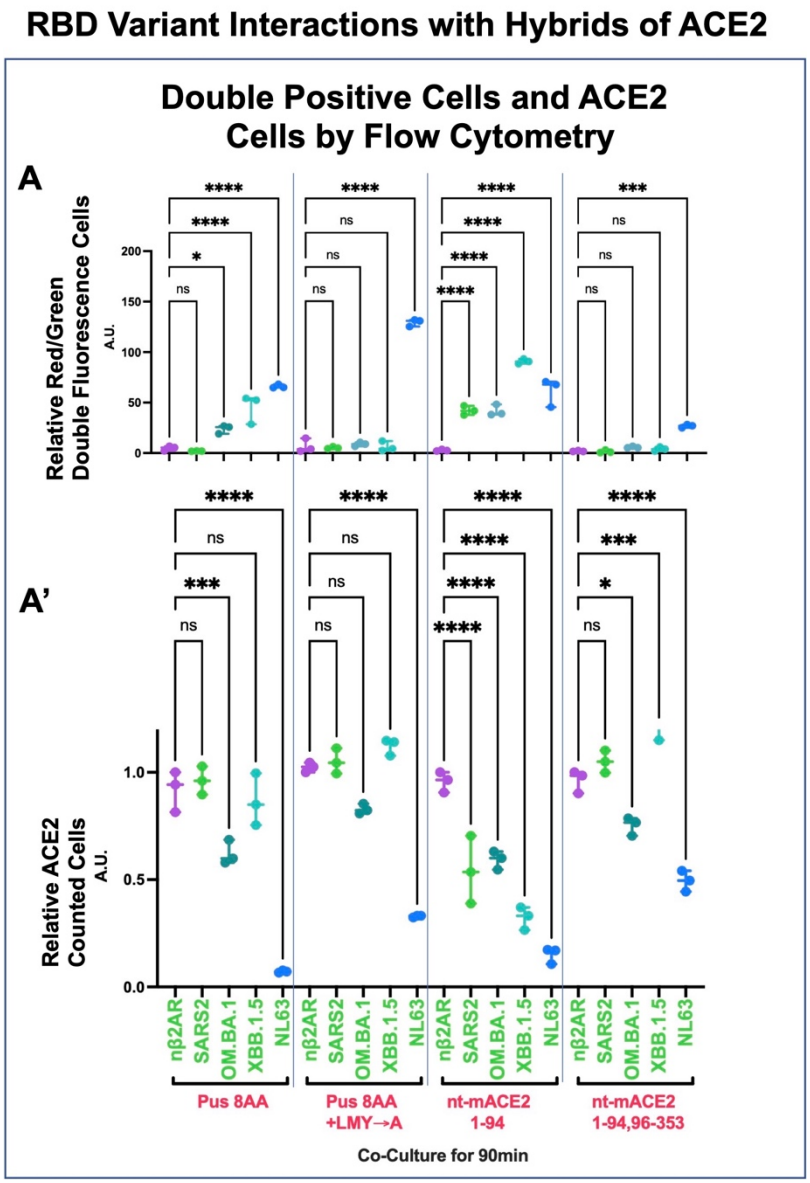

Figure 10: RBD Variants interactions with Mutated ACE2

A. Results from visual inspection for Pus8AA, Pus8AA+LMY→A and Nt-Mouse residues 1-94 (**Figure 8**) were further quantified by the *DPF assay* for nβ2AR, SARS2-RBD, OM.BA.1-RBD, XBB.1.5-RBD and NL63-RBD. In addition, a near complete swap of human residues 1-353 with equivalent region of mouse residues. NL63-RBD show double fluorescence in all four ACE2 mutants and a reduction of ACE2 fluorescence, revealing all ACE2 constructs have the capacity to function. SARS2 variants show differences (**see Figure 9 and Data File S2**). Values in **A and A'** are normalized to controls (Y-axis arbitrary units, A. U.). *For Pus8AA*: only SARS2-RBD shows no binding and hence no double fluorescence (1.92±0.17). *For Pus8AA+LMY→A*: SARS2-RBD, OM.BA.1-RBD, show no binding (5.23±0.99) and (8.75±1.94), respectively. *For Nt-Mouse residues 1-94*: All variants show binding/double fluorescence (58.22±28.20). *For Nt-Mouse 1-94,96-353:* All variants show **no** binding/double fluorescence (3.71±2.14). **A'**. The ACE2 levels showed variability for XBB.1.5-RBD, as it does not downregulate Pus8AA (a loss

of 13.3%±12.1%) as was previously shown for ACE2 but does downregulate the Nt-Mouse residues 1-94 ACE2 chimera (a loss of 67.8%±5.3%). To date, XBB.1.5 is the only variant where binding **can be** decorrelated from an ACE2 decrease in level of expression. GraphPad Prism 9.3.1 used to generate **A and A'**.

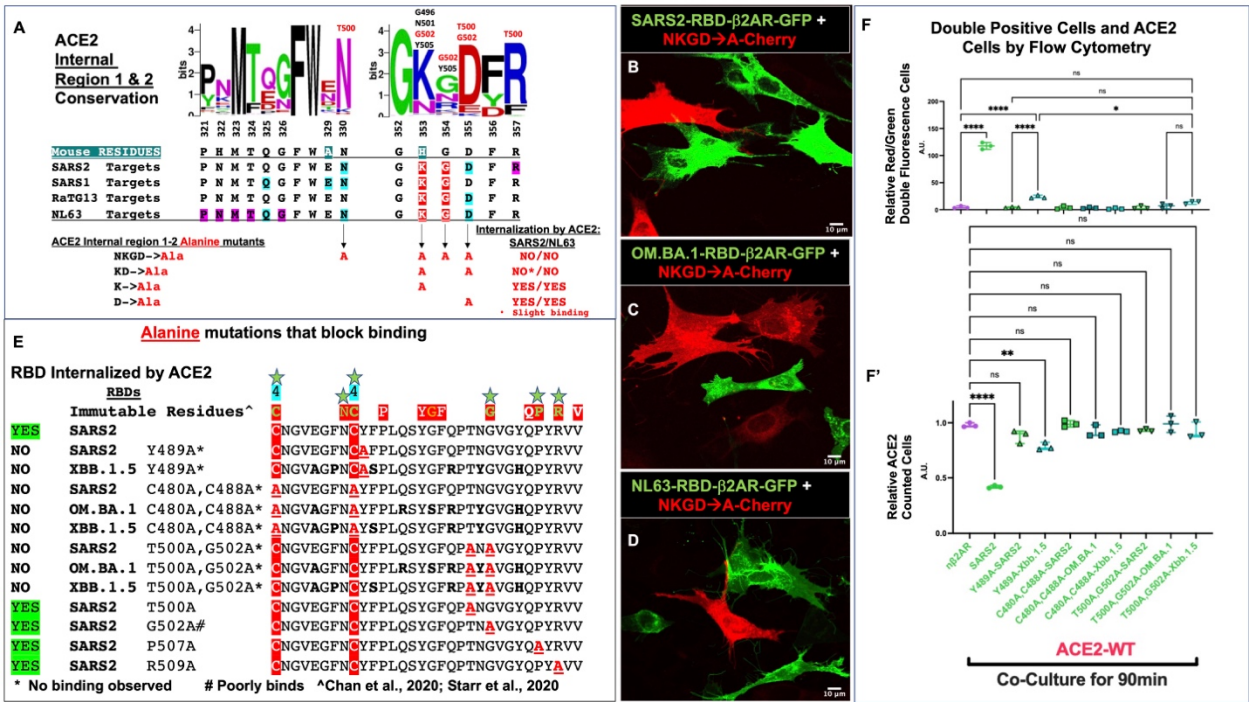

Figure 11: Internal human ACE2 mutants and RBD interaction mutants
A. ACE2 Internal Region. Predicted binding sites of human ACE2 for SARS2, SARS2, RaTG13 and NL63 (Residues: blue highlighted occur in $^{3}/_{4}$ RBDs, red highlighted occur in $^{4}/_{4}$ RBDs, purple highlight is SARS2 specific). ACE2 mutants tested based on conserved predicted binding sites: 1) N330A, K353A, G354A, D355A (NKGD→A); 2) K353A, D355A (KD→A); 3) K353A; 4) D355A. Both SARS2 and NL63 RBDs were tested in two ways: cotransfection or separate transfections followed by overnight co-plating (**see Supplemental Figure S14**); Co-transfection of RBD-β2AR-GFP and ACE2-Cherry, which could interact, typically internalized membrane distribution of both proteins. Mutant NKGD→A, which poorly traffics to the plasma membrane, shows no binding to either SARS2 or NL63 RBDs, KD→A shows no binding to NL63 RBD, but some binding to SARS2-RBD without internalization. By contrast, the single K353A and D355A mutants both revealed binding and internalization of both NL63 and SARS2 RBDs. **B-D.** Utilizing LSM510, representative confocal images for co-plated RBD variants and mutated NKGD→A ACE2-Cherry cells. Neither **B.** SARS2-RBD, **C**. OM.BA.1-RBD, nor **D**. NL63-RBD show internalization into mutant ACE2-Cherry cells. **E.** Alignment of different SARS2/OM.BA.1/XBB.1.5 mutants and that were tested for block binding (**see Supplemental Figure S13**); the region consists of residues 480-511 from SARS2. Bolded residues differ from SARS2. Bolded Red and underlined residues are alanine mutations. Mutants tested were Y489A and the double mutant C480A, C488A on SARS2, OM.BA.1, XBB.1.5 that previously showed no binding. In addition, the T500A, G502A double mutant, which is predicted to bind to KGD region of human ACE2. Visual observations were noted and quantified. **F and F'.** *DPF assay* quantification for mutants that did not predict binding by visual inspection. Only XBB.1.5-Y489A-RBD showed slight binding as some double positive Red/Green cells could be observed (23.67±2.87) and some loss of ACE2-Cherry fluorescence is shown (21.7%±3.4%). Values in **F and F'** are normalized to controls (Y-axis arbitrary units, A. U.), **see Data File S2**. GraphPad Prism 9.3.1 used to generate **F and F'**.

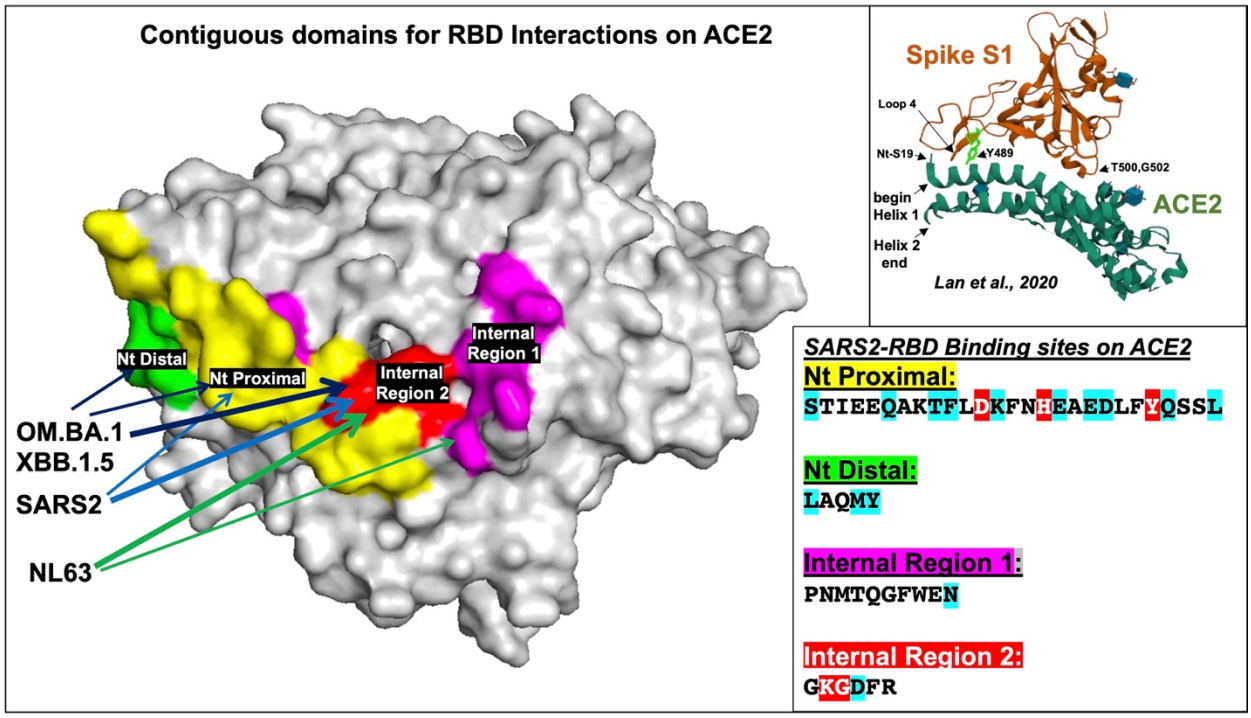

Figure 12: Proposed interpretation of RBD interactions on ACE2 structure. Space filling model of ACE2 structure from pdb_6M0J (27) modified by highlighting interactions for both SARS2 and NL63 RBDs: Nt proximal (yellow), Nt distal (green), and Internal regions 1 (purple) and 2 (red). SARS2-RBD does not bind/internalize if *either* Nt proximal or Internal region 2 (K353, D355) are mutated. OM.BA.1 and OM.BA2-RBDs are not bond/internalized if *either* mutation in both Nt proximal and distal ACE2 or Internal region 2 (K353, D355). NL63-RBD requires Internal region 2 (K353 and D355) for both binding/internalization. **Top Inset** shows crystal structure of Spike S1(burgundy) and RBM of ACE2 (green) modified from Lan et al, 2020. ACE2 residues 19-52 are represented by Helix 1 and 55-81 by Helix 2. Y489 residue shows a main interaction with Helix 1. N487 within Loop 4 interacts with Q24 (not shown). **Bottom Inset** shows **RBD** interactions within the four domains (**see Figures 7, 11**) (residues with blue highlights are predicted binding sites that occur in ¾ of SARS2, SARS1, RaTG13, and NL63-RBDs (26-28); residues with red highlights are predicted binding sites in all 4 RBDs). The RBD interaction data taken together suggest that Internal region 2 binding for SARS1/SARS2/RaTG13 is weak and requires Nt proximal and distal contacts for stabilization (dark blue, light blue arrows), whereas NL63 has additional contacts in the Internal region 1 (green arrows) that supports binding to Internal region 2 (thick arrows). The ability of Y489A to nearly abolish SARS2-RBD binding to ACE2 suggests that none of the domains by themselves have strong binding to ACE2. Overall, the data suggests that Internal region 2 is critical for internalizations of RBDs.

Supplemental information inventory:

Supplemental Figures and legends:

S1 (relates to Figure 1): Internalized Membrane of RBD-β2AR-GFP within ACE2-Cherry Cell Binds β2AR Ligand.

S2 (relates to Figures 1 and 2): Flow cytometry counts of double positive cells and ACE2 levels in control experiments.

S3 (relates to Figures 1 and 2): Neither the non-membrane bound SARS2-RBD nor XBB1.5-RBD reduce ACE2-Cherry fluorescence.

S4 (relates to Figure 3): RBD-Venus affects ACE2-Cherry expression, but not gapTeal.

S5 (relates to Figure 4): Conservation of Disulfide Loop 4 Residues.

S6 (relates to Figures 4 and 5): NL63-RBD Alignment to SARS2-RBD.

S7 (relates to Figures 3 and S3): RpYN06 Alignment to SARS2 and RaTG13-RBDs.

S8 (relates to Figures 4 and 5): Flow cytometry counts of double positive cells and ACE2 levels for RBD mutants.

S9 (relates to Figure 5): Hi-Magnification Visualization of SARS2-RBD Mutants in Cell-Based Assay.

S10 (relates to Figures 4 and 5): Low-Magnification Visualization of SARS2 and OM.BA.1-RBD mutants in Cell-Based assay.

S11 (relates to Figure 8): RBD mutations tested with Pus8AA.

S12 (relates to Figures 8 and 9): AlphaFold predictions of the first two helices of ACE2 for WT, Pus7AA, Pus8AA and Pus8AA+LMY→A.

S13 (relates to Figure 8): Mouse vs Human ACE2 among the first 357 residues.

S14 (relates to Figure 10): Co-EP with RBD mutations and ACE2.

S15 (relates to Figure 10: Co-EP with RBD variants and ACE2 mutants.

S16 (relates to Figure 11): KGD containing peptides do not antagonize RBD binding to ACE2-Cherry.

S17 (relates to Figure 12): Proposed interpretation of RBD interactions on ACE2 structure with demarcated domains.

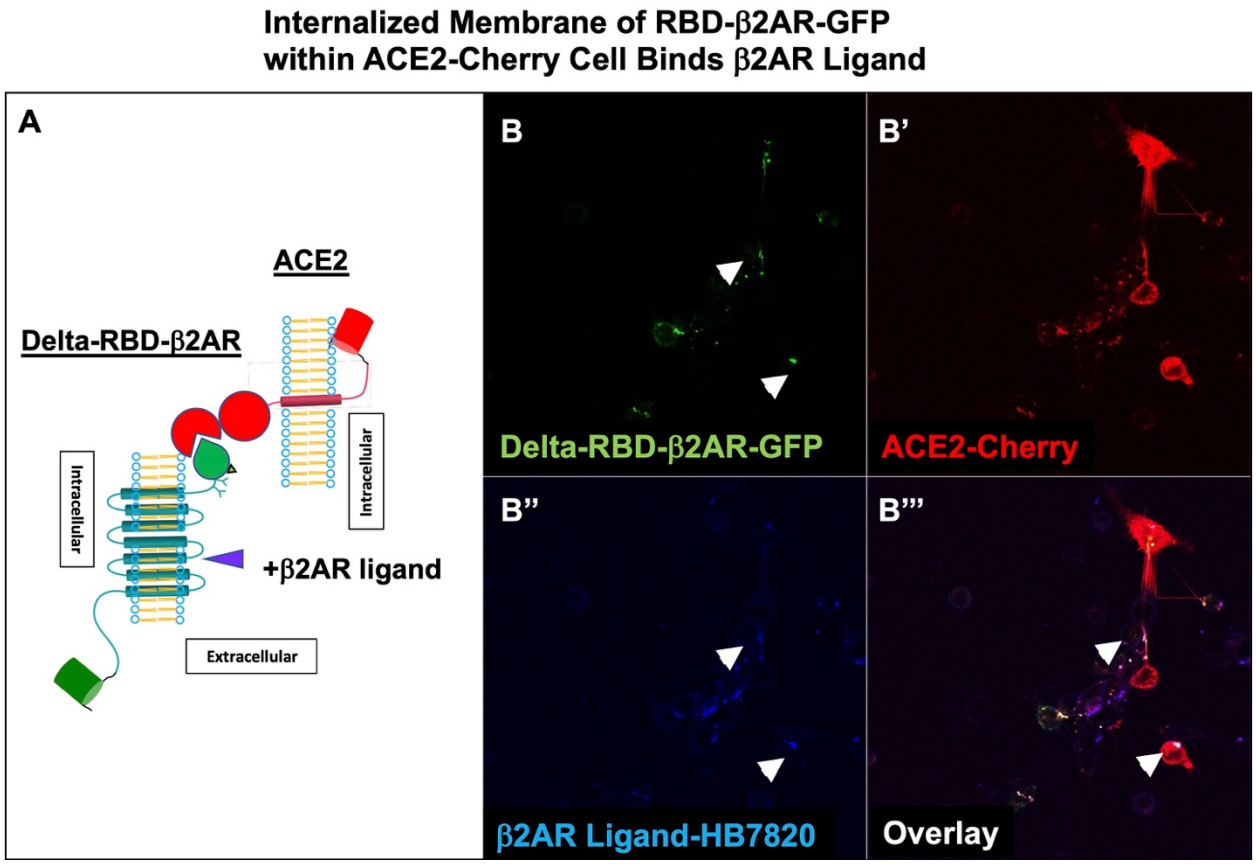

Figure S1: Internalized Membrane of RBD-β2AR-GFP within ACE2-Cherry Cell Binds β2AR Ligand.

A. Schematic of protein interaction and a β2AR ligand binding**. B-B'''.** Overnight Delta-RBD-β2AR-GFP co-cultured with ACE2-Cherry cells. β2AR fluorescent ligand HB7820 (70nM, 1:500 dilution of 35μM stock) added to media for 10min and imaged. **B**. Green fluorescence from Delta-RBD-β2AR-GFP. **B'.** ACE2-Cherry expressing cells show Delta-RBD-β2AR-GFP internalized along with ACE2-Cherry. **B''.** β2AR ligand HB7820 fluorescence. **B'''.** Overlay shows β2AR ligand HB7820 bound to Delta-RBD-β2AR-GFP within ACE2 expressing cells (white arrowheads).

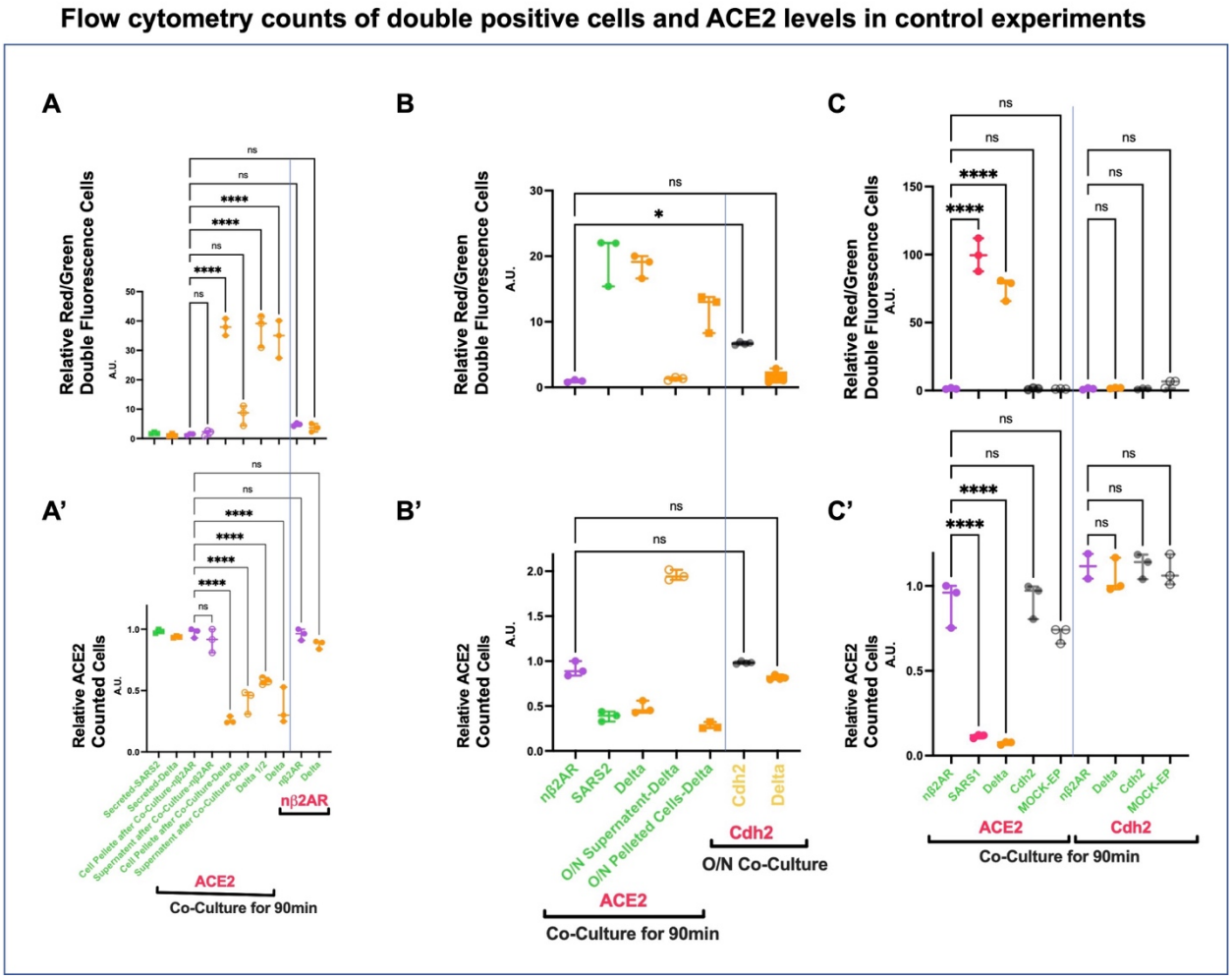

Figure S2: Flow cytometry counts of double-positive cells and ACE2 levels in control experiments.

A-C *DPF assay*: Values are normalized to controls (Y-axis arbitrary units, A. U.). Overnight (O/N) transfection and flow cytometry counts of Co-plating GFP or Venus expressing cells at 90min with RBD or Cdh2 with ACE2-Cherry, nβ2AR-Cherry, or Cdh2-Cherry expressing cells followed by trypsinization. **A'-C'.** *DPF assay*: Values are normalized to controls (Y-axis arbitrary units, A. U.). relative to controls. Green labeling represents GFP fusion proteins. Red labeling represents Cherry fusion proteins. Yellow labeling represents Venus fusion proteins. **A and A'.** Secreted-SARS2 or Secreted-Delta represents the non-transmembrane RBD expressing cells. No double fluorescent cells (green and red) were observed. Supernatants were collected separately from attached cells for nβ2AR or Delta-RBD-nβ2AR (Delta) expressing cells after co-culturing with ACE2-Cherry for 90min. No double fluorescent cells (green and red) were observed in the supernatant relative to control. Only attached cells showed double fluorescent cells for Delta-RBD-β2AR as expected. **B and B'.** SARS2-RBD-nβ2AR (SARS2) shows indistinguishable results to Delta: more double fluorescent cells relative to controls and loss of ACE2-Cherry fluorescence. Supernatant from overnight (O/N) growth of electroporated Delta cells do not yield double fluorescent cells when plated onto ACE2-Cherry cells but attached cells that were incubated with ACE2-Cherry yielded double fluorescent cells and loss of ACE2-

2035 Cherry fluorescence. O/N incubation of Cdh2-Venus with Cdh2-Cherry leads to double
2036 fluorescent cells (yellow and red), but not Delta-nβ2AR-Venus with Cdh2-Cherry. No loss of
2037 Cdh2-Cherry fluorescence is observed with either incubation. **C and C'.** nβ2AR, SARS1-RBD-
2038 nβ2AR (SARS1), Delta, Cdh2, or Mock-EP are co-plated with ACE2-Cherry for 90min. Only
2039 SARS1 and Delta show double fluorescence and loss of ACE2-fluorescence. In a separate set of
2040 experiments, nβ2AR, Delta, Cdh2 and Mock-EP are co-plated with Cdh2-Cherry for 90min. No
2041 double fluorescence for any of these four incubations, nor loss of Cdh2-Cherry fluorescence, was
2042 observed. It should be noted that Cdh2-Venus/Cherry double fluorescence was not observed in
2043 90min compared to the O/N co-plating.
2044
2045
2046

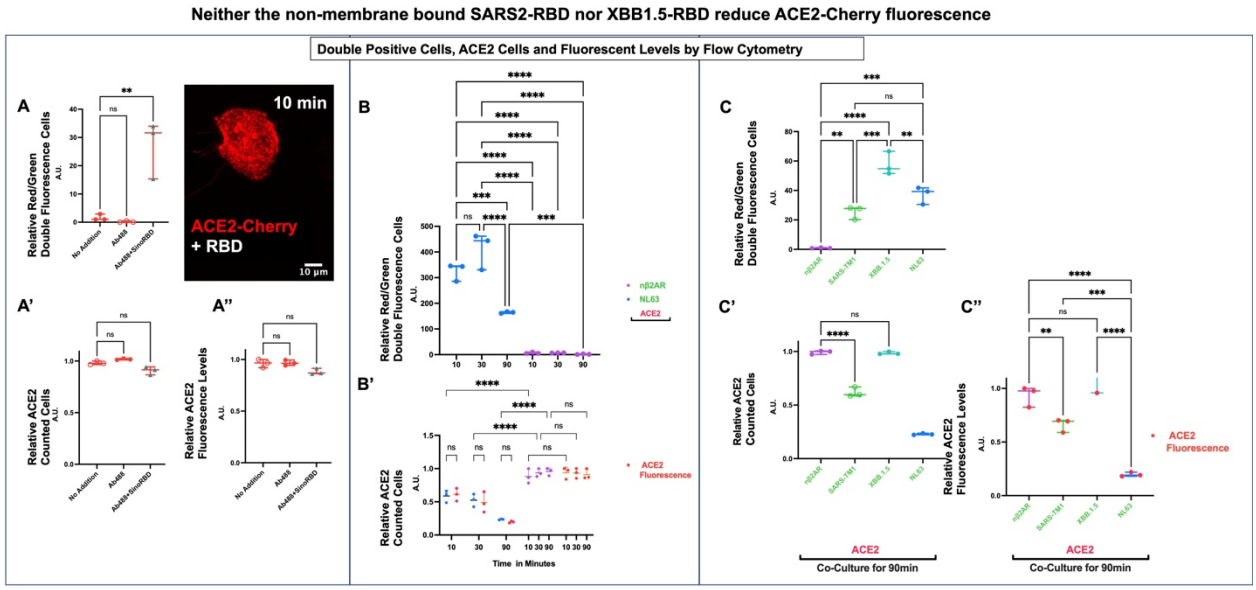

Figure S3: Neither the non-membrane bound SARS2-RBD nor XBB1.5-RBD reduce ACE2-Cherry fluorescence.

A-A''. *DPF assay*: values in are normalized to controls (Y-axis arbitrary units, A. U.). This data makes is also shown in **Figure S16**. **A**. Double fluorescence after 90minute incubation of ACE2-Cherry cells with Ab488 (1µg/4mls of Goat-anti-HIS-Tag-Alexa488 Goat antibody [R&D#: IC050G]) and with or without Sino-RBD, purified His tagged-RBD protein (60ng/4mls of 2019-nCoV-HisTag-RBD [Cat#40592-V08H; 234 residues, R319-F541]). **A'** ACE2-Cherry cells with Ab488 or Ab488+Sino-RBD show no changes in fluorescence cells. **A''** ACE2-Cherry only cells also show no changes in fluorescence values. **Inset,** Shows ACE2-Cherry cell plus 240ng/5mls Sino-RBD. Punctate fluorescence is observed on the cell surface. **B.** Double fluorescence observed for NL63-RBD at 10min, 30min and 90min interaction with ACE2-Cherry plated cells. **B'.** ACE2-Cherry cells show reduced expression overall as well as cells highly expressing cells (red data points) when in contact with NL63 within 10min**.** Again nβ2AR controls show no difference. **C.** Double fluorescence is observed for SARS2-TM1, XBB.1.5-RBD and NL63-RBD 90min interaction with ACE2-Cherry plated cells. **C'.** ACE2-Cherry cell fluorescence is reduced for SARS2-TM1 and NL63-RBD interactions, but not for XBB.1.5-RBD. **C''.** ACE2-Cherry cells show reduced expression for highly expressing cells (red data points) in contact with SARS2-TM1 and NL63-RBD interactions, but not for XBB.1.5-RBD.

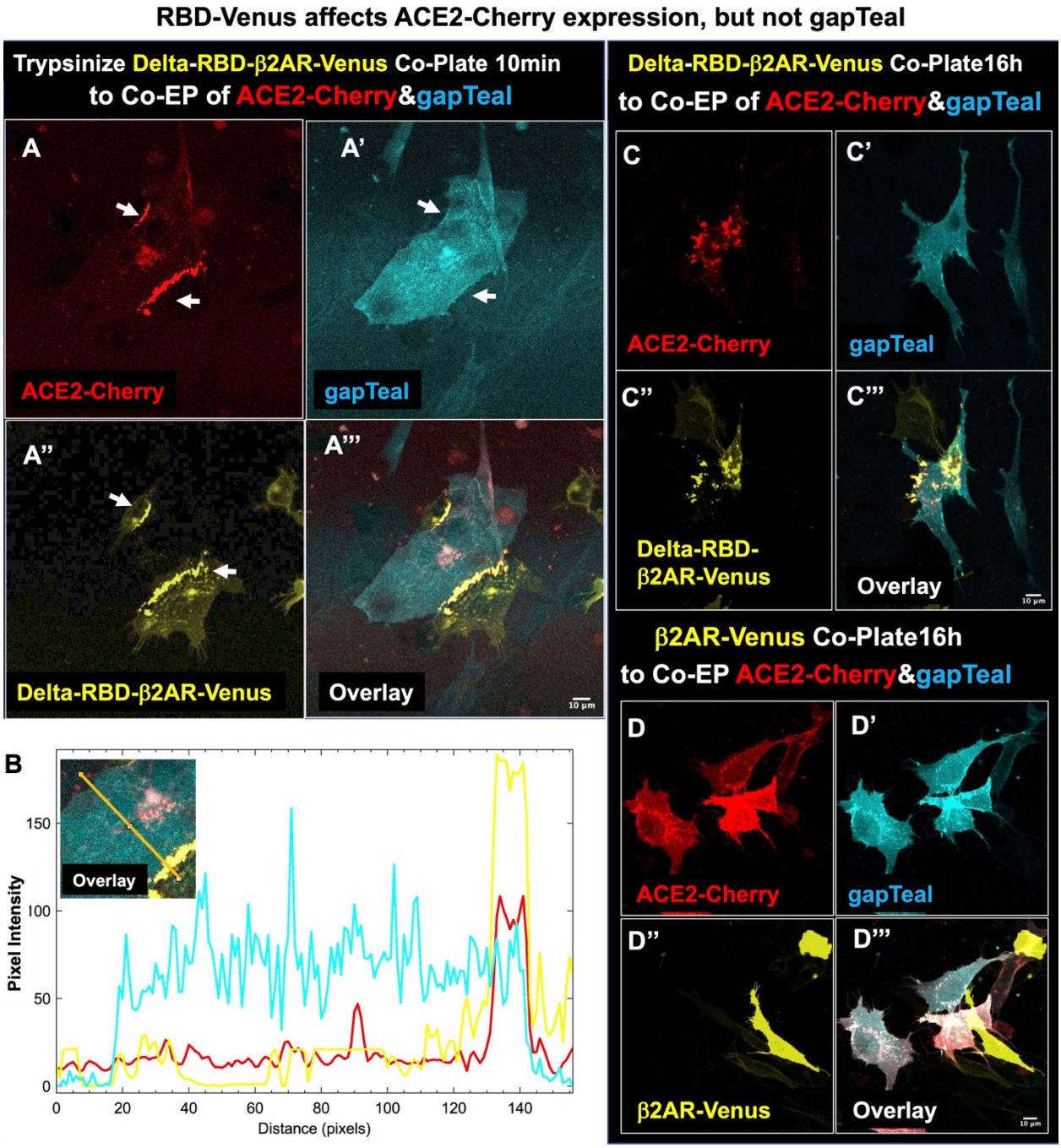

Figure S4: RBD-Venus affects ACE2-Cherry expression, but not gapTeal.
A-A'''. Confocal images for Co-EP of ACE2-Cherrry and gapTeal co-plated with Delta-RBD-β2AR-Venus cells from acute trypsinization. **A-A'''**. In less than 30min, aggregation of both Delta-RBD and ACE2 fusion proteins is observed (white arrows). **B**. Histogram of fluorescence intensity changes also reveals aggregation of Delta-RBD and ACE2 fusion proteins, but not the membrane localized protein gapTeal. **C-C'''.** 16hr co-plating also shows gapTeal stays membrane-bound despite all the ACE2-Cherry fusion protein found in aggregates. **D-D'''.** Co-EP of ACE2-Cherrry and gapTeal co-plated O/N with β2AR-Venus cells. No aggregation of β2AR-Venus and ACE2-Cherry protein.

Conservation of Disulfide Loop 4 Residues

11 known β-RBD Cys480-Cys488 Loop 4 and known Kd of RBD-ACE2

1)SARS2	PCNGVEGFNCYFPL	16nM*
2)RaTG13	PCNGQTGLNCYYPL	3.86uM**
3)P5L	PCNGQVGLNCYYPL	no data
4)MP789	PCNGVEGFNCYFPL	no data
5)SARS1	PCT-PPALNCYWPL	58nM*
6)LYRal1	PCT-PPAFNCYWPL	91nM*
7)Rs7327	PCT-PPAFNCYWPL	63nM*
8)Rs4231	SCS-AIGPNCYNPL	69nM*
9a)Rs4084	SCS-AVGPNCYNPL	85nM*
9b)RsSHCO14	SCS-AVGPNCYNPL	29nM*
10)RShSTT200	PCS-VEGPDCYYPL	no data
11)RSYN04	GCN-PSEADCYWPL	15uM^

α-RBD + variant Cys550-Cys577 Loop 3 and known# Kd of RBD-ACE2

1)NL63	C...CFSTVEVPGSCNFPL	35nM#
2)NL63,N578Y	C...CFSTVEVPGSCYFPL	~17nM^^

*Chan et al., 2021;** Liu et al., 2021; ^Zhou et al., 2021
#Wu et al., 2011;^^ Li et al, 2007

Figure S5: Conservation of Disulfide Loop 4 Residues.
A curious finding by Zhou and colleagues found that *Rhinolophus pusillus* virus RpYN06 had strong homology the SARS2 virus but did not contain the disulfide bridge homology between Cysteine-480 to 488 (Loop 4) (**See Figure S7**); The *R. pusillus* RpYN06-RBD did not bind to ACE2 (41). The Loop 4 region that lies within the SARS2-RBM is well conserved among eleven betacoronavirus species, eight of which are known to bind to ACE2 (8, 21, 22, 40, 41, 43, 44**)**. The only homology between the alpha coronavirus NL63-RBD and SARS2-RBD overlaps the Loop 4 region (**See Figure S9**). An N578Y mutation can increase the NL63-RBD binding affinity to ACE2 despite this domain residing outside of the three RBMs. Conserved Cysteines that form disulfide bridges are highlighted in red, Prolines are highlighted in dark blue, Glycines (alpha helical breakers) are highlighted in yellow, and conserved Asparagines, Tyrosines, and Leucines are highlighted in green.

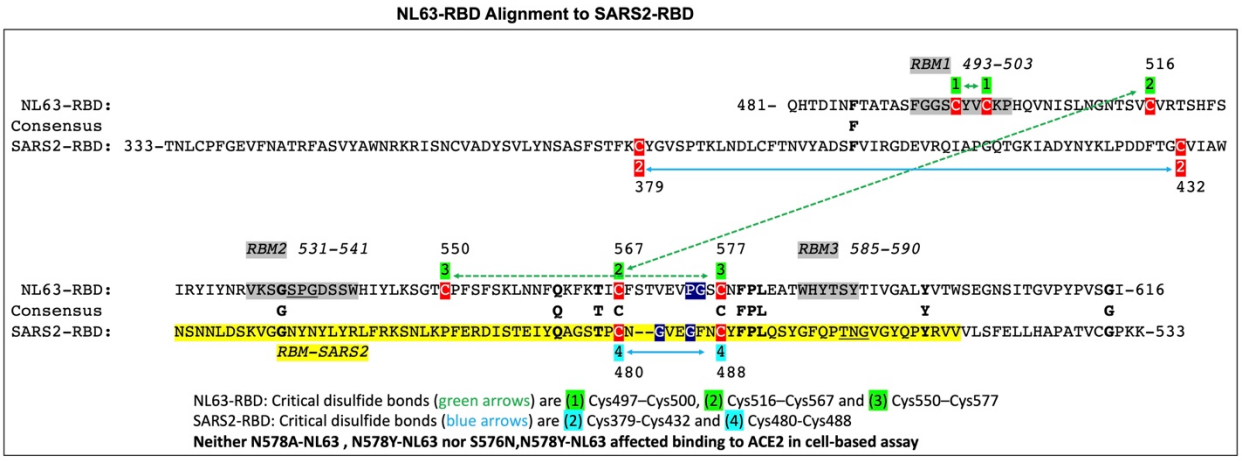

Figure S6: NL63-RBD Alignment to SARS2-RBD.
Both NL63-RBD and SARS2-RBD domains both bind and are internalized by ACE2 expressing cells. NL63-RBD contains three RBM domains (grey highlighted regions) and three predicted disulfide bridges (green numbers and arrows), compared to one RBM for SARS2-RBD (yellow highlighted region) and two critical disulfide bridges (blue numbers and arrows). Manual alignment between 136 residue NL63-RBD and 197 residue SARS-RBD. Consensus sequence reveals only 11 amino acid identities. Four of these residues reside in a 5-amino acid stretch that overlaps Loop 4 region within the RBM of SARS2 (40). Loop 4 alignment in Figure S2 identifies conserved Glycines in Prolines between Cysteine residues. These residues (dark blue highlights) are also found in NL63 and near the conserved CxFPL. It is worth noting that the N578Y mutation in NL63 bringing the identity to 5/5 identities CNFPL, doubles the binding affinity to ACE2 (**see Figure S2**). Residues 535-537(SPG) in NL63 and 500-502 (TNG) in SARS2 are underlined and proposed to interact with critical ACE2 residues K353 and D355.

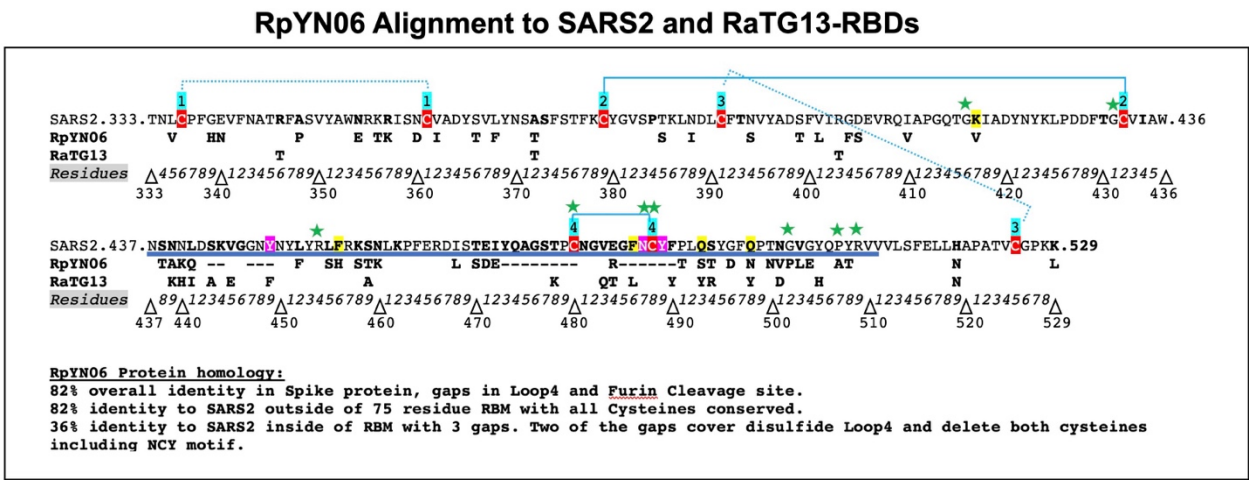

Figure S7: RpYN06 Alignment to SARS2 and RaTG13-RBDs.
The RaTG13 betacoronavirus is one of the most highly homologous betacoronaviruses to SARS2 sharing 96% overall identity including the RBM region (residue differences in brown). By contrast, RpYN06 has 95% nucleotide identity over the 30kb colinear genome, but its RBM region has lost nucleotide homology to SARS2 with the best stretch having 22/57 residues conserved (residue differences in blue). It is notable that two of the eight cysteines are not conserved (highlighted in red), and both make up disulfide Loop 4. Loss of RBM homology correlates with loss of ACE2 binding (41, 42)

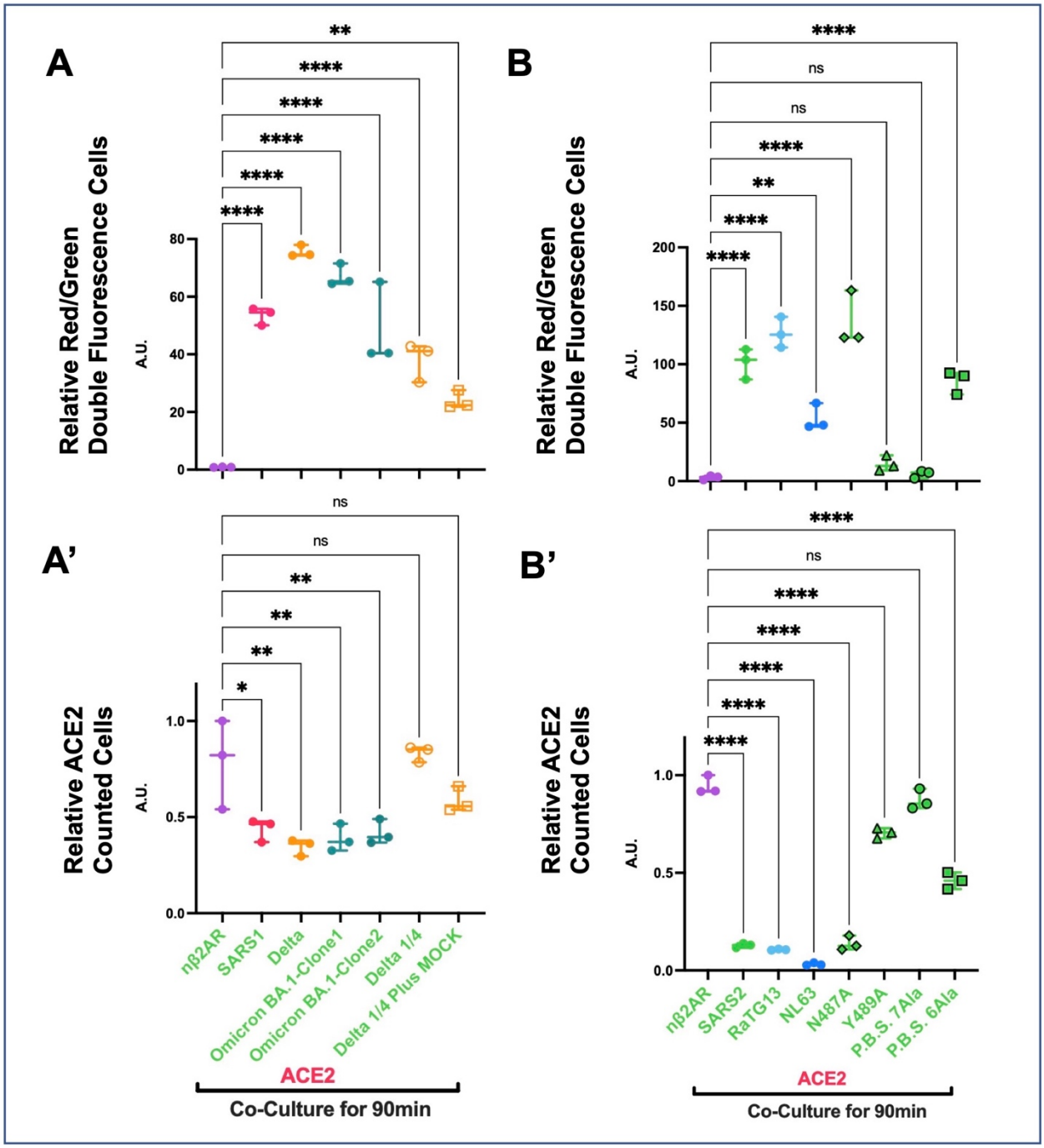

Figure S8: Flow cytometry counts of double positive cells and ACE2 levels for RBD mutants

A-C and A'-C'. *DPF assay*: values in are normalized to controls (Y-axis arbitrary units, A. U.). Overnight (O/N) transfection and flow cytometry counts of Co-plating GFP and Cherry expressing cells at either 90min (RBD cells trypsinized and added to ACE2 expressing cells.

Green labeling represents GFP fusion proteins. Red labeling represents Cherry fusion proteins. **A-B and A'-B'**. Data shows that double fluorescent cells are found with RBDs of SARS1, SARS2, Delta, Omicron, RaTG13, NL63; Concomitant loss of ACE2 expression was observed. The N487A mutant still robustly bound and ACE2 expression was unperturbed, in contrast to Y489A where nearly all binding is abolished, but still shows reduced expression of ACE2. The 7Ala mutation of the Predicted Binding Site (P.B.S. 7Ala: K417A, G446A, L455A, F486A, Q493A, Q498A, N501A) completely abolished binding and no loss of ACE2 expression was observed. By contrast P.B.S. 6Ala mutation (+F486) generated substantial double positives as well as loss of ACE2 expression.

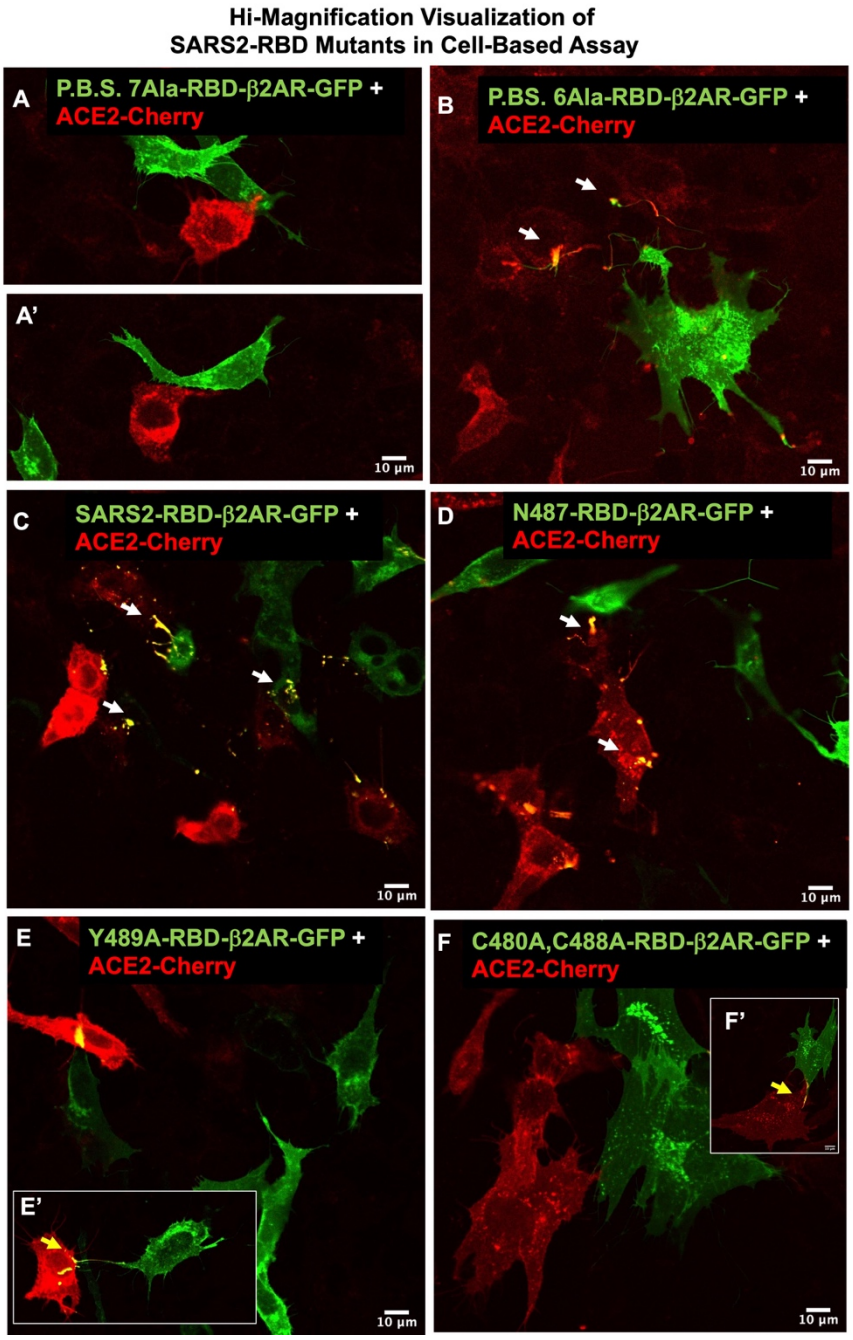

Figure S9: Hi-Magnification Visualization of SARS2-RBD Mutants in Cell-Based Assay **A-F.** Confocal images for co-plated RBD variants and mutants with ACE2-Cherry after 16hrs. **A and A'.** P.B.S. 7 Ala-RBD expressing cells reveal fluorescent filopodia at the membrane (obvious filopodia), but the protein is not found bound to ACE2-Cherry cells. **B.** P.B.S.6 Ala do bind ACE2-Cherry cells. **C.** SARS2-RBD expressing cells robustly bind ACE2-Cherry cells. **D.** N487A-RBD, **E and E'.** Y489A-RBD and **F and F'.** C480-C488A-RBD with ACE2-Cherry Cells. N487A-RBD interactions with ACE2-Cherry are robust, in contrast to Y489A-RBD and C440-C488A-RBDs, which rarely interact with ACE2-Cherry Cells.

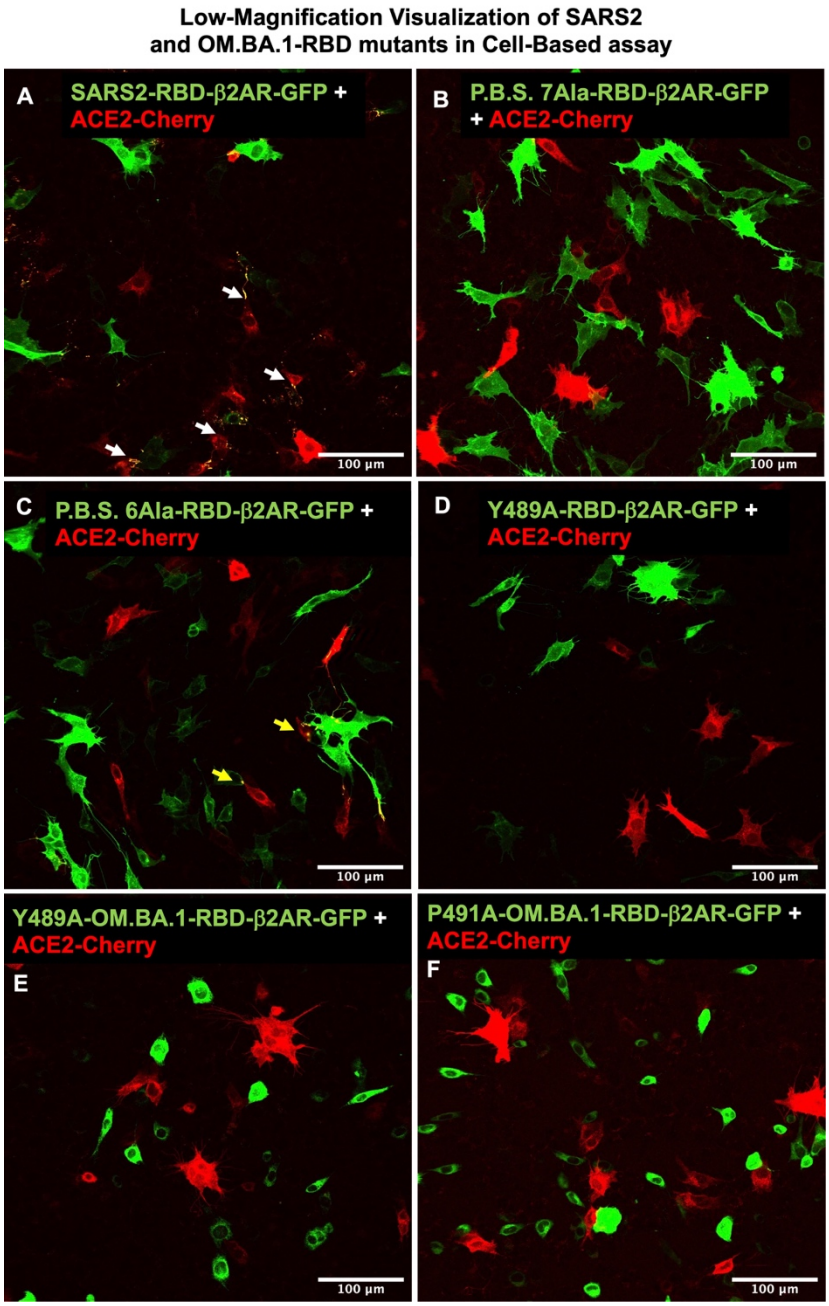

Figure S10: Low-Magnification Visualization of SARS2 and OM.BA.1-RBD mutants in Cell-Based assay

A-F. Low magnification confocal images for co-plated RBD variants and mutants with ACE2-Cherry reveals the pervasiveness of RBD-ACE2 interactions/noninteractions, RBD membrane trafficking/non-trafficking. **A.** SARS2-RBD protein is readily internalized by ACE2-Cherry cells and reduces its membrane expression. **B.** P.B.S. 7 Ala-RBD expressing cells are well expressed at the membrane (obvious filopodia), but the protein is not found bound to ACE2-Cherry cells. **C.** P.B.S. 6 Ala Shows binding ACE2-Cherry cells. **D.** Y489A-RBD expressing cells do not show binding to ACE2-Cherry cells. **E.** Y489A-OM.BA.1-RBD and **F.** P491A-OM.BA.1-RBD Show no filipodia and no interactions with ACE2-Cherry Cells.

RBD Mutations Tested in Cell-Based Assay (Co-Plating)

RBDs Internalized by:		
Pusillus (8AA)	**ACE2**	**Full Length RBD**
NO	YES	SARS2
NO*	YES	Delta
YES	YES	Omicron.BA.1
YES	YES	Omicron.BA.2
NO	YES	Omicron.BA.5
NO	YES	SARS1
NO	YES	RaTG13
NO	YES	SARS2-Hi Frequency 2020 (3Ala)
NO	YES	SARS2-Hi Frequency 2021 (7Ala)
NO	NO	SARS2-P.B.S. (Predicted Binding Sites->7Ala)
NO	YES	SARS2-P.B.S.+F486 (6Ala)
YES	YES	NL63 (alpha coronavirus)

*** Some binding observed.**

Figure S11: RBD mutations tested with Pus8AA+LMY→A-ACE2
Co-plating RBD constructs with Pus8AA-ACE2-Cherry cells. A broad set of RBD mutants and variants of SARS2, SARS1, RaTG13 and NL63 are tested by visual inspection **(see also Figure 8)**. Only OM.BA.1-RBD, OM.BA.2-RBD, and NL63-RBD can robustly bind to Pus8AA-ACE2-Cherry. All three SARS2-RBD mutants that could bind to ACE2-Cherry, did not bind to the Pus8AA-ACE2-Cherry.

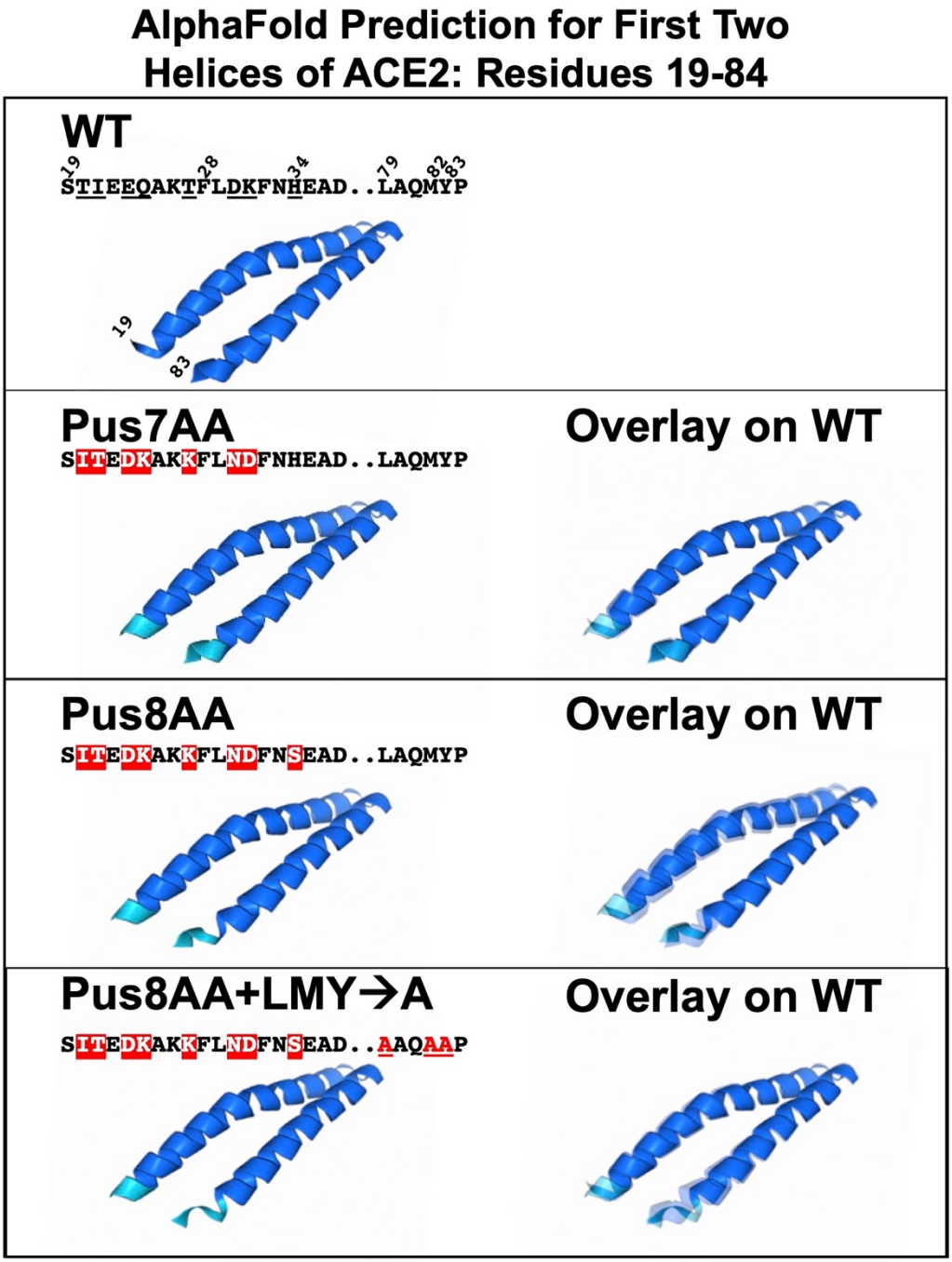

Figure S12: AlphaFold Prediction for the first two helices of ACE2 (residues 19-84) The mature ACE2 protein has its signal sequence cleaved after residue 18. The next 63 residues (19-81) form two helices (helix 1: residues 19-52 and helix 2: residue 55-81). AlphaFoldpredictions (residues 19-84) for WT and Group III mutants: Pus7AA, Pus8AA and Pus8AA+LMY→A all maintain the two-helix structure. Pus8AA has substitutions in ACE2 residues 20, 21, 23, **24**, **27**, **30**, **31**, **34** (bolded residues are predicted to interact with SARS2-RBD, see also **Figure 7**). Overlays with WT show only subtle differences in the helices, but more robust changes at the Nt and artificial Ct of the models.

Mouse vs Human ACE2 Conservation: Residues 1-357

```
     Mouse Signal peptide: 1 MSSSSWLLLSLVAVTRAQ
                             MSSSSWLLLSLVAVT_AQ
     Human Signal peptide: 1 MSSSSWLLLSLVAVTAAQ

     SITEDKAKKFLNDFNS→Pusillus 8AA Changes (Grey highlights)
19   SLTEENAKTFLNNFNQEAEDLSYQSSLASWNYNTNITEENAQKMSEAAAKWSAFYEEQSKTAQSFSLQEIQTPIIKR 95
     S__EE_AKTFL+_FN_EAEDL_YQSSLASWNYNTNITEEN_Q_M+_A__KWSAF_+EQS__AQ_+_LQEIQ___+K_
19   STIEEQAKTFLDKFNHEAEDLFYQSSLASWNYNTNITEENVQNMNNAGDKWSAFLKEQSTLAQMYPLQEIQNLTVKL 95
          Nt Proximal                                            Nt Distal
96   QLQALQQSGSSALSADKNKQLNTILNTMSTIYSTGKVCNPKNPQECLLLEPGLDEIMATSTDYNSRLWAWEGWRAEV 172
     QLQALQQ+GSS_LS_DK+K+LNTILNTMSTIYSTGKVCNP_NPQECLLLEPGL+EIMA_S_DYN_RLWAWE_WR+EV
96   QLQALQQNGSSVLSEDKSKRLNTILNTMSTIYSTGKVCNPDNPQECLLLEPGLNEIMANSLDYNERLWAWESWRSEV 172

173  GKQLRPLYEEYVVLKNEMARANNYNDYGDYWRGDYEAEGADGYNYNRNQLIEDVERTFAEIKPLYEHLHAYVRRKLM 249
     GKQLRPLYEEYVVLKNEMARAN+Y_DYGDYWRGDYE__G_DGY+Y+R_QLIEDVE_TF_EIKPLYEHLHAYVR_KLM
173  GKQLRPLYEEYVVLKNEMARANHYEDYGDYWRGDYEVNGVDGYDYSRGQLIEDVEHTFEEIKPLYEHLHAYVRAKLM 249

250  DTYPSYISPTGCLPAHLLGDMWGRFWTNLYPLTVPFAQKPNIDVTDAMMNQGWDAERIFQEAEKFFVSVGL  320
     +_YPSYISP_GCLPAHLLGDMWGRFWTNLY_LTVPF_QKPNIDVTDAM++Q_WDA+RIF+EAEKFFVSVGL
250  NAYPSYISPIGCLPAHLLGDMWGRFWTNLYSLTVPFGQKPNIDVTDAMVDQAWDAQRIFKEAEKFFVSVGL  320

321  PHMTQGFWANSMLTEPADGRKVVCHPTAWDLGHGDFR  357
     P+MTQGFW_NSMLT+P__+_+K_VCHPTAWDLG_GDFR
321  PNMTQGFWENSMLTDPGNVQKAVCHPTAWDLGKGDFR  357
      Internal 1                   Internal 2

20 mismatches and 5 conserved AA in first 94aa= 69/94 identities (72%)
24 mismatches and 17 conserved AA from 96-357aa/262aa=221/262 identities (84%)
```

Figure S13: Mouse vs Human ACE2 among first 357 residues

First 357 ACE2 residues compared between mouse and human show 87% identity. The consensus sequence shows 45 mismatches (purple shading) of which 22 are conserved. mACE2 Residue Arg95 has been highlighted (blue shading) and is not contained in the m/hACE2 chimera with residues 1-353 of mA CE2 (**see Figures 8 and 10).** Human residues predicted to interact with SARS2-RBD are bolded and shaded turquoise. Nt-Proximal region (residues 19-45), Nt Distal (residues 79-83), Internal region 1 (residues 321-330) and Internal region 2(residues 352-357) are underlined. Pus8AA chimera (residues 19-34) are shown.

2192

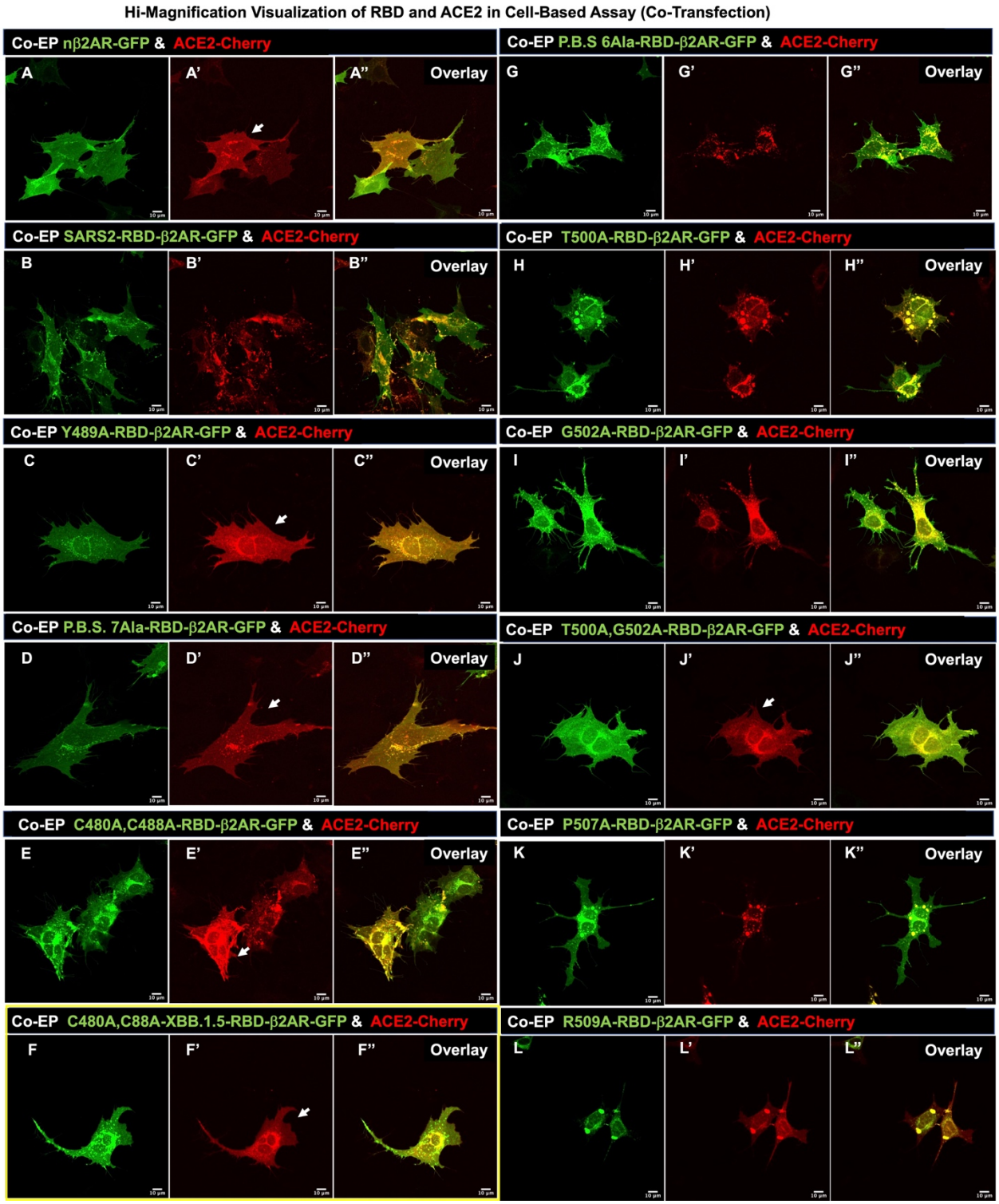

2193

2194 **Figure S14: Co-EP with RBD mutations and ACE2**

2195

2196

2197
2198 ***Figure S14: Co-EP with RBD mutations and ACE2 (continued)***
2199 **A-L, A'-L', A''-L''.** Utilizing LSM501, confocal images for Co-EP of GFP-tagged RBD
2200 variants and mutants and controls along with ACE2-Cherry, imaged after 16hrs. Green **(A-**
2201 **L)** and Red **(A'-L')** channels have been split, and overlay (**A''-L''**). **A-A''**. b2AR and ACE2
2202 show uniform membrane expression. **B-B''.** SARS2-RBD and ACE2 show internalization of all
2203 ACE2-Cherry fluorescence. **C-L, C'-L', C''-L''.** Of the four assays (DPF assay; Cell-
2204 Dissociation assay; Co-plating assay; Co-EP RBD/ACE2 assay) that were set up, the Co-EP
2205 proved to be the most sensitive way to determine any latent binding between RBD and ACE2
2206 proteins. **A', C', D', F', and J'** show no alteration of membrane ACE2
2207 expression. **B', G', H', K', L'** show robust internalization of ACE2-Cherry. **E', I'** show only
2208 modest internalization of ACE2-Cherry. It should be noted that C480A, C488A double mutant in
2209 XBB.1.5-RBD (**F-F''**) abolishes ACE2 internalization more robustly in this assay than C480A,
2210 C488A double mutant in RBD (**E-E''**), but not in DPF assay (**Figure 11F'**).
2211

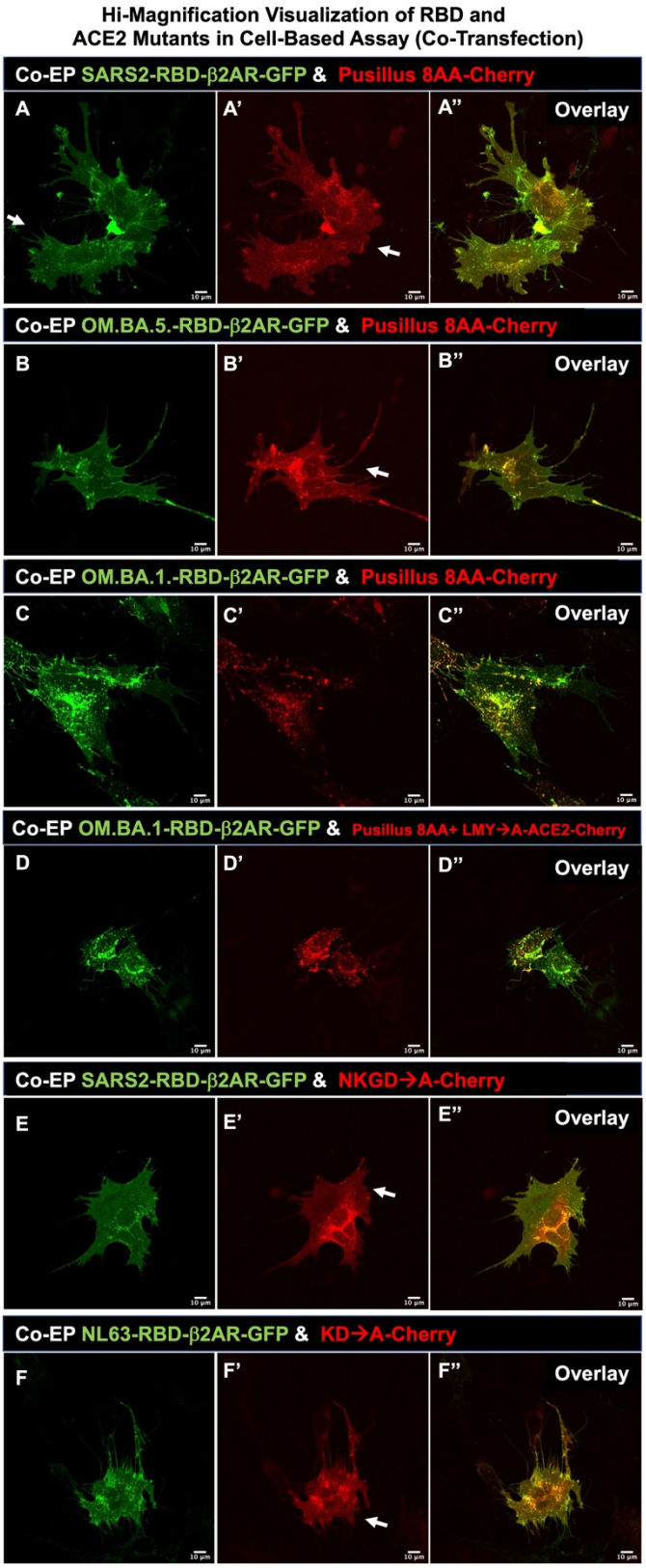

Figure S15: Co-EP with RBD variants and ACE2 mutants

2214 ***Figure S15: Co-EP with RBD variants and ACE2 mutants (continued)***
2215 **A-F, A'-F', A''-F''.** Utilizing LSM510, confocal images for Co-EP of GFP-tagged RBD
2216 variants and mutants and controls along with ACE2-Cherry, imaged after 16hrs. Green **(A-**
2217 **F)** and Red **(A'-F')** channels have been split, and overlay (**A''-F''**). Omicron.BA.1 clearly
2218 shows differential binding to Pusillus 8AA-Cherry compared to SARS2 and OM.BA.5-
2219 RBDs. OM.BA.1-RBD shows some internalization of ACE2-Cherry (**C'**), which shows the
2220 sensitivity of binding in this assay compared to co-plating assay in **Figure S14 A-F** and DPF
2221 assay in **Figure 10**. Both SARS2 and NL63-RBDs show dependence on Internal Region 2 for
2222 binding ACE2-Cherry with no alteration of membrane ACE2 expression (**E', F'**).
2223
2224
2225

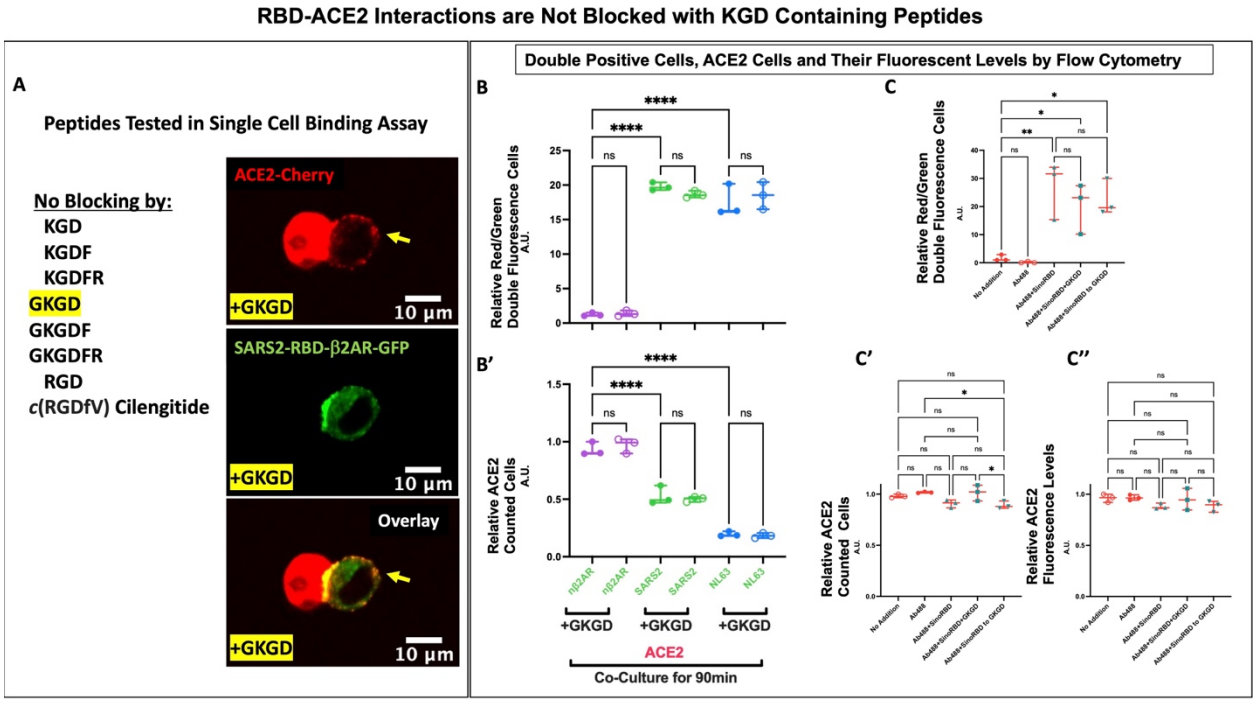

Figure S16: KGD containing peptides do not antagonize RBD binding to ACE2-Cherry **A**. The necessity of K353-G354-D355 sequence in ACE2 suggested that KGD derivative peptides could block RBD binding. Six peptide versions of KGD and two RGD containing peptides were tested for their ability to block SARS2 or NL63 RBDs from binding ACE2-Cherryin the 30min dissociated cell-based assay. Greater than 100 micromolar concentrations for all 8 peptides did not block binding. Utilizing LSM510, confocal images revealed only one peptide GKGD (yellow highlight) appeared to cause a phenotype that was not previously observed: ACE2 protein being redistributed on the adjoining SARS2-RBD cells. **B and B'**. *DPF assay*: analysis of Co-plating GFP and Cherry expressing cells after 90min. Data shows that double florescent cells are found in both SARS2 and NL63 irrespective of preincubation with 120mM GKGD peptide with subsequent 90min incubation at a 1:20 dilution (6mM GKDG). Concomitant loss of ACE2-Cherry expression was observed in both ACE2 cells in all RBD conditions whether the peptide was present. **C-C''**. *DPF assay*: **C**. Double fluorescence after 90minute incubation of ACE2-Cherry cells with Ab488 (1mg/4mls of Goat-anti-HIS-Tag-Alexa488 Goat antibody [R&D#: IC050G]) with and without SinoRBD (60ng/4mls of 2019-nCoV-HisTag-RBD [Cat#40592-V08H; 234 residues, R319-F541]). 1000x-GKGD peptide(49mg) 10min pre-incubated with 1mg Ab488 + 60ng SinoRBD in 200mls PBS, then added to 4mls of media or GKDG added to media (49mg/4mls) plus 200mls PBS with 10min preincubated of 1ug Ab488 + 60ng SinoRBD. No reduction of double fluorescence is observed when GKGD peptide is added. **C'** ACE2-Cherry cells with Ab488, Ab488+SinoRBD, or GKGD+Ab488+SinoRBD show no changes in fluorescence. **C''**. High expressing ACE2-Cherry fluorescence cells also show no changes in fluorescence in all conditions. Values in **B, B', C, C'and C''** are normalized to controls (Y-axis arbitrary units, A. U.)-**see Data File S2**. GraphPad Prism 9.3.1 used to generate **B-C''**.

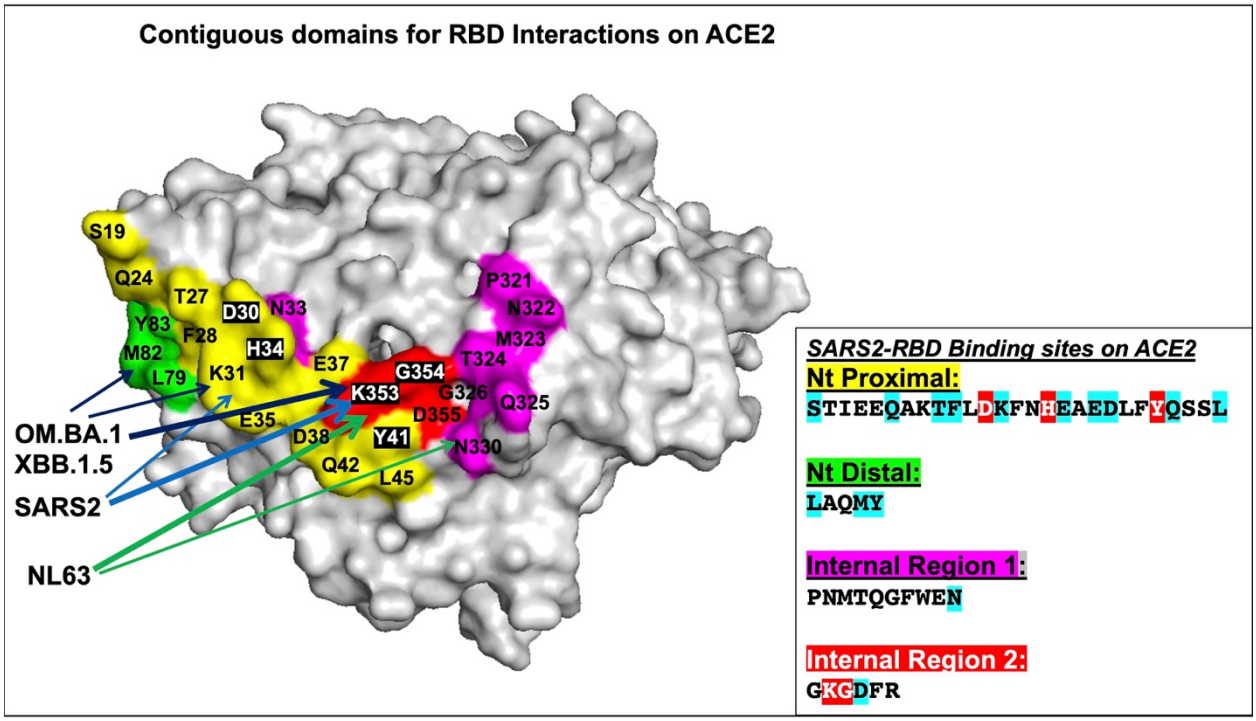

Figure S17: Proposed interpretation of RBD interactions on ACE2 structure with demarcated domains.
Space-filling model of ACE2 structure from pdb_6M0J (14) modified by highlighting interactions for both SARS2 and NL63 RBDs: Nt proximal (**yellow residues**), Nt distal (**green residues**), and Internal regions 1 (**purple residues**) and 2 (**red residues**). Purple residue interactions including N33 are nearly from NL63-RBD. SARS2-RBD does not bind/internalize if *either* Nt proximal or Internal region 2 (K353, D355) are mutated. OM.BA.1 and OM.BA2-RBDs are not bond/internalized if *either* mutation in both Nt proximal and distal ACE2 or Internal region 2 (K353, D355). NL63-RBD requires Internal region 2 (K353 and D355) for both binding/internalization. Inset shows **SARS2-RBD** interactions within the four domains (**see Figures 7, 12**) (residues with blue highlights are predicted binding sites that occur in ¾ of SARS2, SARS1, RaTG13, and NL63-RBDs; residues with red highlights are predicted binding sites in all 4 RBDs). The RBD interaction data taken together suggests that Internal region 2 binding for SARS1/SARS2/RaTG13 is weak and requires Nt proximal and distal contacts for stabilization (dark blue, light blue arrows), whereas NL63 has additional contacts in the Internal region 1 (green arrows) that supports binding to Internal region 2 (thick arrows). The ability of SARS2 mutant Y489A to nearly abolish SARS2-RBD binding to ACE2 suggests that none of the domains by themselves have strong binding to ACE2. Overall, the data points to the Internal region 2 as being critical for internalizations of RBDs.

Figure 1

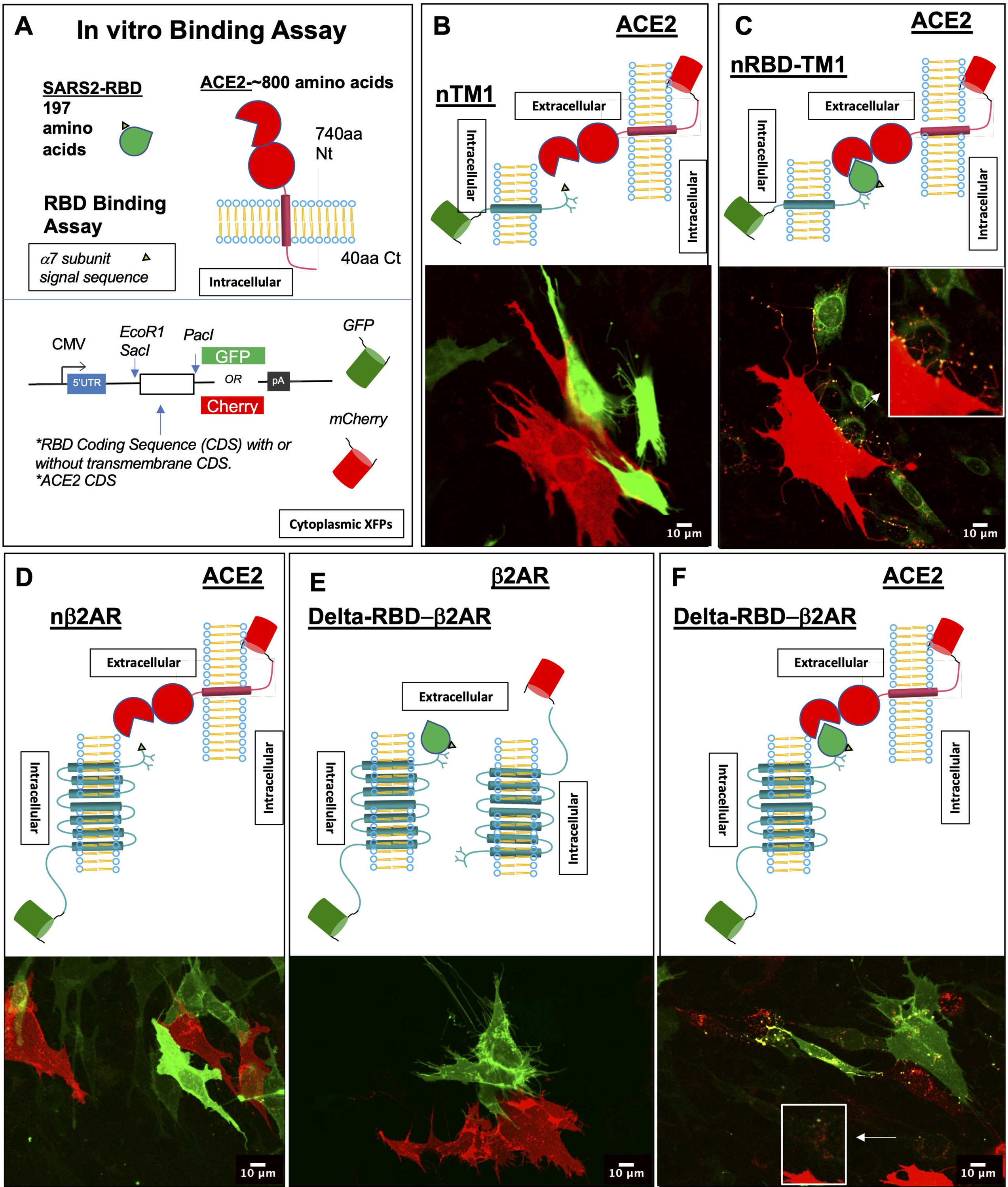
A
In vitro Binding Assay
SARS2-RBD
197 amino acids
ACE2-~800 amino acids
740aa Nt
40aa Ct
Intracellular
RBD Binding Assay
α7 subunit signal sequence
CMV
EcoR1
SacI
PacI
GFP
5'UTR
OR
pA
Cherry
GFP
mCherry
*RBD Coding Sequence (CDS) with or without transmembrane CDS.
*ACE2 CDS
Cytoplasmic XFPs
B
ACE2
nTM1
Extracellular
Intracellular
Intracellular
10 µm
C
ACE2
nRBD-TM1
Extracellular
Intracellular
Intracellular
10 µm
D
ACE2
nβ2AR
Extracellular
Intracellular
Intracellular
10 µm
E
β2AR
Delta-RBD–β2AR
Extracellular
Intracellular
Intracellular
10 µm
F
ACE2
Delta-RBD–β2AR
Extracellular
Intracellular
Intracellular
10 µm

Figure 2

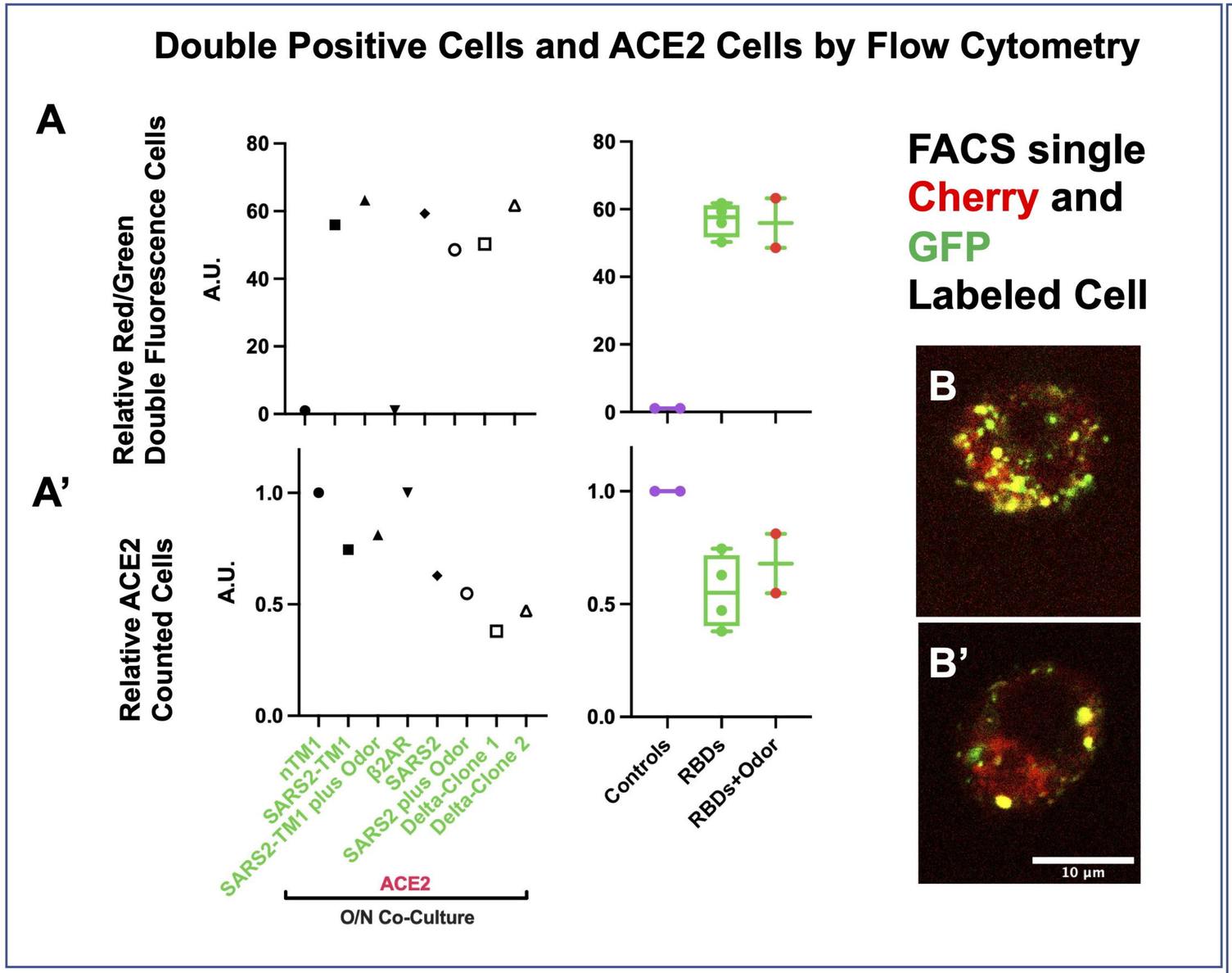
Double Positive Cells and ACE2 Cells by Flow Cytometry
A
Relative Red/Green Double Fluorescence Cells
A.U.
80
60
40
20
0
A'
Relative ACE2 Counted Cells
A.U.
1.0
0.5
0.0
nTM1
SARS2-TM1
SARS2-TM1 plus Odor
β2AR
SARS2
SARS2 plus Odor
Delta-Clone 1
Delta-Clone 2
ACE2
O/N Co-Culture
Controls
RBDs
RBDs+Odor
FACS single Cherry and GFP Labeled Cell
B
B'
10 µm

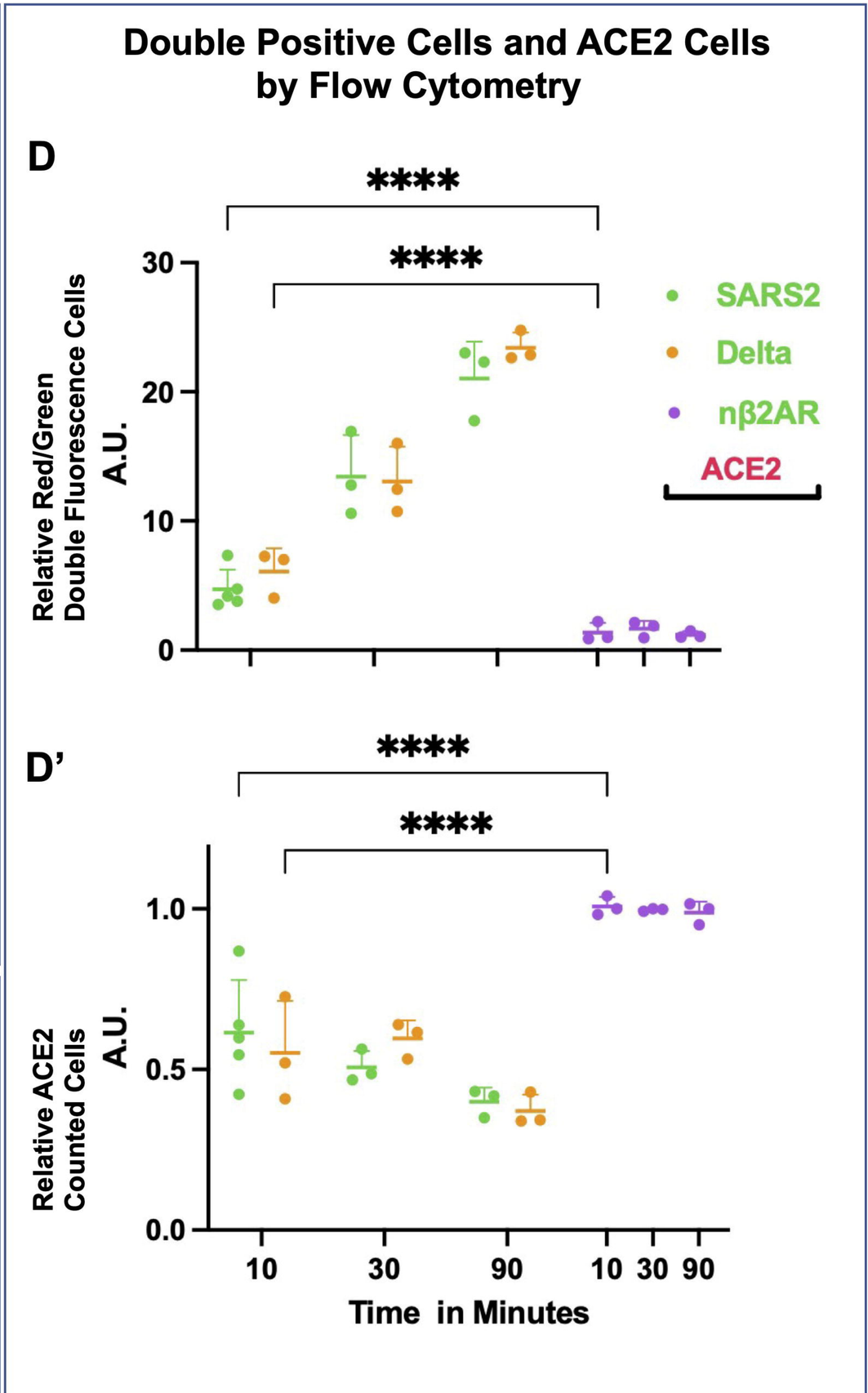
Double Positive Cells and ACE2 Cells by Flow Cytometry
D
****
****
Relative Red/Green Double Fluorescence Cells
A.U.
30
20
10
0
SARS2
Delta
nβ2AR
ACE2
D'
****
****
Relative ACE2 Counted Cells
A.U.
1.0
0.5
0.0
10
30
90
10
30
90
Time in Minutes

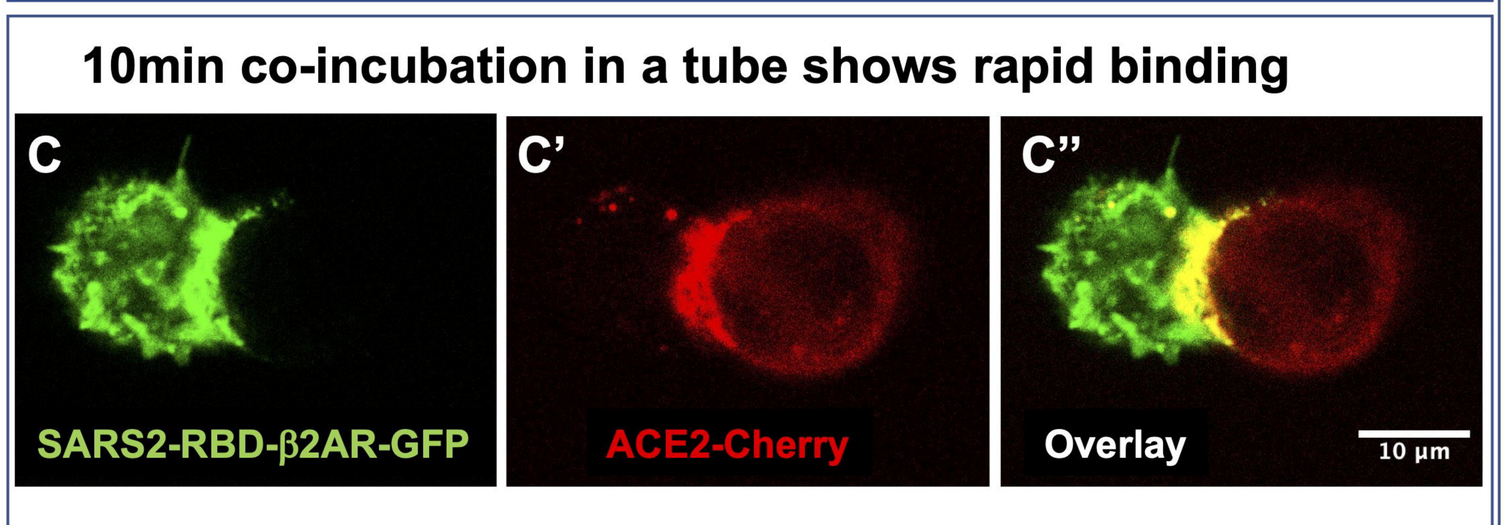
10min co-incubation in a tube shows rapid binding
C
SARS2-RBD-β2AR-GFP
C'
ACE2-Cherry
C''
Overlay
10 µm

Figure 3

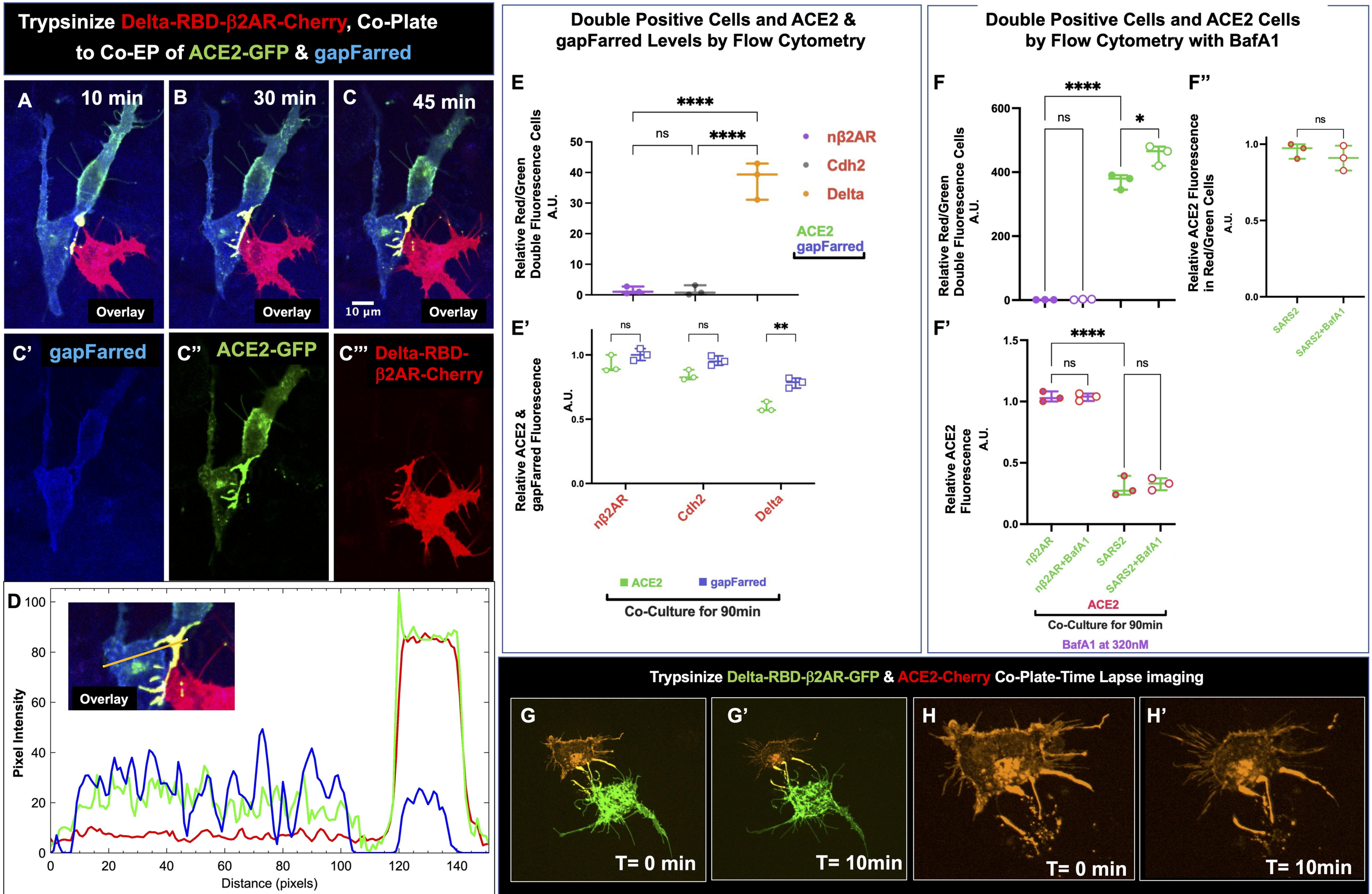
Trypsinize Delta-RBD-β2AR-Cherry, Co-Plate to Co-EP of ACE2-GFP & gapFarred
A 10 min
B 30 min
C 45 min
Overlay
10 µm
C' gapFarred
C'' ACE2-GFP
C''' Delta-RBD-β2AR-Cherry
D
Pixel Intensity
Distance (pixels)
Double Positive Cells and ACE2 & gapFarred Levels by Flow Cytometry
E
Relative Red/Green Double Fluorescence Cells A.U.
nβ2AR
Cdh2
Delta
ACE2
gapFarred
E'
Relative ACE2 & gapFarred Fluorescence A.U.
ACE2
gapFarred
Co-Culture for 90min
Double Positive Cells and ACE2 Cells by Flow Cytometry with BafA1
F
Relative Red/Green Double Fluorescence Cells A.U.
F''
Relative ACE2 Fluorescence in Red/Green Cells A.U.
SARS2
SARS2+BafA1
F'
Relative ACE2 Fluorescence A.U.
nβ2AR
nβ2AR+BafA1
SARS2
SARS2+BafA1
ACE2
Co-Culture for 90min
BafA1 at 320nM
Trypsinize Delta-RBD-β2AR-GFP & ACE2-Cherry Co-Plate-Time Lapse imaging
G
T= 0 min
G'
T= 10min
H
T= 0 min
H'
T= 10min

Figure 4

RBD Meta-Analysis of DMS, Selected Variants and Alanine Substitutions Tested

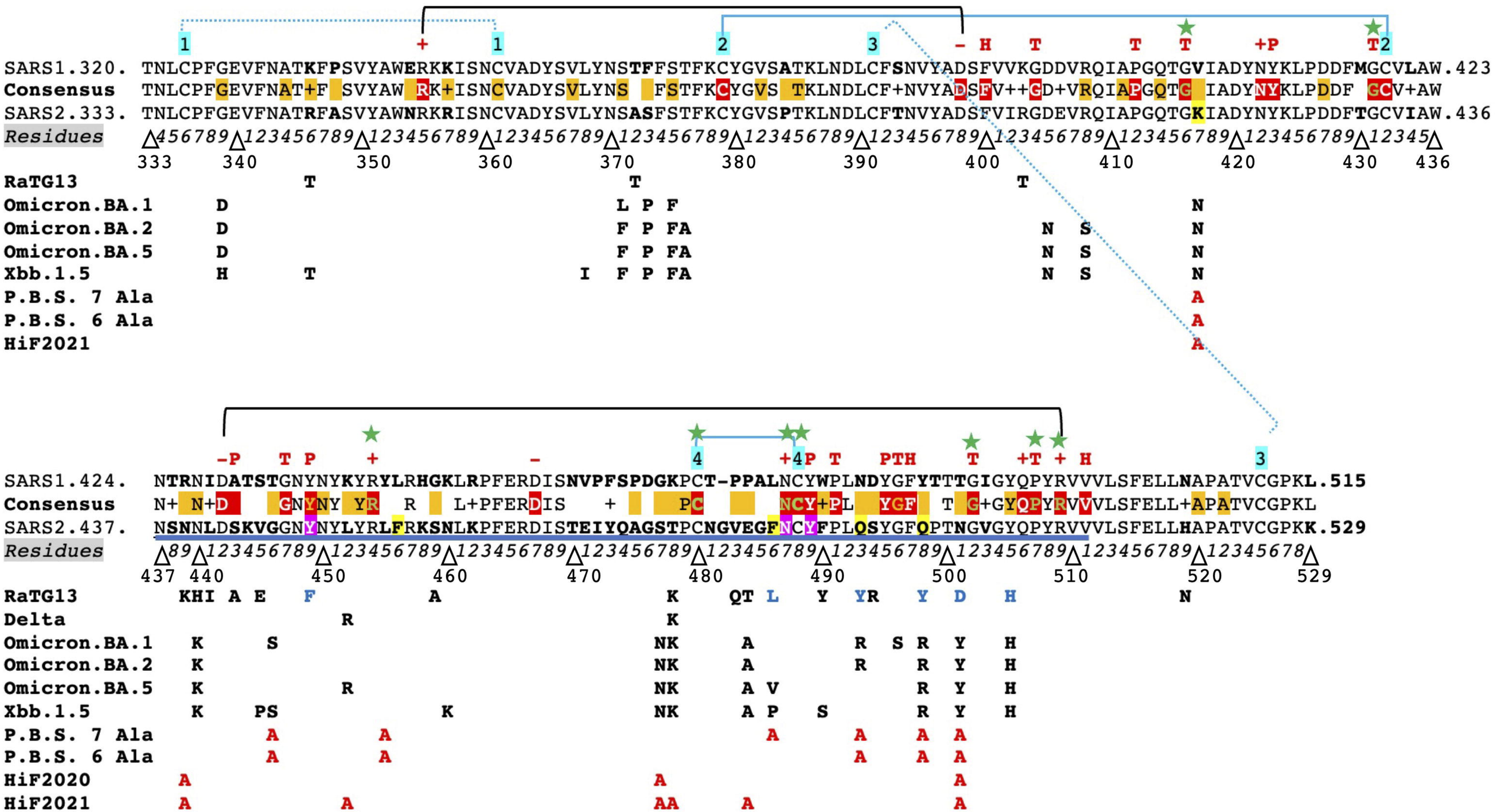

Figure 5

Double Positive Cells and ACE2 Cells by Flow Cytometry

A

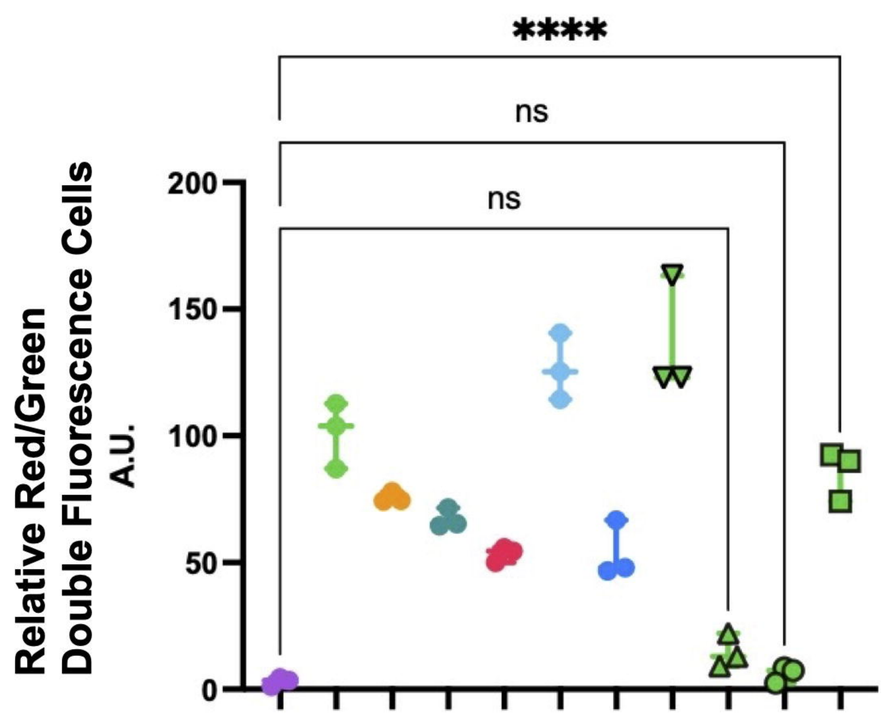

A'

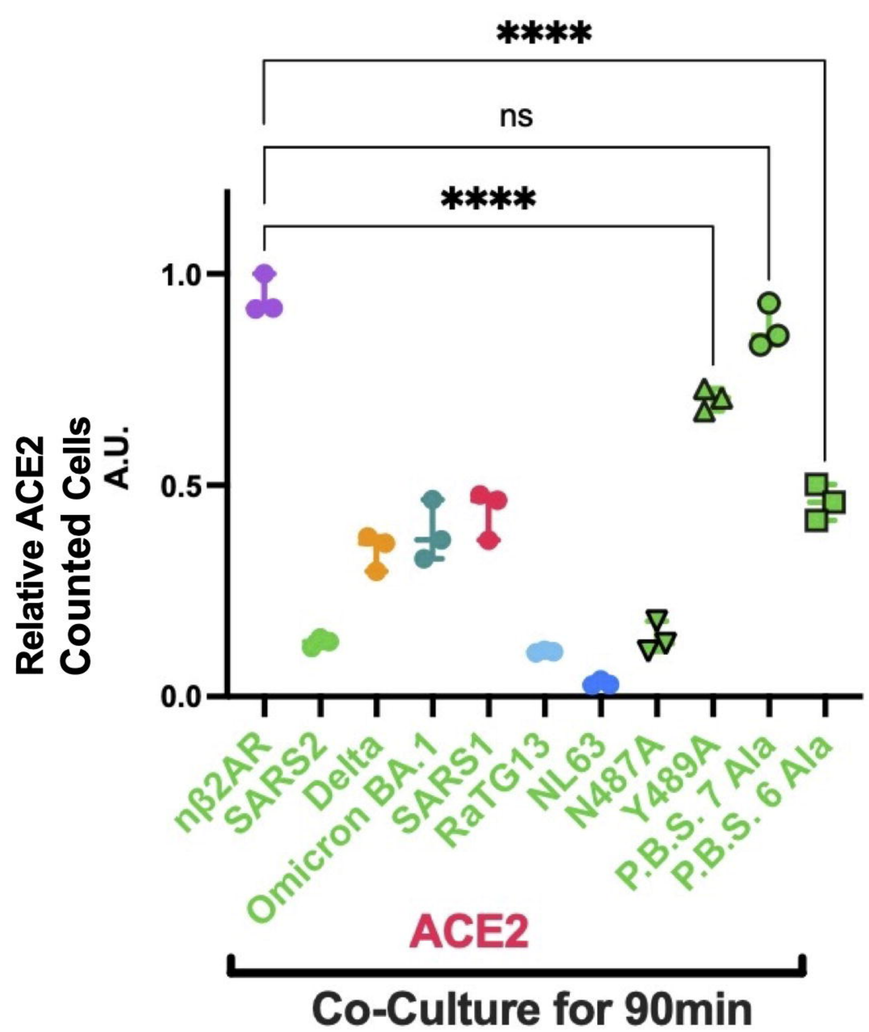

B

Loop 4 Region Mutations Tested

RBD Internalization by ACE2

	RBD
YES	SARS2
YES	T-PPAL(SARS1)
YES	QTL(RaTG13)
YES	F486A
YES	N487A
NO	C488A#
NO	C480A,C488A*
NO	Y489A*
YES	Y489W
YES	Y489H
YES	F490A
YES	P491A
NA	L492A^
YES	Y449A

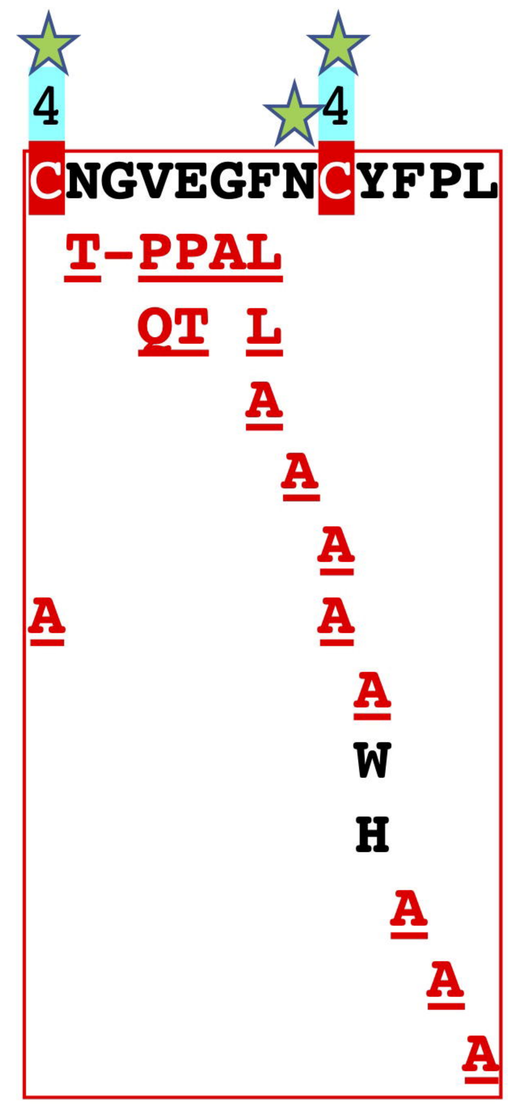

* Traffics well to plasma membrane

\# Poorly traffics to plasma membrane

^ NO trafficking to plasma membrane

Y489A or P491A point mutations in OM.BA.1. do not traffic to plasma membrane.

Figure 6

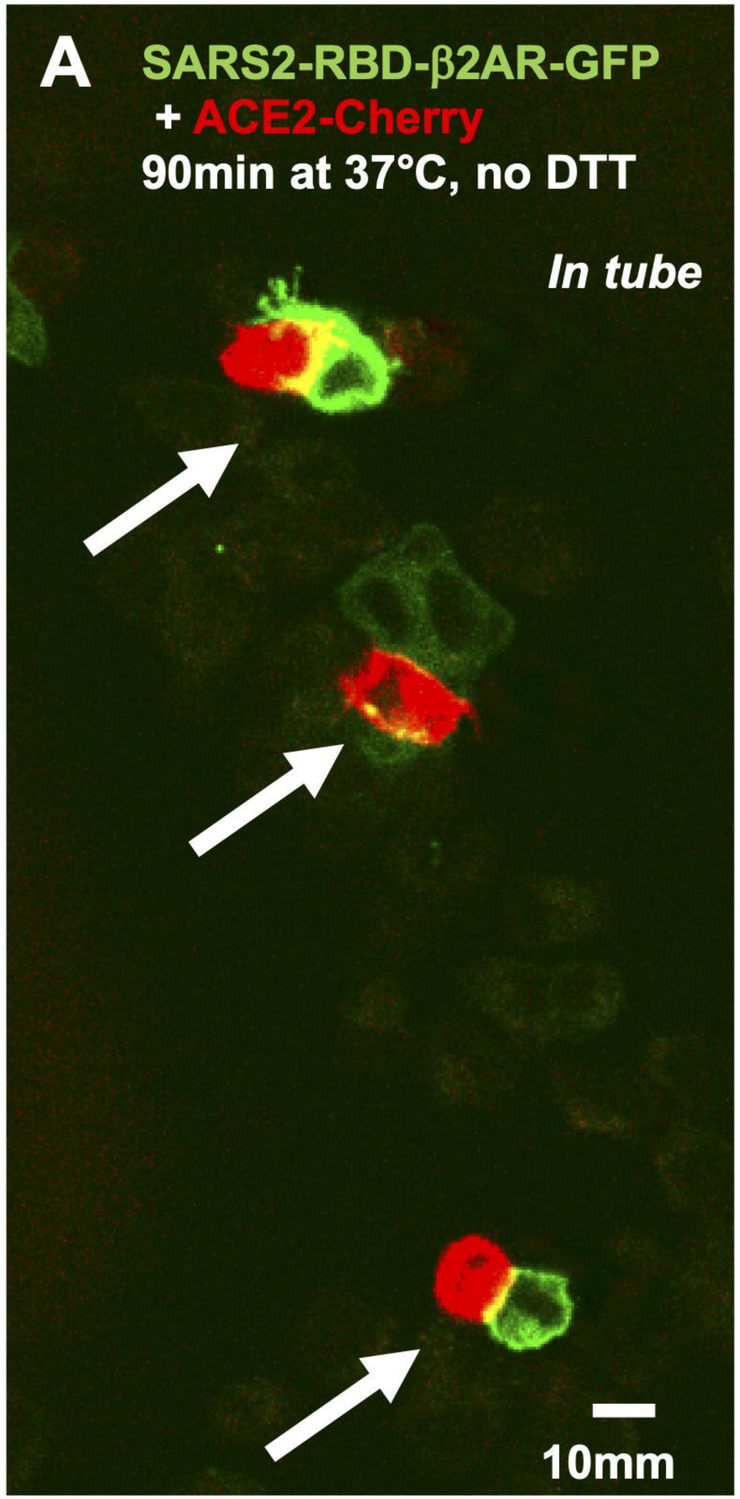

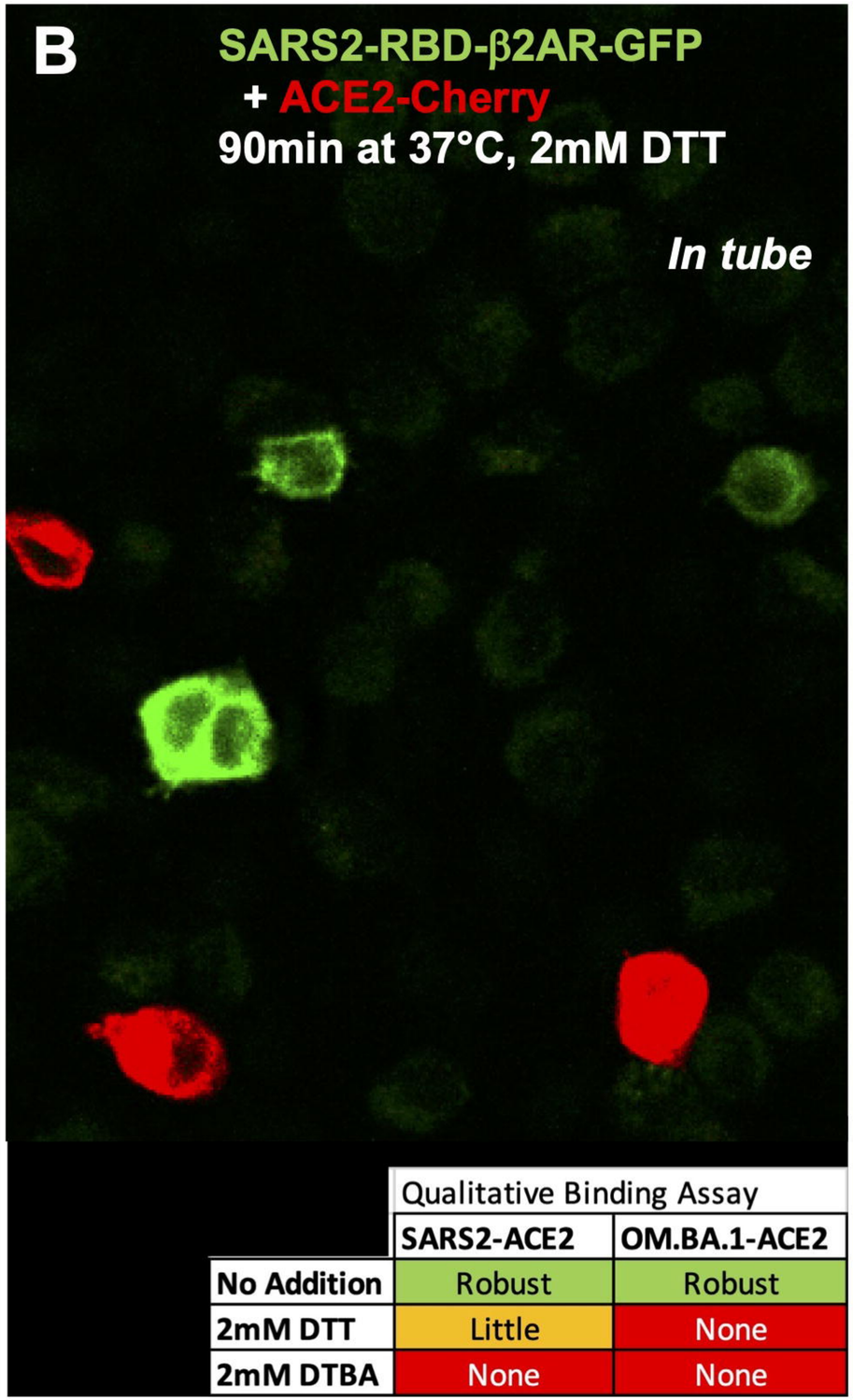

Qualitative Binding Assay

	SARS2-ACE2	OM.BA.1-ACE2
No Addition	Robust	Robust
2mM DTT	Little	None
2mM DTBA	None	None

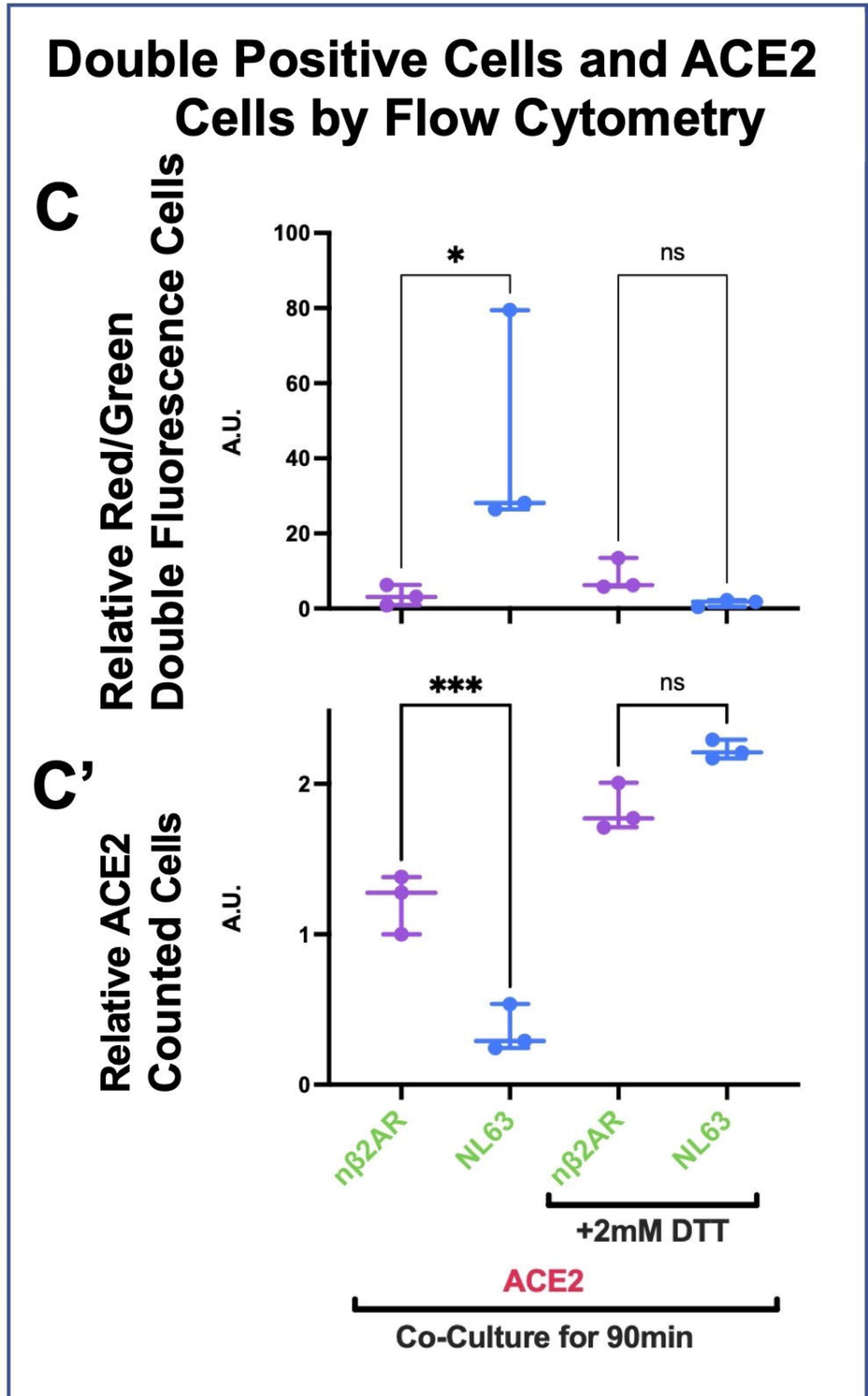

Figure 7

ACE2 Nt Proximal Region Conservation and SARS2 Interactions

A

408 Species Manually Aligned

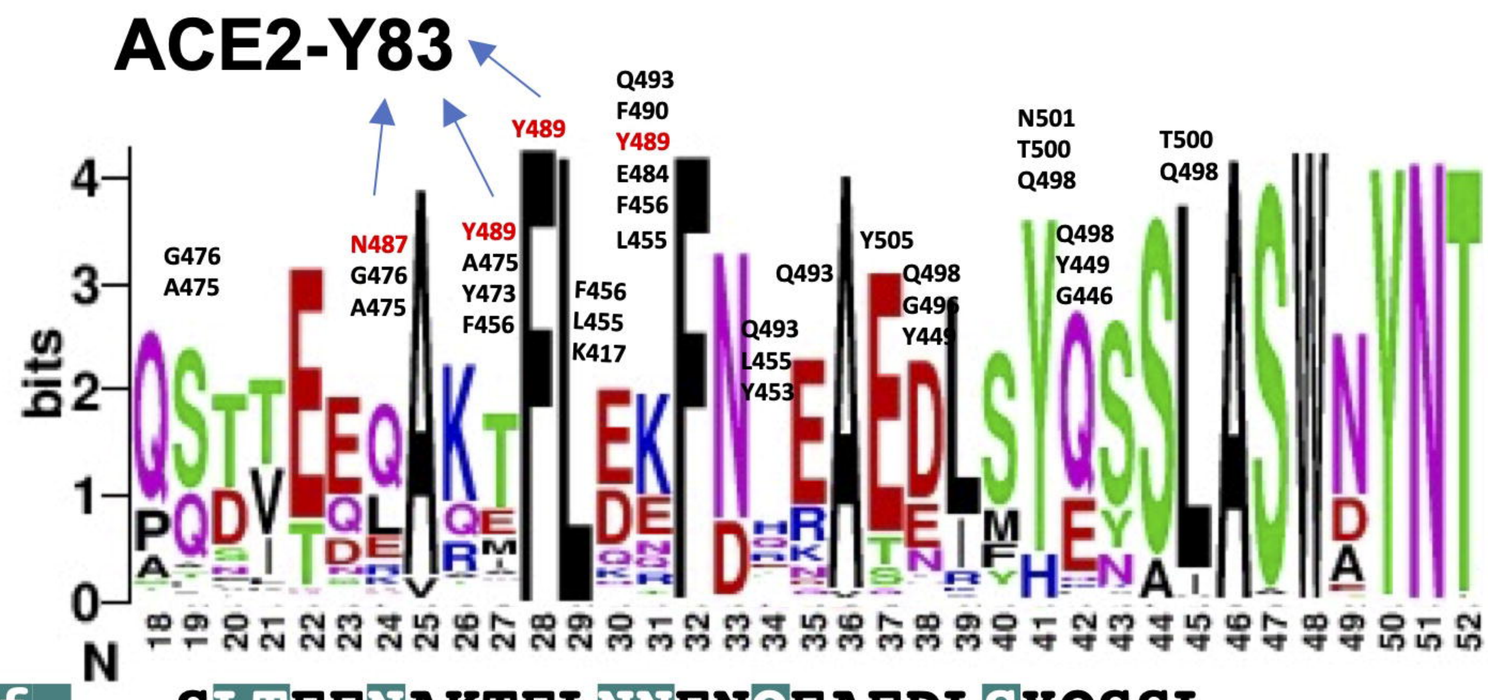


```
Mus ACE2  Diff     SLTEENAKTFLNNFNQEAEDLSYQSSL
SARS2     Targets  STIEEQAKTFLDKFNHEAEDLFYQSSL
SARS1     Targets  STIEEQAKTFLDKFNHEAEDLFYQSSL
RaTG13    Targets  STIEEQAKTFLDKFNHEAEDLFYQSSL
NL63      Targets  STIEEQAKTFLDKFNHEAEDLFYQSSL
```

Aves/Reptilia Manual Aligned

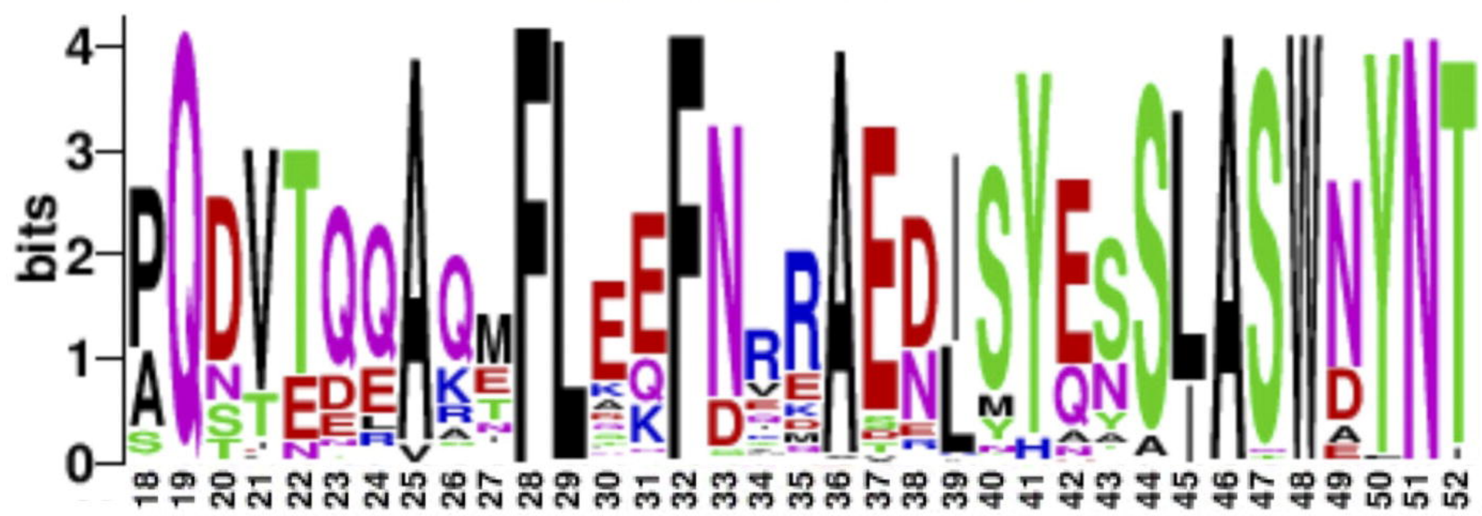

B

ACE2 Nt Distal Region Conservation

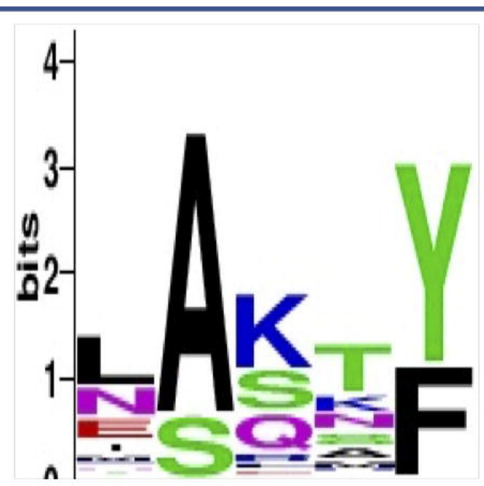


```
SARS2/SARS1 &
RaTG13 Targets   L A Q M Y
NL63 Targets     L A Q M Y
```

Loop 4 residues

N487 Y489 Y489 F486 F486 N487 Y489

Q24 T27 F28 L79 M82 Y83

Nt Proximal **Nt Distal**

Figure 8

A — ACE2 Nt Proximal and Distal Mutants and Hybrids

	RBD Internalized SARS2	RBD Internalized OM.BA.1	ACE2 mutant	Human ACE2 Amino Terminal Mutants: Signal Sequence	Cut ↓	Proximal (19, 28, 34, 45) … Distal (79, 82, 83)
	YES	YES	**WT-Human**	MSSSSWLLLSLVAVTAAQ		STIEEQAKTFLDKFNHEAEDLFYQSSL…LAQMY
I	YES	YES	E22Q,E23Q	MSSSSWLLLSLVAVTAAQ		STI**QQ**QAKTFLDKFNHEAEDLFYQSSL…LAQMY
	YES	YES	E22A,E23A,Q24A	MSSSSWLLLSLVAVTAAQSTI**AAA**		AKTFLDKFNHEAEDLFYQSSL…LAQMY
	YES	YES	E22,E23 del	MSSSSWLLLSLVAVTAAQSTIQA		KTFLDKFNHEAEDLFYQSSL…LAQMY
	YES	YES	Q24K	MSSSSWLLLSLVAVTAAQ		STIEE**K**AKTFLDKFNHEAEDLFYQSSL…LAQMY
	YES	YES	F28A	MSSSSWLLLSLVAVTAAQ		STIEEQAKT**A**LDKFNHEAEDLFYQSSL…LAQMY
	YES	YES	Q24A,Y83A	MSSSSWLLLSLVAVTAAQ		STIEE**A**AKTFLDKFNHEAEDLFYQSSL…LAQM**A**
	YES	YES	T27A,F28A,K31A,Y83A	MSSSSWLLLSLVAVTAAQ		STIEEQAK**AA**LD**A**FNHEAEDLFYQSSL…LAQM**A**
	YES	YES	L79A,M82A,Y83A(LMY→A)	MSSSSWLLLSLVAVTAAQ		STIEEQAKTFLDKFNHEAEDLFYQSSL…**A**AQ**AA**
II	YES	YES	Pusillus(5AA)	MSSSSWLLLSLVAVTAAQ		S**IT**E**DK**AK**K**FLDKFNHEAEDLFYQSSL…LAQMY
	YES	YES	Pusillus(7AA)	MSSSSWLLLSLVAVTAAQ		S**IT**E**DK**AK**K**FL**ND**FNHEAEDLFYQSSL…LAQMY
	NO	YES	Pusillus(8AA)	MSSSSWLLLSLVAVTAAQ		S**IT**E**DK**AK**K**FL**ND**FN**S**EAEDLFYQSSL…LAQMY
	NO	YES	Pusillus(8AA)+F28A	MSSSSWLLLSLVAVTAAQ		S**IT**E**DK**AK**KA**L**ND**FN**S**EAEDLFYQSSL…LAQMY
	NO	**NO***	Pusillus(8AA)+LMY→A	MSSSSWLLLSLVAVTAAQ		S**IT**E**DK**AK**K**FL**ND**FN**S**EAEDLFYQSSL…**A**AQ**AA**
III	YES	YES	Chicken(10AA)	M**LLHF**WLL**CG**L**S**AV**VTP**		**QDVTQE**A**QT**FLDKFNHEAEDLFYQSSL…LAQMY
	YES	YES	Chicken(14AA)	M**LLHF**WLL**CG**L**S**AV**VTP**		**QDVTQE**A**QT**FL**AE**FN**VR**AEDLFYQSSL…LAQMY
	YES	YES	Chicken(10AA)+LMY→A	M**LLHF**WLL**CG**L**S**AV**VTP**		**QDVTQE**A**QT**FLDKFNHEAEDLFYQSSL…**A**AQ**AA**
	YES	YES	Chicken(14AA)+LMY→A	M**LLHF**WLL**CG**L**S**AV**VTP**		**QDVTQE**A**QT**FL**AE**FN**VR**AEDLFYQSSL…**A**AQ**AA**
	YES**	YES	Chicken(18AA)+LMY→A	M**LLHF**WLL**CG**L**S**AV**VTP**		**QDVTQE**A**QT**FL**AE**FN**VR**AED**IS**Y**EN**SL…**A**AQ**AA**
	NA	*NA*	Hu Chicken(18AA)+LMY→A	MSSSSWLLLSLVAVTAA	**TPQDVTQE**A**QT**FL**AE**FN**VR**AED**IS**Y**EN**SL…**A**AQ**AA**	
IV	YES	YES	Mouse Nt	MSSSSWLLLSLVAVTTAQ		SLTEENAKTFLNNFNQEAEDLSYQSSL…TAQSF

* Pusillus (8AA)+LMY→A does not bind to OM.BA.2-RBD, XBB.1.5, but does bind to NL63-RBD

** Fewer cells with SARS2-RBD internalizations compared to OM.BA.1

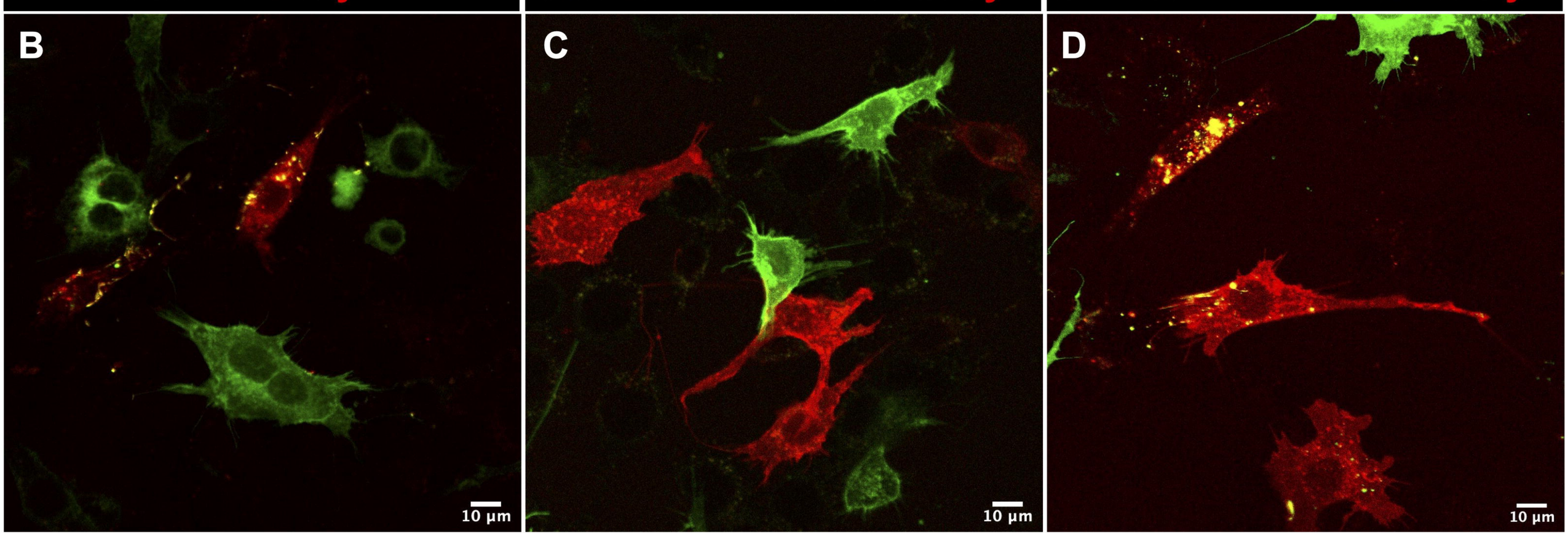

Figure 9

Hi-Magnification Visualization of OM.BA.1 RBD, OM.BA.2 and NL63 with ACE2 Mutants in Cell-Based Assay

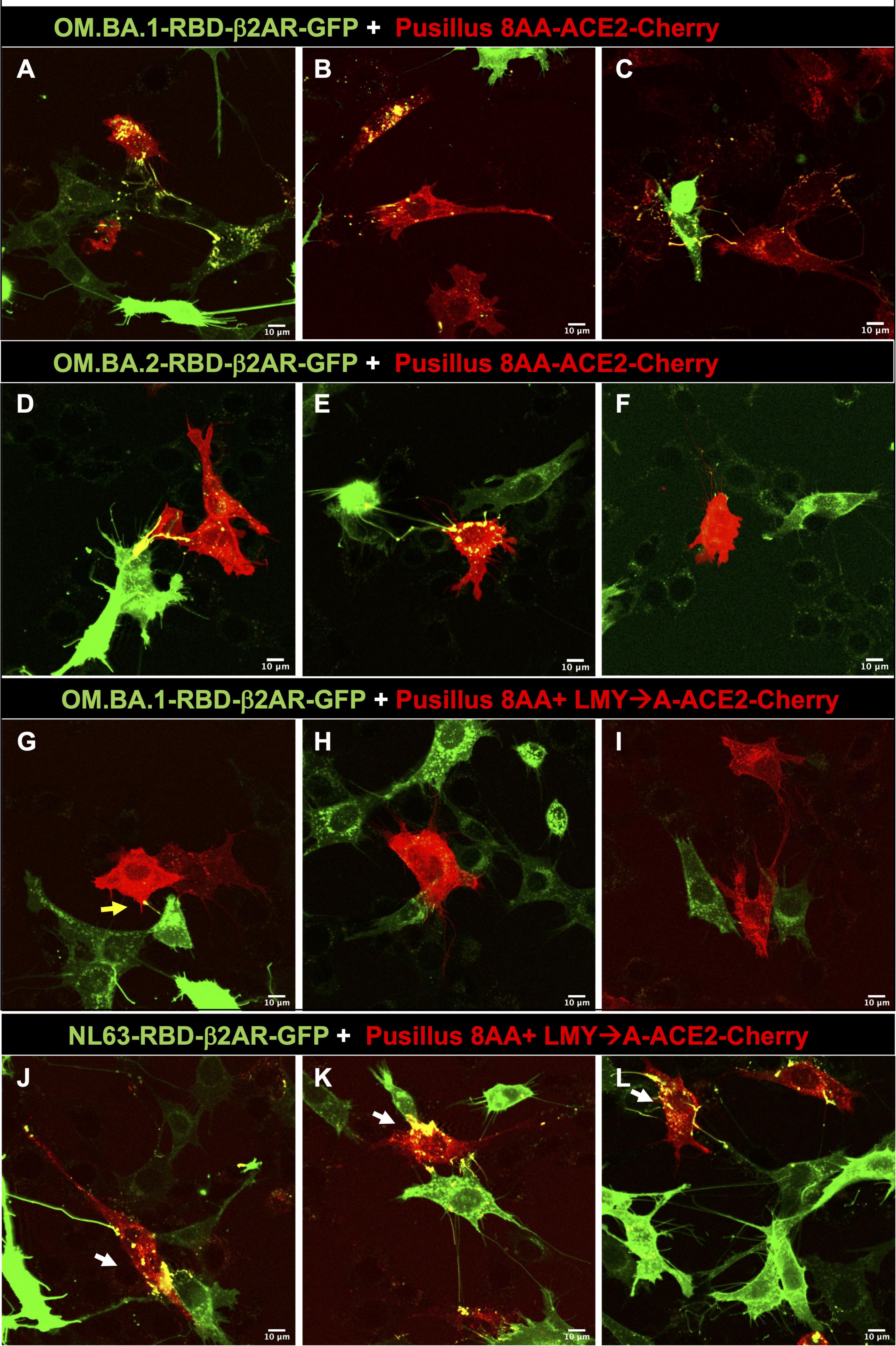

Figure10

RBD Variant Interactions with Hybrids of ACE2

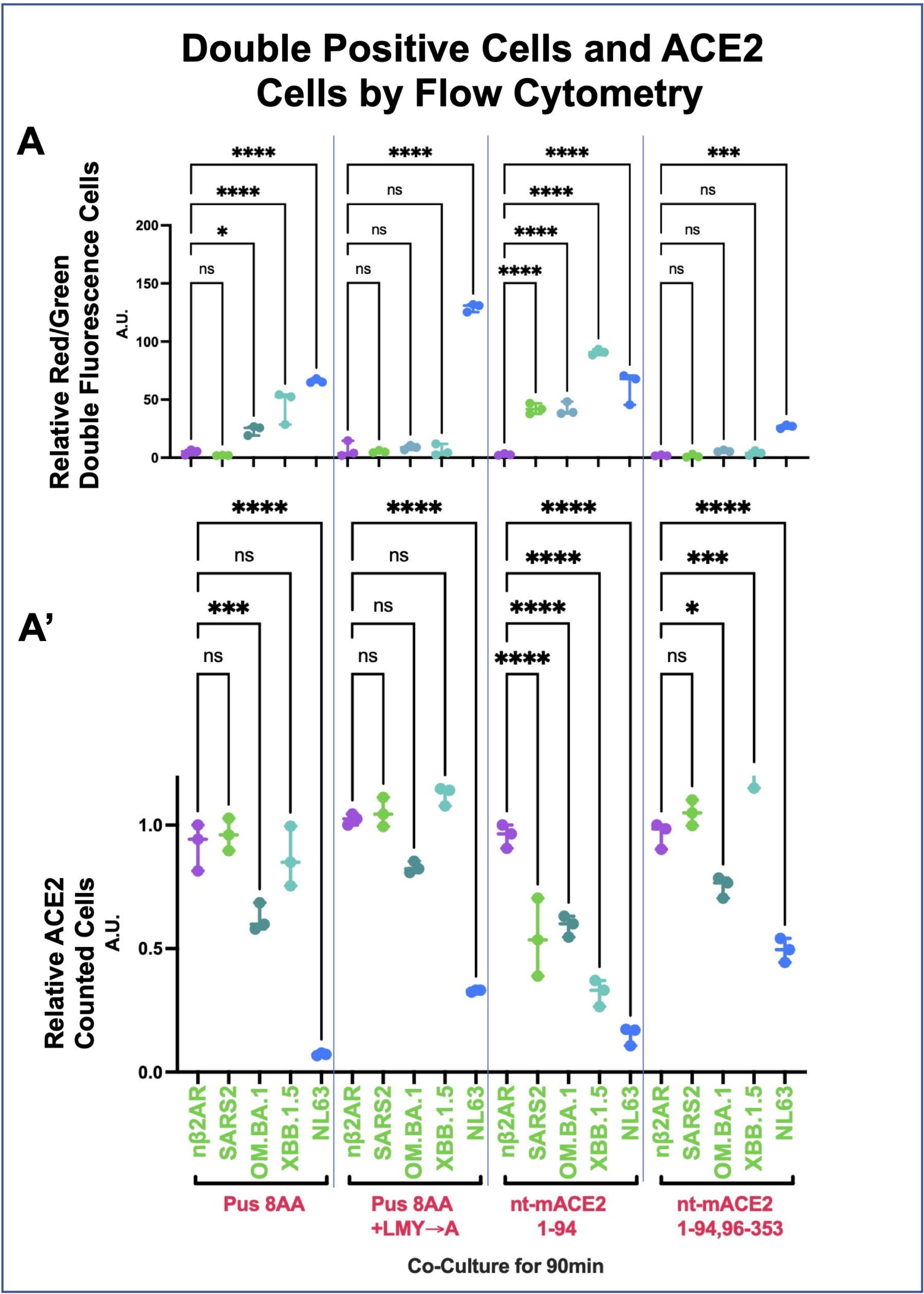

Figure 11

A

ACE2 Internal Region 1 & 2 Conservation

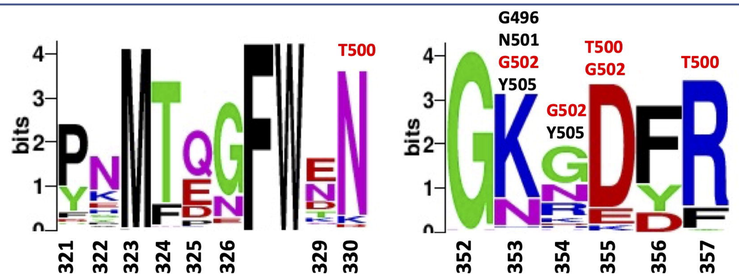

Mouse RESIDUES		P	H	M	T	Q	G	F	W	A	N	G	H	G	D	F	R
SARS2	Targets	P	N	M	T	Q	G	F	W	E	N	G	K	G	D	F	R
SARS1	Targets	P	N	M	T	Q	G	F	W	E	N	G	K	G	D	F	R
RaTG13	Targets	P	N	M	T	Q	G	F	W	E	N	G	K	G	D	F	R
NL63	Targets	P	N	M	T	Q	G	F	W	E	N	G	K	G	D	F	R

ACE2 Internal region 1-2 Alanine mutants

				Internalization by ACE2: SARS2/NL63
NKGD->Ala	A	A	A	NO/NO
KD->Ala		A	A	NO*/NO
K->Ala		A		YES/YES
D->Ala			A	YES/YES

* Slight binding

E

Alanine mutations that block binding

RBD Internalized by ACE2

	RBDs		
	Immutable Residues^		C NC P YGF G QP R V
YES	SARS2		CNGVEGFNCYFPLQSYGFQPTNGVGYQPYRVV
NO	SARS2	Y489A*	CNGVEGFNCAFPLQSYGFQPTNGVGYQPYRVV
NO	XBB.1.5	Y489A*	CNGVAGPNCASPLQSYGFRPTYGVGHQPYRVV
NO	SARS2	C480A,C488A*	ANGVEGFNAYFPLQSYGFQPTNGVGYQPYRVV
NO	OM.BA.1	C480A,C488A*	ANGVAGFNAYFPLRSYSFRPTYGVGHQPYRVV
NO	XBB.1.5	C480A,C488A*	ANGVAGPNAYSPLQSYGFRPTYGVGHQPYRVV
NO	SARS2	T500A,G502A*	CNGVEGFNCYFPLQSYGFQPANAVGYQPYRVV
NO	OM.BA.1	T500A,G502A*	CNGVAGFNCYFPLRSYSFRPAYAVGHQPYRVV
NO	XBB.1.5	T500A,G502A*	CNGVAGPNCYSPLQSYGFRPAYAVGHQPYRVV
YES	SARS2	T500A	CNGVEGFNCYFPLQSYGFQPANGVGYQPYRVV
YES	SARS2	G502A#	CNGVEGFNCYFPLQSYGFQPTNAVGYQPYRVV
YES	SARS2	P507A	CNGVEGFNCYFPLQSYGFQPTNGVGYQAYRVV
YES	SARS2	R509A	CNGVEGFNCYFPLQSYGFQPTNGVGYQPYAVV

* No binding observed # Poorly binds ^Chan et al., 2020; Starr et al., 2020

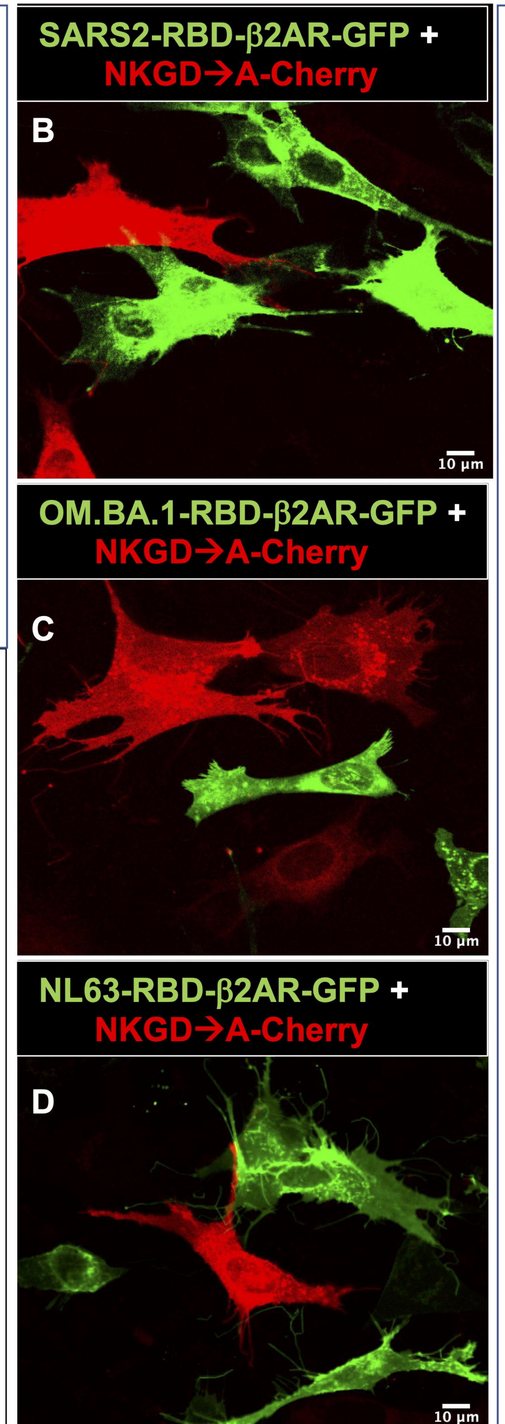

F

Double Positive Cells and ACE2 Cells by Flow Cytometry

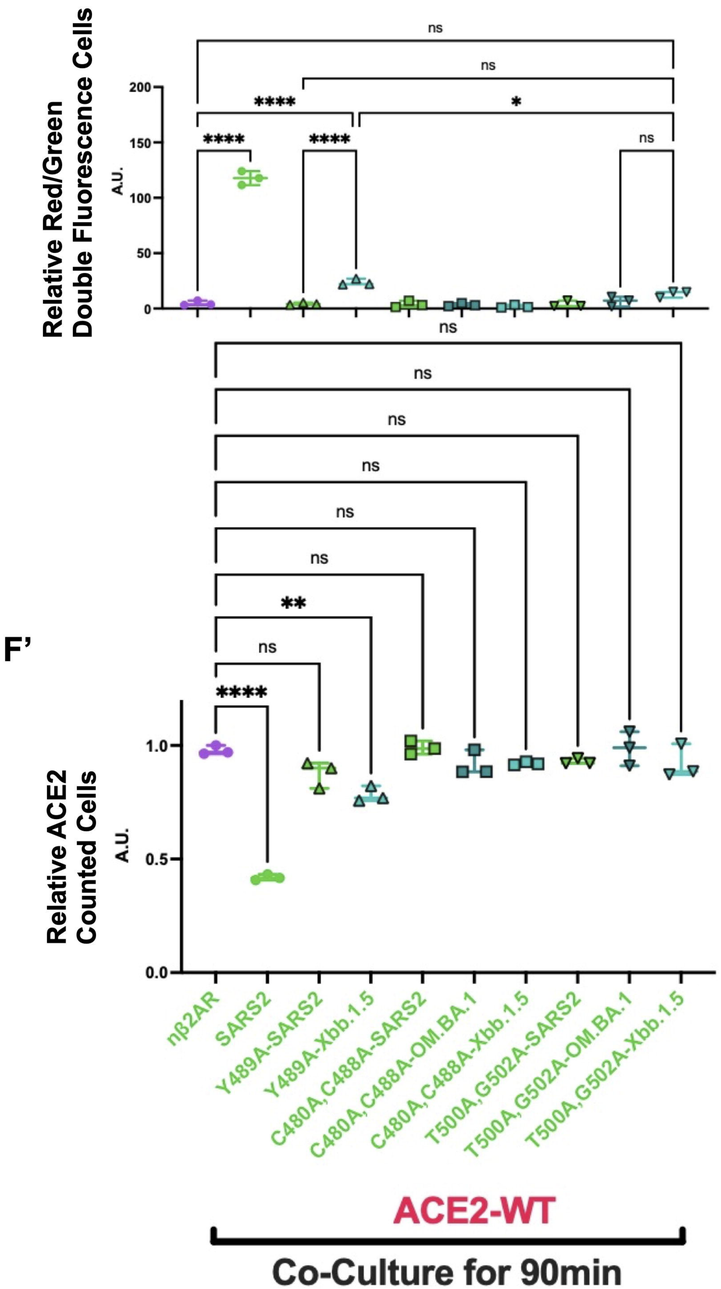

Figure 12

Contiguous domains for RBD Interactions on ACE2

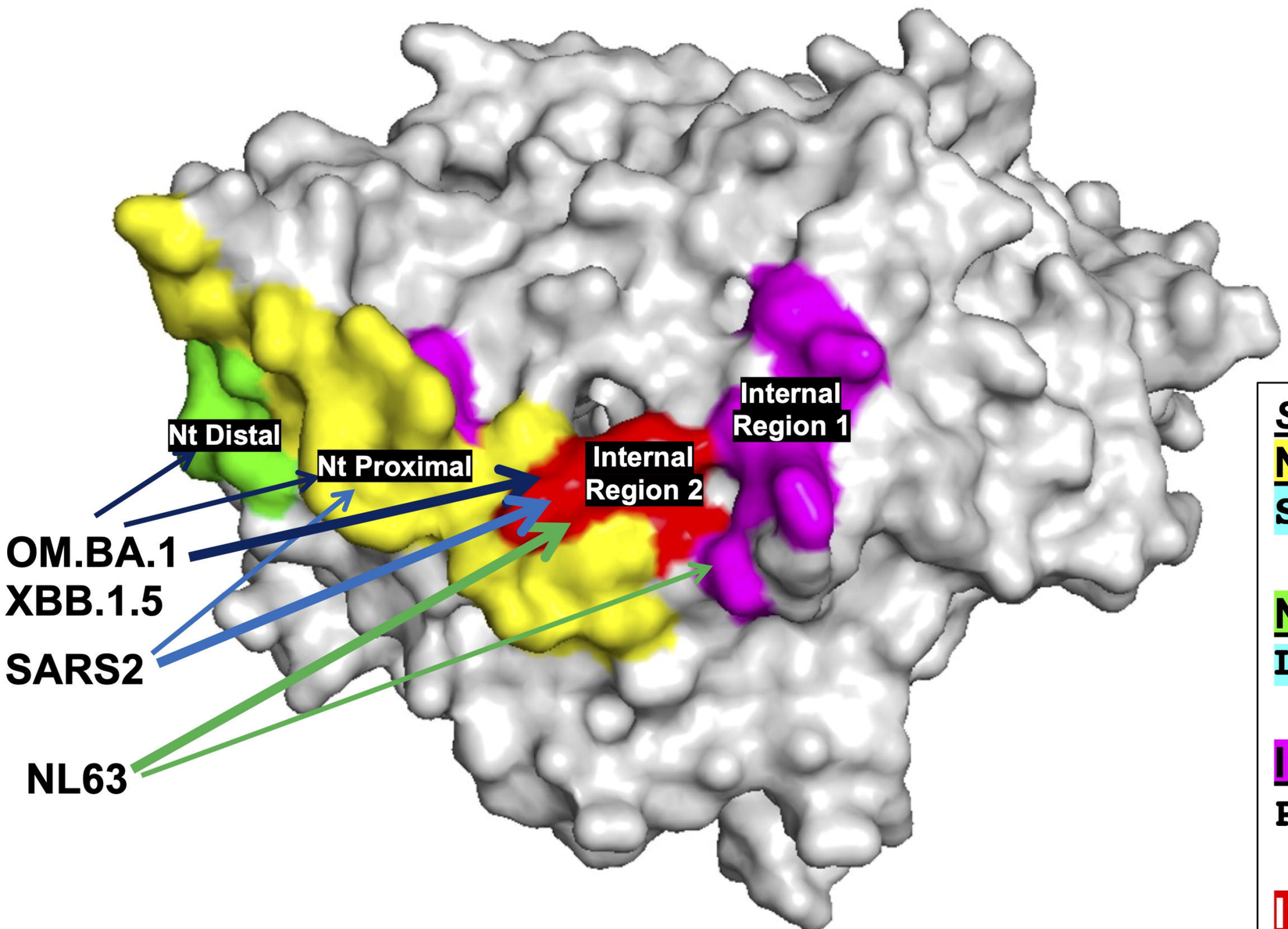

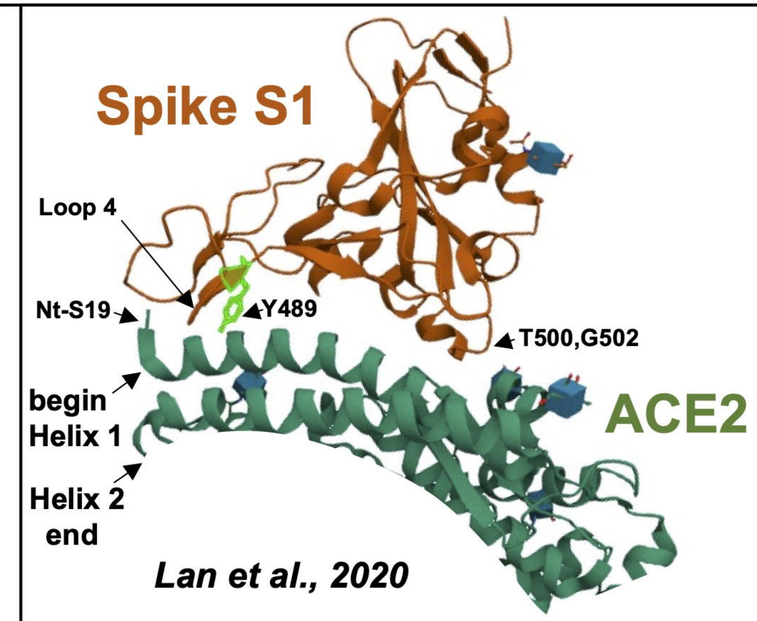

SARS2-RBD Binding sites on ACE2

Nt Proximal:

STIEEQAKTFLDKFNHEAEDLFYQSSL

Nt Distal:

LAQMY

Internal Region 1:

PNMTQGFWEN

Internal Region 2:

GKGDFR